

Fall 2011

Understanding the Effect of Cation and Solvation on the Structure and Reactivity of Nitrile Anions

Michael Ziegler

Follow this and additional works at: <https://dsc.duq.edu/etd>

Recommended Citation

Ziegler, M. (2011). Understanding the Effect of Cation and Solvation on the Structure and Reactivity of Nitrile Anions (Doctoral dissertation, Duquesne University). Retrieved from <https://dsc.duq.edu/etd/1414>

This Immediate Access is brought to you for free and open access by Duquesne Scholarship Collection. It has been accepted for inclusion in Electronic Theses and Dissertations by an authorized administrator of Duquesne Scholarship Collection. For more information, please contact phillips@duq.edu.

UNDERSTANDING THE EFFECT OF CATION AND SOLVATION ON THE
STRUCTURE AND REACTIVITY OF NITRILE ANIONS

A Dissertation

Submitted to The Bayer School of Natural and Environmental Science

Duquesne University

In partial fulfillment of the requirements for
the degree of Doctor of Philosophy

By

Michael J. Ziegler

December 2011

Copyright by
Michael J. Ziegler

2011

UNDERSTANDING THE EFFECT OF CATION AND SOLVATION ON THE
STRUCTURE AND REACTIVITY OF NITRILE ANIONS

By

Michael J. Ziegler

Approved November 18, 2011

Dr. Jeffrey D. Madura
Professor of Chemistry
(Committee Chair)

Dr. Jeffrey D. Evanseck
Professor of Chemistry
(Committee Member)

Dr. Charles F. Kahle II
Vice President Coatings R&D,
Chief Technology Officer, PPG Industries
(Committee Member)

Dr. Tomislav Pintauer
Professor of Chemistry
(Committee Member)

Dr. Ralph A. Wheeler
Chair, Department of Chemistry and
Biochemistry
Professor of Chemistry

Dr. David W. Seybert
Dean, Bayer School of Natural and
Environmental Sciences
Professor of Chemistry and Biochemistry

ABSTRACT

UNDERSTANDING THE EFFECT OF CATION AND SOLVATION ON THE STRUCTURE AND REACTIVITY OF NITRILE ANIONS

By

Michael J. Ziegler

November 18, 2011

Dissertation supervised by Professor Jeffry D. Madura

This Ph.D. dissertation is focused on the investigation the structure of nitrile anion containing molecules and how the structure and reactivity of those molecules are affected by solvation and counter ion. A systematic approach was employed in this investigation, beginning with an evaluation of the accuracy of three commonly used model chemistries (Hartree-Fock (HF), Second-order Møller-Plesset perturbation theory (MP2), the Becke three-parameter exchange functional coupled with the nonlocal correlation functional of Lee, Yang, and Parr (B3LYP), all paired with the 6-31+G(d) basis set). A series of complexes of various cations with a number of explicit molecules of tetrahydrofuran (THF) and dimethyl ether (DME) were studied with these model chemistries and the results were compared, where possible, with experimental results. From this work, it was determined that the B3LYP models gave the most accurate results for the complexes in question. This work was then extended to acetonitrile anion containing complexes of

solvent and cation. Based on the results of that extension, it was determined that cation size and charge density on the cation were critical factors in determining the structure of the acetonitrile anion molecule and in determining if the anion was metalated at the nitrogen or α -carbon position, with larger cations favoring carbon metalation and more significant deformation of the α -carbon from the expected sp^2 hybridization. The final aspect of this dissertation was the determination of reaction coordinate energy profiles for a pair of substitution reactions involving nitrile anion containing cycloaliphatic molecules. The results of this study showed that, due to steric and kinetic factors, the axial products and transition states associated with these reactions were favored, and that the degree of preference was kinetically controlled.

DEDICATION

To my wife Terri and my mother Theresa, who in so many ways have made this possible.

ACKNOWLEDGMENT

I would first and foremost like to thank Professor Jeffrey D. Madura for his patience, wisdom, creativity, and genuine care for my growth during our work together. Professor Madura demonstrated a constant and energizing optimism in this work, and without his advice, guidance, and encouragement this dissertation would not have been possible. The most profound lesson that I learned from Professor Madura has been to always embrace and cultivate my own intellectual curiosity, as this, far more than any facts or equations, is what truly makes a scientist a scientist.

I would also like to thank my committee my dissertation committee for graciously sharing their time, energy, insight and guidance with me. The depth of Professor Evanseck's knowledge and his ability to teach others by encouraging their own critical thinking on a subject are talents that have helped me significantly in my research on this dissertation, and which I have tried to emulate in my own career. I have known Professor Pintauer for almost 15 years, and during that time I have found an immense respect for, and benefited in my own work from, his determined pursuit of understanding and his passion for answering the question "why?". Doctor Khale's ability to visualize the future and encourage others make that vision a reality combined with his willingness to embrace innovative ways to do traditional things has not only allowed me to pursue my dream of completing a PhD dissertation but has also inspired me in other ways to look past what is and to see what could be.

I would like to thank Doctor Doug Fox for numerous discussions and significant assistance in understanding the Gaussian Software Package. I would thank Professor Fraser Fleming for numerous helpful discussions on nitrile anion chemistry. I would also like to thank Ms. Sarah Gibbons and Ms. Lisa Morkowchuk for their contributions to the work discussed in Chapter 4 of this dissertation.

I would like to thank Doctor Richard Foukes for his encouragement, mentoring and advice, and for challenging me to begin this journey. I would like to thank my mom, Ms. Theresa Ziegler for her unwavering faith and support. And finally, I need to thank my wife, Doctor Terri Ziegler for her patience, support, love, and friendship throughout this work and always.

TABLE OF CONTENTS

Abstract.....	Error! Bookmark not defined.	iv
Dedication.....	Error! Bookmark not defined.	vi
Acknowledgement	Error! Bookmark not defined.	vii
List of Tables	Error! Bookmark not defined.	xii
List of Figures.....	Error! Bookmark not defined.	xiv
1 Introduction.....		1
1.1 Theoretical Background.....		2
1.1.1 Ab Initio Methods.....		6
1.1.2 Post Hartree-Fock Methods		10
1.1.3 Density Functional Theory Methods		12
1.1.4 Self-Consistent Reaction Field Methods		15
1.2 Nitrile Anions Background		16
1.2.1 Nitrile Anion Reactivity.....		17
1.2.2 Nitrile Anion Utility.....		18
1.2.3 Nitrile Anion Structure		20
1.3 Objectives of this Dissertation		21
1.4 References		22
2 Cation / Solvent Complexes.....		32
2.1 Introduction		32
2.2 Computational Methods.....		34
2.3 Results and Discussions		35

2.3.1	Explicit DME Solvation.....	35
2.3.2	Explicit – Continuum DME Solvation.....	45
2.3.3	Explicit THF Solvation.....	50
2.3.4	Explicit – Continuum THF Solvation.....	59
2.4	Conclusions	66
2.5	References	67
3	Effect of Solvent and Cation on the Structure of Acetonitrile Anion.....	76
3.1	Introduction	76
3.2	Computational Methods.....	79
3.3	Results and Discussions	80
3.3.1	Comparison of Model Chemistries	80
3.3.2	Determination of Carbon or Nitrogen Metalation for DME Complexes	86
3.3.3	Determination of Carbon or Nitrogen Metalation for THF Complexes	90
3.3.4	Natural Bond Order Analysis.....	94
3.4	Conclusions	99
3.5	References	101
4	Selectivity of Substitution Reactions Involving Nitrile Anion Containing Molecules.	108
4.1	Introduction	108
4.2	Computational Methods.....	113
4.3	Results and Discussions	114

4.3.1	Reactant and Product Energies for the Reaction of the Five Membered Ring	115
4.3.2	Reactant and Product Energies for the Reaction of the Six Membered Ring.	119
4.3.3	Transition State Calculations	122
4.3.3.1	Density Functional Theory Calculations	123
4.3.3.2	Semi-Empirical Calculations	128
4.3.3.3	Alternate Software Calculations	129
4.4	Conclusions	141
4.5	References	143
5	Conclusion and Future Directions	149

LIST OF TABLES

Table 2.1. Calculated values for selected structural features of DME-cation complexes.	36
Table 2.2. Thermochemical values calculated at standard pressure and 298 °K (all values are given in Hartrees)......	37
Table 2.3. Bond dissociation energies calculated at standard pressure and 298 °K (all values are given in kJ/mol)	38
Table 2.4. Root mean squared differences between calculated and experimentally measured bond dissociation enthalpies (bond dissociation energy for Cu+) in kJ/mol....	44
Table 2.5. $\Delta G(\text{solvation})$ calculated with a continuum approximation of solvation and the number of explicit solvent molecules listed. Calculated at standard pressure and 298° K (all values are in kJ/mol).....	46
Table 2.6. Calculated values for selected structural features of cation / solvent complexes	51
Table 2.7. Thermochemical values calculated at standard pressure and 298° K (all values are given in Hartrees).....	52
Table 2.8. Bond dissociation energies and enthalpies calculated at standard pressure and 298° K (all values are in kJ/mol)	53
Table 2.9. $\Delta G(\text{solvation})$ calculated with a continuum approximation of solvation and the number of explicit solvent molecules listed. Calculated at standard pressure and 298° K (all values are in kJ/mol).....	60
Table 3.1. Calculated values for selected structural features of cation / DME complexes using various model chemistries.....	80
Table 3.2. Calculated values for selected structural features of cation / THF complexes using various model chemistries.....	81
Table 3.3. Calculated values for selected structural features of cation / THF complexes using various levels of Møller-Plesset perturbation theory and sizes of basis set.....	82
Table 3.4. Calculated values for selected structural features and electronic energy of cation / DME complexes using various types of solvation models and the B3LYP/6- 31+G(d) model chemistry	88
Table 3.5. Calculated values for selected structural features and electronic energy of cation / THF complexes using various types of solvation models and the B3LYP/6- 31+G(d) model chemistry.....	91
Table 3.6. Energetically favored metalation site for each cation under various solvation conditions.....	95
Table 3.7. Electronic energies, natural charges, and cation natural charge densities for DME solvated complexes using various solvation models.....	96
Table 3.8. Electronic energies, natural charges, and cation natural charge densities for THF solvated complexes using various solvation models.....	97
Table 4.1. Relative enthalpies, in kJ/mol, for the three possible conformations of the reactant of the 5 membered ring reaction calculated with the B3LYP/6-31+G(d) model chemistry.....	118
Table 4.2. Dipole moments, in Debyes, for the three possible conformations of the reactant of the 5 membered ring reaction.	118

Table 4.3. Relative enthalpies, in kJ/mol, for the three possible conformations of the reactant of the 6 membered ring reaction calculated with the B3LYP/6-31 ⁺ G(d) model chemistry.....	120
Table 4.4. Dipole moments, in Debyes, for the three possible conformations of the reactant of the 6 membered ring reaction.	121
Table 4.5. Selected structural data for the two lithium based transition structures for the 5 membered ring reaction.	128
Table 4.6. Summary of semi-empirical results for the calculations of transition structures using Gaussian 09.	129
Table 4.7. Relative energies of the MOPAC optimized transition structures.....	130
Table 4.8. Selected structural data for the PM6 transition structures for the 5 membered ring reaction.	131
Table 4.9. Selected structural data for the PM6 transition structures for the 6 membered ring reaction.	131

LIST OF FIGURES

Figure 1.1. Overview of electronic structure calculations	3
Figure 1.2. Resonance structures for acetonitrile anion.....	16
Figure 1.3. Representative nitrile anion bond lengths	17
Figure 1.4. Unexpected retention of stereochemistry	18
Figure 1.5. Effects of solvent on stereochemistry of an annulation product	19
Figure 1.6. Three nitrile anion complexes	21
Figure 2.1. Dimethyl ether bond dissociation energy	38
Figure 2.2. Comparison of Li ⁺ - DME bond dissociation enthalpies calculated at HF/6-31+G(d),MP2/6-31+G(d), and B3LYP/6-31+G(d) with experimentally measured values	39
Figure 2.3. Comparison of Na ⁺ - DME bond dissociation enthalpies calculated at HF/6-31+G(d),MP2/6-31+G(d), and B3LYP/6-31+G(d) with experimentally measured values	40
Figure 2.4. Comparison of K ⁺ - DME bond dissociation enthalpies calculated at HF/6-31+G(d),MP2/6-31+G(d), and B3LYP/6-31+G(d) with experimentally measured values	41
Figure 2.5. Comparison of Cu ⁺ - DME bond dissociation energies calculated at HF/6-31+G(d),MP2/6-31+G(d), and B3LYP/6-31+G(d) with experimentally measured values	42
Figure 2.6. Comparison of Li ⁺ - DME Gibbs Free Energy of Solvation calculated at HF/6-31+G(d),MP2/6-31+G(d), and B3LYP/6-31+G(d) using continuum solvation approximated by the PCM method and theoretical value calculated using the Born Equation	47
Figure 2.7. Comparison of Na ⁺ - DME Gibbs Free Energy of Solvation calculated at HF/6-31+G(d),MP2/6-31+G(d), and B3LYP/6-31+G(d) using continuum solvation approximated by the PCM method and theoretical value calculated using the Born Equation	48
Figure 2.8. Comparison of K ⁺ - DME Gibbs Free Energy of Solvation calculated at HF/6-31+G(d),MP2/6-31+G(d), and B3LYP/6-31+G(d) using continuum solvation approximated by the PCM method and theoretical value calculated using the Born Equation	49
Figure 2.9. Comparison of Cu ⁺ - DME Gibbs Free Energy of Solvation calculated at HF/6-31+G(d) and B3LYP/6-31+G(d) using continuum solvation approximated by the PCM method and theoretical value calculated using the Born Equation.....	50
Figure 2.10. Tetrahydrofuran bond dissociation energy	54
Figure 2.11. Comparison of Li ⁺ - THF bond dissociation enthalpies calculated at HF/6-31+G(d),MP2/6-31+G(d), and B3LYP/6-31+G(d)	54
Figure 2.12. Comparison of Na ⁺ - THF bond dissociation enthalpies calculated at HF/6-31+G(d),MP2/6-31+G(d), and B3LYP/6-31+G(d)	55
Figure 2.13. Comparison of K ⁺ - THF bond dissociation enthalpies calculated at HF/6-31+G(d),MP2/6-31+G(d), and B3LYP/6-31+G(d)	56
Figure 2.14. Comparison of Cu ⁺ - THF bond dissociation enthalpies calculated at HF/6-31+G(d),MP2/6-31+G(d), and B3LYP/6-31+G(d)	57

Figure 2.15. Comparison of MgCl ⁺ - THF bond dissociation enthalpies calculated at HF/6-31+G(d),MP2/6-31+G(d), and B3LYP/6-31+G(d).....	58
Figure 2.16. Comparison of Li ⁺ - THF Gibbs Free Energy of Solvation calculated at HF/6-31+G(d),MP2/6-31+G(d), and B3LYP/6-31+G(d) using continuum solvation approximated by the PCM method and theoretical value calculated using the Born Equation	61
Figure 2.17. Comparison of Na ⁺ - THF Gibbs Free Energy of Solvation calculated at HF/6-31+G(d),MP2/6-31+G(d), and B3LYP/6-31+G(d) using continuum solvation approximated by the PCM method and theoretical value calculated using the Born Equation	62
Figure 2.18. Comparison of K ⁺ - THF Gibbs Free Energy of Solvation calculated at HF/6-31+G(d),MP2/6-31+G(d), and B3LYP/6-31+G(d) using continuum solvation approximated by the PCM method and theoretical value calculated using the Born Equation	63
Figure 2.19. Comparison of Cu ⁺ - Gibbs Free Energy of Solvation calculated at HF/6-31+G(d),MP2/6-31+G(d), and B3LYP/6-31+G(d) using continuum solvation approximated by the PCM method and theoretical value calculated using the Born Equation	64
Figure 2.20. Comparison of MgCl ⁺ - Gibbs Free Energy of Solvation calculated at HF/6-31+G(d),MP2/6-31+G(d), and B3LYP/6-31+G(d) using continuum solvation approximated by the PCM method and theoretical value calculated using the Born Equation	65
Figure 3.1. Deformation angle around the α -carbon of the nitrile anion	77
Figure 3.2. Deformation angle around the α -carbon of the nitrile anion (calculated at B3LYP/6-31+G(d) and HF/6-31+G(d)) as a function of the covalent radius of the counter ion present in the DME complex	83
Figure 3.3. Deformation angle around the α -carbon of the nitrile anion (calculated at B3LYP/6-31+G(d) and HF/6-31+G(d)) as a function of the covalent radius of the counter ion present in the THF complex.....	84
Figure 3.4. Deformation angle around the α -carbon of the nitrile anion (calculated at B3LYP/6-31+G(d) and HF/6-31+G(d)) as a function of model chemistry and solvent. The lines show the range of values, and the triangles show the mean values of deformation angle for all cations using that specific solvent and theory combination.....	86
Figure 3.5. (a) Nitrogen metalated lithium / acetonitrile complex, explicitly solvated with DME. (b) Carbon metalated lithium / acetonitrile complex, explicitly solvated with DME. White spheres represent hydrogen atoms, gray spheres represent carbon atoms, red spheres represent oxygen atoms, the blue sphere represents a nitrogen atom, and the purple sphere represents a Li ⁺ cation.	87
Figure 3.6. (a) Nitrogen metalated copper / acetonitrile complex, explicitly solvated with DME. (b) Carbon metalated copper / acetonitrile complex, explicitly solvated with DME. White spheres represent hydrogen atoms, gray spheres represent carbon atoms, red spheres represent oxygen atoms, the blue sphere represents a nitrogen atom, and the pink sphere represents a Cu ⁺ cation	90
Figure 3.7. Carbon metalated lithium / acetonitrile complex, explicitly solvated with THF. White spheres represent hydrogen atoms, gray spheres represents carbon atoms, red	

spheres represent oxygen atoms, the blue sphere represents a nitrogen atom, and the purple sphere represents a Li ⁺ cation.	93
Figure 4.1. Reaction scheme for 5 membered ring, where M is Li, Na, K, or Cu, showing first the nitrogen metalated reactant going through the two possible transition structures to two possible products, followed by the two different carbon metalated starting points each going through a single transition structure to a single product.....	110
Figure 4.2. Reaction scheme for 6 membered ring, where M is Li, Na, K, or Cu, showing first the nitrogen metalated reactant going through the two possible transition structures to two possible products, followed by the two different carbon metalated starting points each going through a single transition structure to a single product.....	111
Figure 4.3. An experimental example of a cation influenced alkylation reaction.	112
Figure 4.4. Structures and relative enthalpies of the two products of the 5 membered ring reaction.....	116
Figure 4.5. Structures and relative enthalpies of the two products of the 6 membered ring reaction.....	119
Figure 4.6. Two transition structures for the 5 membered ring reaction.	122
Figure 4.7. Two transition structures for the 6 membered ring reaction.	123
Figure 4.8. A starting point geometry showing the reaction axis highlighted in red. White spheres represent hydrogen atoms, gray spheres represent carbon atoms, red spheres represent oxygen atoms, the blue sphere represents a nitrogen atom, the green sphere represents a chlorine atom, and the purple sphere represents a K ⁺ cation.	124
Figure 4.9. (a) Starting point geometry for the trans transition structure of the 5 membered ring reaction with the Na ⁺ . (b) Unoptimized geometry for the trans transition structure of the 5 membered ring reaction with the Na ⁺ after ~3,000 SCF iterations. White spheres represent hydrogen atoms, gray spheres represent carbon atoms, red spheres represent oxygen atoms, the blue sphere represents a nitrogen atom, the green sphere represents a chlorine atom, and the purple sphere represents a Na ⁺ cation.	126
Figure 4.10. The B3LYP reaction coordinate for the 5 membered ring reaction with Li ⁺ starting from the nitrogen metalated reactant. Data shown is based on explicit / continuum hybrid solvation in THF.....	127
Figure 4.11. The PM6 reaction coordinate for the 5 membered ring reaction with Li ⁺ starting from the nitrogen metalated reactant. Data shown is based on explicit / continuum hybrid solvation in THF.....	133
Figure 4.12. The PM6 reaction coordinate for the 5 membered ring reaction with Na ⁺ starting from the nitrogen metalated reactant. Data shown is based on explicit / continuum hybrid solvation in THF.....	134
Figure 4.13. The PM6 reaction coordinate for the 5 membered ring reaction with K ⁺ starting from the nitrogen metalated reactant. Data shown is based on explicit / continuum hybrid solvation in THF.....	135
Figure 4.14. The PM6 reaction coordinate for the 5 membered ring reaction with Cu ⁺ starting from the nitrogen metalated reactant. Data shown is based on explicit / continuum hybrid solvation in THF.....	136
Figure 4.15. The PM6 reaction coordinate for the 6 membered ring reaction with Li ⁺ starting from the nitrogen metalated reactant. Data shown is based on explicit / continuum hybrid solvation in THF.....	137

Figure 4.16. The PM6 reaction coordinate for the 6 membered ring reaction with Na ⁺ starting from the nitrogen metalated reactant. Data shown is based on explicit / continuum hybrid solvation in THF.....	138
Figure 4.17. The PM6 reaction coordinate for the 6 membered ring reaction with K ⁺ starting from the nitrogen metalated reactant. Data shown is based on explicit / continuum hybrid solvation in THF.....	139
Figure 4.18. The PM6 reaction coordinate for the 6 membered ring reaction with Cu ⁺ starting from the nitrogen metalated reactant. Data shown is based on explicit / continuum hybrid solvation in THF.....	140

1 Introduction

Scientists in all fields of science are constantly faced with the challenge of developing new compounds as diverse as drug molecules, building materials, chemical sensors, high performance coatings, semi-conductors, nanoparticles, and countless others. In order to answer this challenge scientists have historically gone to the lab, and through a fundamental understanding of chemistry, intuition, and trial and error, they have attempted to make molecules that have certain desirable properties. Over the past sixty years, the availability of high performance computers and novel methods of approximating the solutions to quantum mechanical equations have led to new tools which allow researchers to have at their disposal a virtual laboratory which they can use to gain a deeper understanding and make predictions about what is happening on an atomic level in the laboratory reaction vessel.¹⁻³ This higher level of understanding is not merely a simplification of the research and development process, but is in fact a tool that is necessary to allow scientific advances to keep pace with the ever increasing challenges facing mankind.

The overall objective of this investigation is to apply electronic structure calculations to help increase our understanding how solvents and cations affect the structure of nitrile anion containing molecules and how in turn those structures can be used to predict the reactivity of those molecules.

1.1 Theoretical Background

Quantum Chemistry is the application of quantum mechanics to the study of molecular systems. Electronics structure calculations, which are the principle quantum chemical method used in this dissertation work, use quantum mechanics to calculate the energy of molecular systems. Useful extensions of these energy calculations are the determination of optimized molecular structure, calculation of the vibrational frequencies associated with intramolecular motions within the molecular system, and molecular properties such as partial charge. An optimized molecular structure is one in which the forces between atoms are zero and the energy is at a minimum. The first derivative of the total energy of the system with respect to atomic position is used to determine the optimized molecular structure. The second derivative of the total energy of the system with respect to atomic position is used to determine the vibrational frequencies and whether the optimized structure is a global minimum or a transition state.

Figure 1.1 shows a general overview of how various quantum mechanical concepts and computational techniques are related and how they build upon each other to form the different types of model chemistries used in this dissertation.

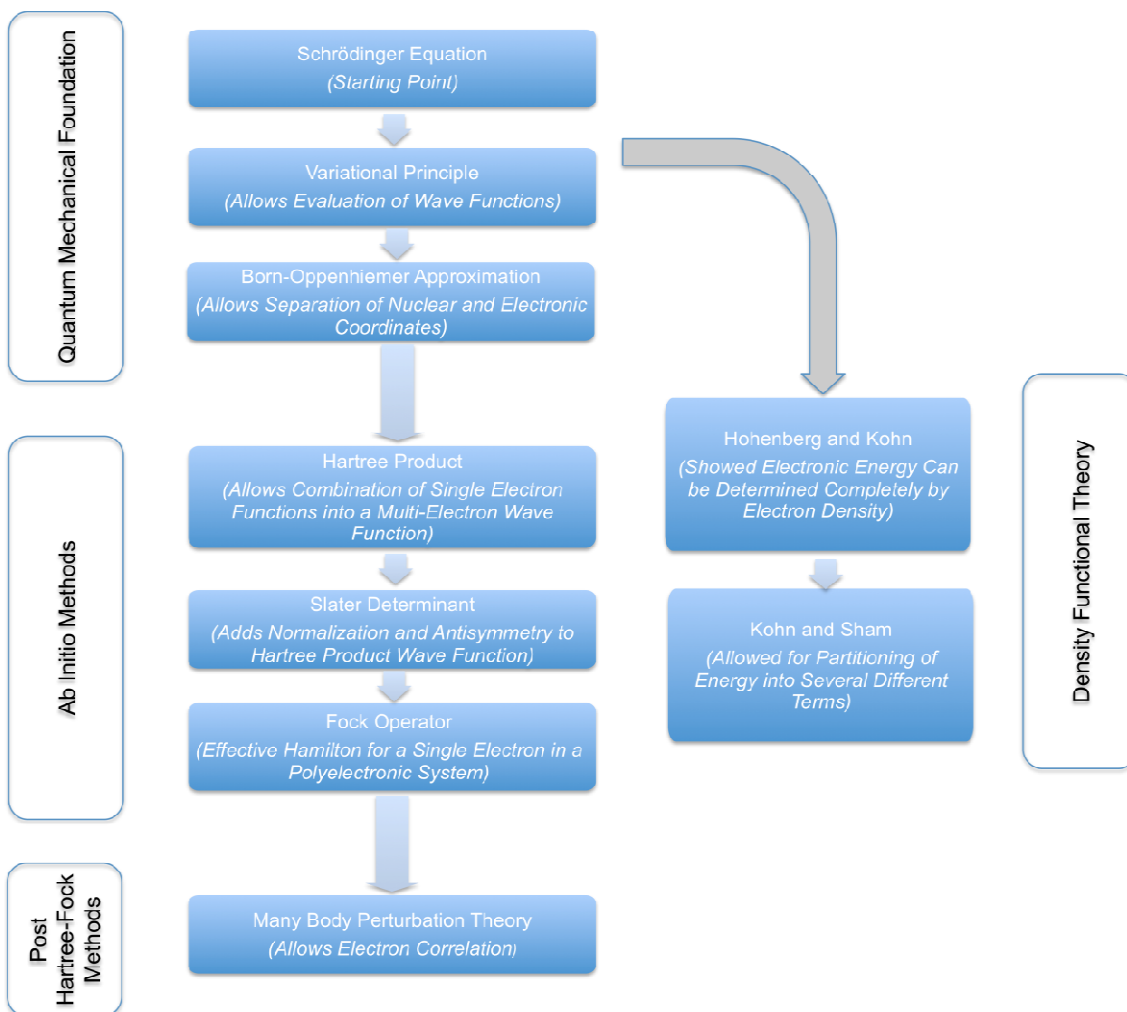


Figure 1.1. Overview of electronic structure calculations

As show in Figure 1.1, the basis electronic structure calculations is the Schrödinger equation [1.1], where H is the Hamiltonian operator, ψ is the wave function, and E is the total energy. The Hamiltonian operator, which is comprised a kinetic energy operator and a potential energy operator, operates upon the wave function of a molecular system in such a way that it returns the wave function multiplied by the total energy of the system.

The Schrödinger equation is analytically solvable only for the smallest of systems, such as the hydrogen cation or the hydrogen atom. As such, the various electronic structure calculation methods aim to find an approximate solution to equation, and are differentiated from one another by the nature of the approximations used.

One critical aspect of these approximations, which is shared by all methods, is the use of the Variational Principle (or Variation Theorem), which states that the wave function which gives the lowest value of total energy (E) is greater than or equal to the true ground state of that molecular system. Since it is not possible to determine an analytical solution to the Schrödinger equation for larger systems the Variational Principle allows for a criterion which can be used to determine “the best” approximate solution.

The next step in building these methodologies, is to further breakdown the molecular Hamiltonian from kinetic (T) and potential energy (V) terms, as shown in equation [1.2], to five terms representing the kinetic energy of the nuclei (T_{nuc}), the kinetic energy of the electrons (T_{elec}), the potential energy of nuclear-electron interactions ($V_{\text{nuc-elec}}$), the potential energy of nuclear-nuclear interactions ($V_{\text{nuc-nuc}}$), and the potential energy of electron-electron interactions ($V_{\text{elec-elec}}$), as shown in equation [1.3].

$$H = T + V \quad [1.2]$$

$$H = T_{\text{nuc}} + T_{\text{elec}} + V_{\text{nuc-elec}} + V_{\text{nuc-nuc}} + V_{\text{elec-elec}} \quad [1.3]$$

The first key assumption that will be made in order to allow for approximate solutions of the Schrödinger equation is the application of the Born-Oppenheimer approximation.⁴ This approximation treats the kinetic energy of the nuclei as independent of the rest of the system, and is based on the fact that nuclei are normally moving significantly slower than electrons in a molecule, and that electrons are in turn able to relax relative to changes in the motion of the nuclei in an essentially instantaneous way. This allows the molecular system being studied to be considered as being composed of moving electrons and unmoving nuclei with fixed positions. In considering such a system the nuclear kinetic energy term of the Hamiltonian would be ignored and the nuclear-nuclear interaction term would be a constant based on the fixed positions of the nuclei, allowing the Schrödinger equation to be rewritten, such as in equation [1.4], to return the electronic energy of the system based on the operation of an electronic Hamilton on the electronic wave function plus the energy of the nuclear-nuclear interaction.

$$(H_{\text{elec}} + V_{\text{nuc-nuc}})\Psi_{\text{elec}} = E_{\text{elec}}\Psi_{\text{elec}} \quad [1.4]$$

$$\text{Where: } H_{\text{elec}} = T_{\text{elec}} + V_{\text{nuc-elec}} + V_{\text{elec-elec}}$$

In addition to simplifying the Hamilton used in the Schrödinger equation, Born also provides an interpretation of the nature of the wave function, as the description of the probability of an electron being in a given region of space.^{5, 6} Based on this interpretation, some restrictions must be placed on the electronic wave function. First, the absolute value of the square of the wave function is interpreted as being the probability density of the electrons that it describes, leading to the restriction that Ψ be

normalized. In other words, it must be guaranteed that the electrons will be found somewhere in all space. A second restriction is that, in keeping with the Pauli Exclusion Principle, the wave functions of the electronics must be antisymmetric. When two identical electronics are exchanged, the sign of the wave function must be changed.

The next steps in the methodologies of three main types of electronic structure calculations are Ab Initio methods, Post Hartree-Fock methods, and Density Functional Theory methods, are described in the following sections.

1.1.1 Ab Initio Methods

Ab initio methods are, as the name implies, based on the first principles of the laws of quantum mechanics and in general, very accurate but very computationally expensive methods. The most direct, and in many ways, the simplest application of these first principles of is Hartree-Fock (HF) Theory^{1-3, 7-12}.

Molecular orbital theory allows Ψ for a given molecular system to be considered to be composed of a combination of the molecular orbitals of that system. In turn each molecular orbital can be constructed from linear combination of atomic orbitals, as shown in Equation [1.5], where Φ is a molecular orbital, a_i is a coefficient known as the molecular orbital expansion coefficient, and φ_i is the a function corresponding to an atomic orbital. This construction is carried out using a basis set expansion approximation, which is the use of a combination of small, conveniently solved functions (basis sets) to approximate an arbitrary function, in this case the molecular orbital.

$$\Phi = \sum_{i=1}^N a_i \varphi_i \quad [1.5]$$

For a many electron system the total electronic wave function can be constructed as a Hartree product of the all of the single electron wave functions in the system. Further, those single electron wave functions can be considered as molecular orbitals resulting in the expression for the total wave function shown in equation [1.6]. A wave function of the form of equation [1.6] is conventionally known as Hartree-Product wavefunction

$$\Psi_{\text{elec}} = \Phi_1 \Phi_2 \Phi_3 \dots \Phi_n \quad [1.6]$$

A convenient way of enforcing the required restrictions of normalization and antisymmetry upon a Hartree-Product wave function is to build the wave function from Slater determinants. The columns in a Slater determinant are spin orbitals (single electron wave functions) and the rows represent the electronic coordinates. The spin orbitals, χ_N , used in the determinant, are the products of spatial molecular orbital (Φ_n) and a spin function (α or β). In the generic Slater determinant shown in equation [1.7], N is total number of electrons in the system.

$$\Psi_{\text{SD}} = \frac{1}{\sqrt{N!}} \begin{vmatrix} \chi_1(1) & \chi_2(1) & \dots & \chi_N(1) \\ \chi_1(2) & \chi_2(2) & \dots & \chi_N(2) \\ \dots & \dots & \dots & \dots \\ \chi_1(N) & \chi_2(N) & \dots & \chi_N(N) \end{vmatrix} \quad [1.7]$$

Given the simplifications and assumption discussed thus far, the next step in the use of Hartree-Fock theory is to evaluate the quality of a trial wave function in light of the variational principle. As mentioned above, the variational principle states that the correct energy of a system is the lower bound of calculated values, meaning that the

lower the energy calculated from operation of the Hamilton on the trial wave function, the closer to “correct” that wave function is. In order to calculate these energies, the electronic Hamiltonian described in equation [4], must first be more rigorously defined.

The total electronic Hamiltonian is separable, and may be expressed as the sum of all single electron Hamiltonians in a system of N total electronics, as shown in equation [1.8].

$$H_{\text{elec}} = \sum_{i=1}^N h_i \quad [1.8]$$

An effective single electron Hamilton is the Fock Operator, which contains a term for the kinetic energy of the electrons (T_{elec}), the potential energy of nuclear-electron interactions ($V_{\text{nuc-elec}}$). A single electron Hamilton of this type is of the form shown in equation [1.9], where x,y, and z are the Cartesian coordinates of the electron, M is the total number of nuclei in the molecule, Z is the atomic number of nucleus k, and r is the distance between electron i and nucleus k.

$$h_i = -\frac{1}{2} \left(\frac{\partial^2}{\partial x_i^2} + \frac{\partial^2}{\partial y_i^2} + \frac{\partial^2}{\partial z_i^2} \right) + \sum_{k=1}^M \left(\frac{Z_k}{r_{ik}} \right) + V_i\{j\} \quad [1.9]$$

The third term on the right hand side of the equation is a term accounting for electron – electron repulsion interaction potential with all of the other electrons occupying orbitals (j). Defining the form of this term is made extremely complicated by its dependence on the simultaneous pairwise interactions of all electrons in the system.

HF methodology uses an approximation of electron – electron repulsion potential of the form of equation [1.10], in which ρ_j is the charge density associated with electron j .

$$V_i\{j\} = \sum_{j \neq i} \int \frac{\rho_j}{r_{ij}} dr \quad [1.10]$$

The final step in HF methodology is to determine a reasonably accurate estimate of the wave function and energy associated with a molecular system using an iterative self-consistent field (SCF) approach. In this approach, an initial guess of wave functions of the occupied molecular orbitals is made and is used to construct the necessary one electron Hamiltonian operators. These operators are then used to provide a new set of, presumably more accurate, wave functions. This process is repeated until a pre-established convergence criterion threshold, such as maximum energy change in each step, is met. The tighter the threshold used, the more computationally expensive the process is, but the closer to the correct wave function the approximation is presumed to be.

Hartree-Fock theory is used extensively in this dissertation, despite the obvious limitations inherent in the method's treatment of electron – electron interaction potentials. As stated above this limitation is due to the fact that individual electron – electron interactions (or electron correlations) are ignored and instead replaced by the interaction of an individual electron with an average field of charge density from the other electrons of the system. Numerous computational methods have been developed to provide more accurate approximations, by improving upon the treatment of electron – electron interaction used in HF theory. The addition of individual electron correlation in these

methods typically provides increases in accuracy accompanied by increased computational costs.

1.1.2 Post Hartree-Fock Methods

Møller-Plesset Perturbation Theory¹³⁻¹⁵ is one such electron correlation containing extension of HF theory, which was used in frequently in this dissertation. Møller-Plesset Perturbation Theory is an extension of Rayleigh – Schrödinger Perturbation Theory,¹⁶ and falls within the general framework of the mathematical concept of Many Body Perturbation Theory.¹⁷ In simplest terms, perturbation theory suggests that the solution to an extremely complex problem is very close to the solution of a problem which has already been solved (at least approximately), and as such should be estimated by making a small change or perturbation to the existing solution. As shown in equation [1.11], in terms of quantum mechanics this is done mathematically by defining the Hamiltonian operator as the sum of a reference Hamilton (H_0) and a term containing a correction or perturbation Hamilton (H') and a parameter (λ) which determines the strength of the perturbation. When the value of λ is equal to zero, the defined Hamiltonian is equal to the reference Hamiltonian, and when λ is equal to one the defined Hamiltonian is equal to the “True” Hamiltonian.

$$H = H_0 + \lambda H' \quad [1.11]$$

If this newly defined Hamiltonian is then used to construct a perturbed version of the Schrödinger equation, it will be necessary to continuously change the energy and wave function terms in the equation as the value of λ is increased from zero. These

energy and wave function terms can be expressed as Taylor expansions in powers of λ . When λ is equal to zero the terms are equal to their reference, unperturbed values, and are considered to be zeroth-order perturbation of the Schrödinger equation. When the Taylor expansion adds one additional term to the energy or wave function, it is considered to be a first order perturbation, when two terms are added it becomes a second order perturbation and so on. Conceptually, these additional energy terms represent a correction to the total energy of the system which corresponds to the the potential energy associated with electron correlation. The further mathematical implementation of perturbation theory to the approximate solution to the Schrödinger equation is somewhat rigorous and is described in detail in numerous sources.¹⁻³ However, the practical consequence of the use of the perturbation theory is a calculated value of electronic energy which is typically significantly more accurate than standard HF theory. Jensen² estimates that 2nd order Møller-Plesset Perturbation Theory (MP2) typically yields a correction to HF theory which accounts for 80-90% of electron correlation energy, that 3rd order Møller-Plesset Perturbation Theory (MP3) typically captures 90-95% of correlation energy, and that 4th order Møller-Plesset Perturbation Theory (MP4) typically accounts for 95-98% of correlation energy. All of these corrections, however, come at the cost of significantly increased computational expense.

1.1.3 Density Functional Theory Methods

Density functional theory methods are based on the work of Hohenberg and Kohn¹⁸, which showed that the ground state electronic energy of a molecular system can be determined completely by the electron density of that system, and can be described by a unique functional of electron density. A functional is a form that produces a scalar from a function, which in turn is a form that produces a scalar from another set of scalars. The electronic energy can be described as shown in equation [1.12], where the term U_{ext} represents the energy associated with the interaction of the system's electrons and a constant external potential (in other words with the unmoving nuclei) and the functional $F[\rho(r)]$ represents the kinetic energy of the electrons and the energy arising from interelectronic interactions.

$$E[\rho(r)] = \int U_{\text{ext}}(r)\rho(r) dr + F[\rho(r)] \quad [1.12]$$

Based on the subsequent work of Kohn and Sham¹⁹, modern density functional theory methods partition the total energy of the molecular system into three terms, as shown in equation [1.13]. The first term (E_{KE}) describes the kinetic energy of the system's electrons, ignoring any effects of electron – electron interaction, the second term of the system (E_{H}) describes the columbic or Hartree electrostatic energy of the electrons in the system, which ignores the correlation of motion of the electrons, and the third term (E_{XC}) which contains the energetic contributions of spin exchange, electron correlation, and the difference between the true kinetic energy of the system and the kinetic energy approximated by E_{KE} .

$$F[\rho(r)] = E_{KE}[\rho(r)] + E_H[\rho(r)] + E_{XC}[\rho(r)] \quad [1.13]$$

The majority of these terms can be described in a straightforward classical manner. The key to the accuracy of this approach is the definition of the exchange-correlation term (E_{XC}). The choice of the functional form of E_{XC} is what separates and defines the various DFT methods that are currently used to calculate electronic structure. Traditionally, the exchange-correlation term has been considered as a combination of two separate terms, one related purely to the exchange energy (E_X), and one related to the correlation energy (E_C), as shown in equation [1.14].

$$E_{XC}[\rho] = E_X[\rho] + E_C[\rho] = \int \rho(r) \varepsilon_X[\rho(r)] dr + \int \rho(r) \varepsilon_C[\rho(r)] dr \quad [1.14]$$

The simplest starting point for defining the exchange and correlation functional is the extensively used Local Density Approximation (LDA). LDA assumes that the local density of a system can be treated as a uniform electron gas. Based on this approximation the exchange energy can be defined by the Dirac formula²⁰ as shown in equation [1.15].

$$E_X^{LDA}[\rho] = -C_x \int \rho^{4/3}(r) dr \quad [1.15]$$

The LDA based correlation energy, however, cannot be described in the same straight forward analytical form as the exchange energy. Several parameterized formulas, such as VWN²¹ and PW²², have been constructed based on the results of highly precise quantum Monte Carlo simulations.²³

In many cases, DFT calculations based on the local density approximation perform quite well, particularly for the organometallic species that are the focus of this investigation.²⁴ However, LDA has been shown to be inadequate for some problems.²⁴⁻²⁶ To overcome these limitations, a method must be used which considers the non-uniformity of the system's electron density. A first step toward realistic non-uniformity is to consider not only electron density, but also the derivatives of electron density. A class of DFT methods known as Generalized Gradient Approximation (GGA) methods includes the first derivative of electron density as a variable. An early and common example of GGA functional is the Becke's B88 exchange functional.²⁷ This method involves the addition of a parameterized correction factor to the standard LDA based exchange functional, resulting in a two orders of magnitude reduction in error in the exchange energy relative to the LDA method.²⁸ This concept of incorporation of first derivatives of electron density also been employed to develop gradient corrected correlation functional. The most common of which is likely the Lee, Yang and Parr (LYP) functional which is based on parameters obtained from the fitting data for the helium atom.²⁹

In addition to the traditional DFT methods described above, which calculate E_{XC} by pairing an exchange functional with a correlation functional, newer hybrid functional exist which improve accuracy by containing at least some proportion of exact exchange energy as determined by Hartree-Fock theory.^{30, 31} The most popular is the Becke three parameter functional (B3) including the semiempirical combination of exact exchange, the local spin density approximation and gradient correction,^{30, 32} which is often combined with the LYP gradient corrected correlation functional to yield the functional

form shown in equation [1.16], where a, b, and c are parameters determined by least squares fitting to experimental data.

$$E_{XC}^{B3LYP} = (1 - a)E_X^{LDA} + aE_X^{exact} + b\Delta E_X^{B88} + (1 - c)E_C^{VWM} + cE_C^{LYP} \quad [1.16]$$

The B3LYP functional is used exclusively in this thesis for all density functional calculations.

1.1.4 Self-Consistent Reaction Field Methods

Thus far, this description of electronic structure calculations has only considered interactions of the atoms in the system with each other. At times it is useful to consider also how the atoms in the system interact with each other and with the environment, e.g. solvent, in which the system exists. This interaction with between the system and solvent can be approached in three ways. First, solvent molecules could be explicitly added to the system and evaluated as part of the system. Alternatively, a much less computational expensive approach would be to approximate solvent as a continuous medium.³³ Finally, a hybrid approach could be used in which some solvent molecules are explicitly added to the system in addition to the addition of a continuous medium.

Continuum models consider the solvent to be a uniform continuum with a given dielectric constant. This continuum is then considered to have an appropriately sized and shaped cavity in which the solute exists.³⁴ The various models that are commonly used differ in how the size and shape of the cavity are defined, how the charge distribution of the solute is represented, how the cavity/dispersion contributions are calculated and how

the dielectric medium is described. When the solute is described quantum mechanically, as is the case with the electronic structure calculations described here, the interaction with the solvent model must be calculated by an iterative process. Models that use an iterative calculation process are known as self-consistent reaction field models.²

The self-consistent reaction field model used in this dissertation is the PCM model. The PCM model employs a van der Waals cavity formed by combining atomic van der Waals radii scaled by an empirical factor. The PCM model parameterizes the cavity/dispersion contributions based on the surface area of the cavity.³⁵

1.2 Nitrile Anions Background

Nitrile anions were selected as the main topic of this dissertation due to their unique reactivity,³⁶⁻⁴⁰ their usefulness in the synthesis of biologically relevant molecules,^{37-39, 41-49} and the ambiguity surrounding the structure in solution.⁵⁰⁻⁵⁹ As shown in Figure 1.2, nitrile anions can exhibit two resonance structures which imply two different hybridizations around the α -carbon.

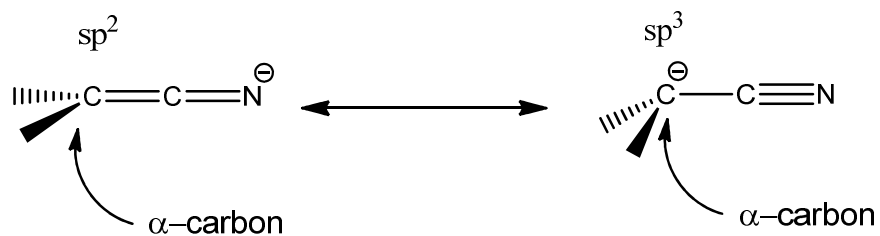


Figure 1.2. Resonance structures for acetonitrile anion

1.2.1 Nitrile Anion Reactivity

The interesting reactivity of metalated nitrile anions is due to several key structural and electrostatic features of these molecules. First and foremost is their powerful nucleophilicity^{36, 43} stemming from the powerful inductive stabilization^{60, 61} of negative charge density within the functional group. A second key feature of nitrile anions is their excellent hydrogen bond acceptor properties.⁶² The compact size of nitrile anion groups are another key feature in their reactivity. This small size has been shown through x-ray analysis,⁵⁰ with the carbon-nitrogen bond of a crystal with the structure shown in Figure 1.3 having a length of 1.17 Å and the carbon- α -carbon bond having a length of 1.38 Å. In addition to compact bond lengths of nitrile anions, they also exhibit one of the smallest (3.6 Å) diameter π -systems known.⁶³

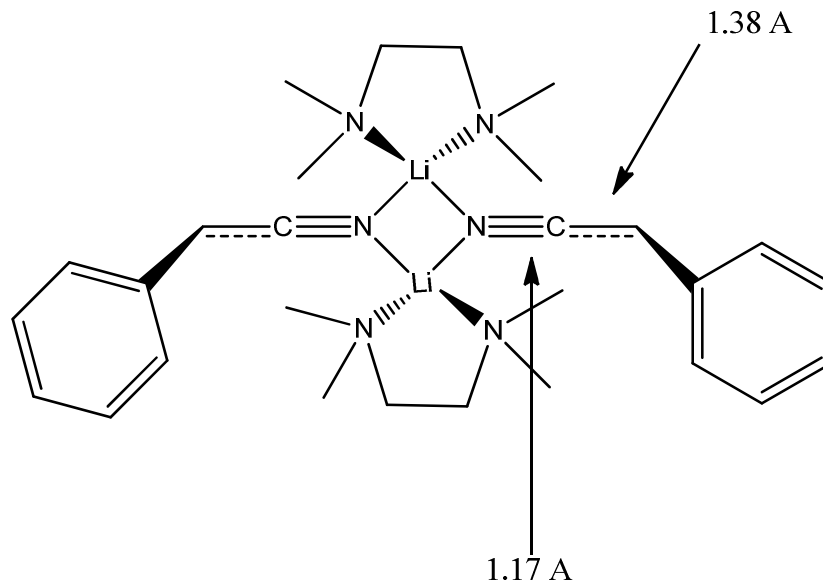


Figure 1.3. Representative nitrile anion bond lengths⁵⁰

A final, and extremely important feature of nitrile anion reactivity, is their highly unusual ability stabilize adjacent radicals,^{64, 65} cations,^{66, 67} and anions,³⁶ which is likely to explain their unique chemo-, regio-, and stereo-selectivity.³⁸

1.2.2 Nitrile Anion Utility

The reactivity of nitrile anions, discussed in the previous section, makes them extremely useful functional groups for synthetic chemists to employ in the design of reaction schemes requiring these features of nitrile anions to drive specific unique effects, such as the chemo-, regio-, or stereo-selectivity mentioned previously.

For instance, the reaction shown in Figure 1.4 results in a product that has a 99.9% retention of the (-)- stereochemistry of the starting material.⁴⁰ If this reaction proceeds through the expected sp^2 hybridized transition state, there would be no retention of stereochemistry. The fact that the stereochemistry of the starting material is conserved suggests that there is at least some sp^3 character the transition state. Interestingly, this behavior is only seen when sodium is used as the cation. Understanding the role that the nitrile anion's counterion is contributing to this unusual hybridization is of particular interest.

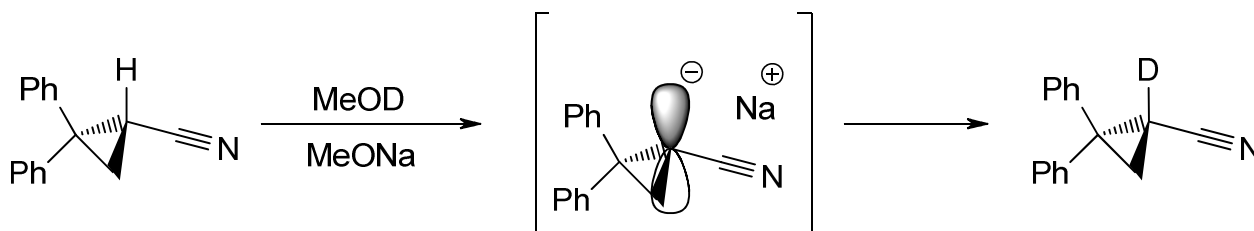


Figure 1.4. Unexpected retention of stereochemistry

Examples can be found which also show that the nature of the solvation of a metalated nitrile anion is a key determinant of the structure of the complex and its resultant reactivity. One example of this behavior is shown in Figure 1.5. The investigators who conducted this research contend that this strong dependence on solvent polarity is attributable to the geometry of the transition state.⁶⁸ In the case of the cis-decalin product it is believed that the transition state is “planar” or has a linear angle between the nitrogen of the nitrile group and the α -carbon. As the polarity of the reaction medium increases the deviation from the linear angle or pyramidalization of the carbon increases resulting in a stronger preference for the trans-decalin product. This increase in pyramidalization of the α -carbon is conceptually similar to the increase in the sp^3 character of the α -carbon in the substitution reaction described above.

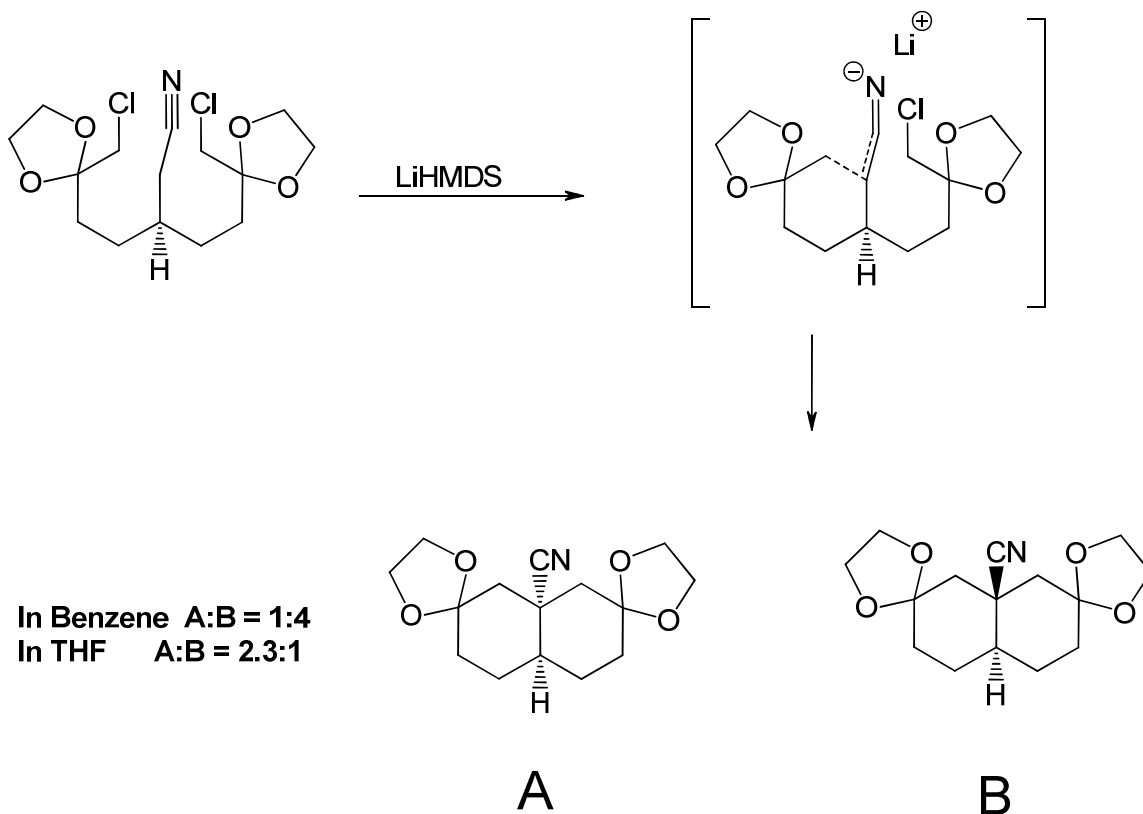


Figure 1.5. Effects of solvent on stereochemistry of an annulation product⁶⁸

The reaction in Figure 1.5 is of particular interest due to the nature of the cis- and trans- decalin reaction products. Nitrile anions are receiving considerable attention for their usefulness in driving the stereoselectivity of cis-³⁹ and trans-⁴⁹ decalins. These molecules are part of the frameworks of numerous biologically important natural products such as terpenoids and steroids, where the stereochemistry of the molecule determines its biological activity. The ability of nitrile anions to tune the stereochemistry offers significant advantage in the quest of simple synthetic routes to enantiomerically pure natural products.

1.2.3 Nitrile Anion Structure

The crystallographic,⁵⁰ spectroscopic,^{51, 52, 54-59, 69-73} and computational^{53-55, 58} study of the structure of nitrile anions has seen significant recent activity. Two fundamental questions at the core of these investigations are, where is the cation associated with the nitrile anion (the nitrogen or the α -carbon) and whether the complexes exist in solution as aggregates of monomers.

As shown in Figure 1.3, early x-ray analysis led to the conventional view that the metal cations in nitrile anion complexes are associated at the nitrogen atom, and that the complexes exist as dimers. Subsequent spectroscopic and computational investigation in Li-nitrile anion systems, however, showed results which supported this view in some cases,⁵¹⁻⁵³ but other reports supported the existence of α -carbon metalated or mixed nitrogen and α -carbon metalated aggregates.^{57, 59} Figure 1.6 shows three constitutional isomers of a lithiated nitrile anion complex with both nitrogen and α -carbon contact points which have been shown to exist in a fast intermolecular exchange equilibrium in

solutions of diethyl ether and also of tetrahydrofuran. In general, however, lithiated nitrile anions seem to have an inherent preference for nitrogen metalation, and the majority of experimental and computation results reflect this preference.

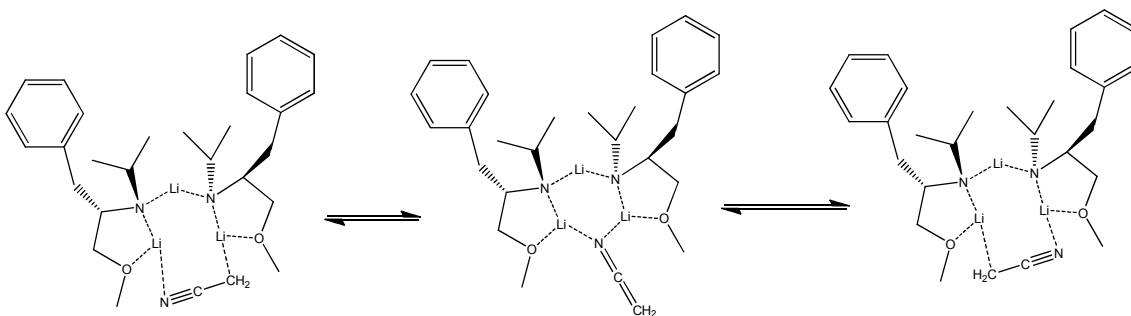


Figure 1.6. Three nitrile anion complexes⁵⁹

Outside of lithium, other cations do not seem to share this preference. Transition metals have been shown to exhibit equal preference for α -carbon or nitrogen metalation,⁶⁹⁻⁷¹ and magnesium complexes seem to have an exclusive preference for α -carbon or nitrogen metalation.^{72, 73} These types of counterions also do not show a preference for dimerization and have been shown to exist monomerically in solution.⁶⁹⁻⁷³

1.3 Objectives of this Dissertation

The fundamental hypothesis of this dissertation is the assertion that the structure and resultant reactivity of nitrile anions is strongly influenced by the nature of the cation that acts as counterion and the nature of the solvent in which the complex exists. This hypothesis was explored exclusively through the use of electronic structure calculations.

The dissertation is divided into three specific projects ultimately supporting the investigation of the fundamental hypothesis. The first of these projects is described in Chapter 2 and is based on the study of various cation – solvent complexes using several

different electronic structure calculation methods. The aim of this project is to determine the most effective method for study these types of systems by comparing the calculated theoretical results with known experimental results. The second project, which is described in Chapter 3, was an extension of the work in Chapter 2 in which acetonitrile anions are added to the cation – solvent complexes. The aim of this project is to better understand the direct effect of cation and solvent on the structure of acetonitrile anion. The final project, which is described in Chapter 4, is investigation into the relative energies of several different reaction coordinates for a simple nucleophilic substitution reaction involving a nitrile anion containing cycloaliphatic molecule. The aim of this project was to determine if calculated differences in the electronic energies of the various reactants and transition structures could be used to predict the structure of the reaction product.

1.4 References

1. Cramer, C. J., *Essentials of Computational Chemistry*. Second ed.; John Wiley & Sons, Ltd: West Sussex, England, 2004; p 596.
2. Jensen, F., *Introduction to Computational Chemistry*. Second ed.; John Wiley & Sons, Ltd: West Sussex, England, 2007; p 599.
3. Leach, A. R., *Molecular Modeling Principles and Applications*. Pearson Education Limited: Essex, England, 2001; p 744.
4. Born, M.; Oppenheimer, R., Zur Quantentheorie der Molekeln. *Annalen der Physik* **1927**, 389, (20), 457-484.

5. Born, M., Zur Quantenmechanik der Stoßvorgänge. *Zeitschrift für Physik A Hadrons and Nuclei* **1926**, 37, (12), 863-867.
6. Born, M., Quantenmechanik der Stoßvorgänge. *Zeitschrift für Physik A Hadrons and Nuclei* **1926**, 38, (11), 803-827.
7. Fock, V. A., Näherungsmethode zur Lösung des quantenmechanischen Mehrkörperproblems. *Zeitschrift für Physik* **1930**, 61, 126-148.
8. Hartree, D. R., The Wave Mechanics of an Atom with a Non-Coulomb Central Field. Part I. Theory and Methods. *Proceedings of the Cambridge Philosophical Society* **1927**, 24, 89-110.
9. Hartree, D. R., The Wave Mechanics of an Atom with a Non-Coulomb Central Field. Part II. Some Results and Discussion. *Proceedings of the Cambridge Philosophical Society* **1927**, 24, 111-132.
10. Hartree, D. R., The Wave Mechanics of an Atom with a non-Coulomb Central Field. Part III. Term Values and Intensities in Series in Optical Spectra. *Proceedings of the Cambridge Philosophical Society* **1928**, 24, 426-437.
11. Hartree, D. R., The Distribution of Charge and Current in an Atom consisting of many Electrons obeying Dirac's equations. *Proceedings of the Cambridge Philosophical Society* **1929**, 25, 225-236.
12. Hartree, D. R., The Wave Mechanics of an Atom with a Non-Coulomb Central Field. Part IV. Further Results relating to Terms of the Optical Spectrum. *Proceedings of the Cambridge Philosophical Society* **1929**, 25, 310-314.

13. Krishnan, R.; Frisch, M. J.; Pople, J. A., Contribution of triple substitutions to the electron correlation energy in fourth order perturbation theory. *Journal of Chemical Physics* **1980**, 72, 4244-4245.
14. Krishnan, R.; Pople, J. A., Approximate fourth-order perturbation theory of the electron correlation energy. *Journal of Quantum Chemistry* **1978**, 14, 91-100.
15. Moller, C.; Plesset, M. S., Note on an Approximation Treatment for Many-Electron Systems. *Physical Review* **1934**, 46, 618-622.
16. Schrödinger, E., Quantisierung als Eigenwertproblem. *Annalen der Physik* **1926**, 385, (13), 437-490.
17. Tobocman, W., Many-Body Perturbation Theory. *Physical Review* **1957**, 107, (1), 203.
18. Hohenberg, P.; Kohn, W., Inhomogeneous Electron Gas. *Physical Review* **1964**, 136, (3B), B864.
19. Kohn, W.; Sham, L. J., Self-Consistent Equations Including Exchange and Correlation Effects. *Physical Review* **1965**, 140, (4A), A1133.
20. Dirac, P. A. M., Note on Exchange Phenomena in the Thomas Atom. *Mathematical Proceedings of the Cambridge Philosophical Society* **1930**, 26, (03), 376-385.
21. Vosko, S. J.; Wilk, L.; Nusair, M., Accurate spin-dependent electron liquid correlation energies for local spin density calculations: a critical analysis. *Canadian Journal of Physics* **1980**, 58, 1200-1211.
22. Perdew, J. P.; Wang, Y., Accurate and simple analytic representation of the electron-gas correlation energy. *Physical Review B* **1992**, 45, (23), 13244.

23. Ceperley, D. M.; Alder, B. J., Ground State of the Electron Gas by a Stochastic Method. *Physical Review Letters* **1980**, 45, (7), 566.
24. Head-Gordon, M., Quantum Chemistry and Molecular Processes. *The Journal of Physical Chemistry* **1996**, 100, (31), 13213-13225.
25. Becke, A. D., Completely numerical calculations on diatomic molecules in the local-density approximation. *Physical Review A* **1986**, 33, (4), 2786.
26. Johnson, B. G.; Gill, P. M. W.; Pople, J. A., The performance of a family of density functional methods. *The Journal of Chemical Physics* **1993**, 98, (7), 5612-5626.
27. Becke, A. D., Density-functional exchange-energy approximation with correct asymptotic behavior. *Physical Review A* **1988**, 38, (6), 3098.
28. Ortiz, G.; Ballone, P., Pseudopotentials for non-local-density functionals. *Physical Review B* **1991**, 43, (8), 6376.
29. Lee, C.; Yang, W.; Parr, R. G., Development of the Colle-Salvetti correlation-energy formula into a functional of the electron density. *Physical Review B* **1988**, 37, (2), 785-789.
30. Becke, A. D., Density-functional thermochemistry. III. The role of exact exchange. *Journal of Chemical Physics* **1993**, 98, (7), 5648-5662.
31. Becke, A. D., Density-functional thermochemistry. IV. A new dynamical correlation functional and implications for exact-exchange mixing. *The Journal of Chemical Physics* **1996**, 104, (3), 1040-1046.
32. Stephens, P. J.; Devlin, F. J.; Chabalowski, C. F.; Frisch, M. J., Ab Initio Calculation of Vibrational Absorption and Circular Dichroism Spectra Using Density Functional Force Fields. *The Journal of Physical Chemistry* **1994**, 98, (45), 11623-11627.

33. Cramer, C. J.; Truhlar, D. G., Implicit Solvation Models: Equilibria, Structure, Spectra, and Dynamics. *Chemical Reviews* **1999**, 99, (8), 2161-2200.
34. Tomasi, J.; Persico, M., Molecular Interactions in Solution: An Overview of Methods Based on Continuous Distributions of the Solvent. *Chemical Reviews* **1994**, 94, (7), 2027-2094.
35. Cossi, M.; Barone, V.; Cammi, R.; Tomasi, J., Ab initio study of solvated molecules: a new implementation of the polarizable continuum model. *Chemical Physics Letters* **1996**, 255, (4-6), 327-335.
36. Arseniyadis, S.; Kyler, K. S.; Watt, D. S., *Organic Reactions* **1984**, 31, 1-364.
37. Fleming, F. F.; Wei, Y.; Liu, W.; Zhang, Z., Metalated nitriles: stereodivergent cation-controlled cyclizations. *Tetrahedron* **2008**, 64, (32), 7477-7488.
38. Fleming, F. F.; Zhang, Z., Cyclic nitriles: tactical advantages in synthesis. *Tetrahedron* **2005**, 61, (4), 747-789.
39. Singh, V.; Iyer, S. R.; Pal, S., Recent approaches towards synthesis of *cis*-decalins. *Tetrahedron* **2005**, 61, 9197-9231.
40. Walborsky, H. M.; Motes, J. M., Cyclopropanes. XXV. Cyclopropyl anion. *Journal of the American Chemical Society* **1970**, 92, (8), 2445-2450.
41. Fleming, F. F.; Gudipati, S.; Zhang, Z.; Liu, W.; Steward, O. W., Cyclic Nitriles: Diastereoselective Alkylations. *The Journal of Organic Chemistry* **2005**, 70, (10), 3845-3849.
42. Fleming, F. F.; Liu, W.; Ghosh, S.; Steward, O. W., Metalated Nitriles: Internal 1,2-Asymmetric Induction. *The Journal of Organic Chemistry* **2008**, 73, (7), 2803-2810.

43. Fleming, F. F.; Shook, B. C., Nitrile anion cyclizations. *Tetrahedron* **2002**, 58, (1), 1-23.
44. Fleming, F. F.; Shook, B. C.; Jiang, T.; Steward, O. W., β -Siloxy Unsaturated Nitriles: Stereoselective Cyclizations to cis- and trans-Decalins. *Organic Letters* **1999**, 1, (10), 1547-1550.
45. Fleming, F. F.; Wei, G.; Zhang, Z.; Steward, O. W., Cyclic Oxonitriles: Stereodivergent Grignard Addition[^] Alkylations. *The Journal of Organic Chemistry* **2007**, 72, (14), 5270-5275.
46. Fleming, F. F.; Wei, Y.; Liu, W.; Zhang, Z., Metalated Nitriles: Cation-Controlled Cyclizations. *Organic Letters* **2007**, 9, (14), 2733-2736.
47. Fleming, F. F.; Zhang, Z.; Liu, W.; Knochel, P., Metalated Nitriles: Organolithium, -magnesium, and -copper Exchange of β -Halonitriles. *The Journal of Organic Chemistry* **2005**, 70, (6), 2200-2205.
48. Fleming, F. F.; Zhang, Z.; Wei, G.; Steward, O. W., C-Metalated Nitriles: α -Electrophile-Dependent Alkylations and Acylations. *The Journal of Organic Chemistry* **2006**, 71, (4), 1430-1435.
49. Varner, M. A.; Grossman, R. B., Annulation routes to trans-decalins. *Tetrahedron* **1999**, 55, (49), 13867-13886.
50. Boche, G., The Structure of Lithium Compounds of Sulfones, Sulfoximides, Sulfoxides, Thioethers and 1,3-Dithianes, Nitriles, Nitro Compounds and Hydrazones. *Angewandte Chemie International Edition in English* **1989**, 28, (3), 277-297.

51. Carlier, P. R.; Lo, C. W.-S., $7\text{Li}/31\text{P}$ NMR Studies of Lithiated Arylacetonitriles in THF-HMPA Solution: Characterization of HMPA-Solvated Monomers, Dimers, and Separated Ion Pairs. *Journal of The American Chemical Society* **2000**, 122, 12819-12823.
52. Carlier, P. R.; Lucht, B. L.; Collum, D. B., 6Li PN NMR-Based Solution Structural Determination of EtzO⁻ and TMEDA-Solvated Lithiophenylacetonitrile and a LiHMDS Mixed Aggregate. *Journal of The American Chemical Society* **1994**, 116, 11602-11603.
53. Carlier, P. R.; Madura, J. D., Effective Computational Modeling of Constitutional Isomerism and Aggregation States of Explicit Solvates of Lithiated Phenylacetonitrile. *The Journal of Organic Chemistry* **2002**, 67, 3832-3840.
54. Kaneti, J.; Schleyer, P. v. R.; Clark, T.; Kos, A. J.; Spitznagel, G. W.; Andrade, J. G.; Moffat, J. B., The structures and energies of the lithium, sodium, and magnesium derivatives of the anions CH_2CN^- and CH_2NC^- . Solvation and aggregation of the lithium species. *Journal of the American Chemical Society* **1986**, 108, (7), 1481-1492.
55. Kudo, H.; Hashimoto, M.; Yokoyama, K.; Wu, C. H.; Dorigo, A. E.; Bickelhaupt, F. M.; von Schleyer, P., Structure and Stability of the Li_2CN Molecule. An Experimental and ab Initio Study. *The Journal of Physical Chemistry* **1995**, 99, (17), 6477-6482.
56. Moran, S.; Ellis, H. B.; DeFrees, D. J.; McLean, A. D.; Ellison, G. B., Carbanion spectroscopy: cyanomethide anion (CH_2CN^-). *Journal of the American Chemical Society* **1987**, 109, (20), 5996-6003.
57. Sott, R.; Granander, J.; Hilmersson, G., Mixed Complexes Formed by Lithioacetonitrile and Chiral Lithium Amides: Observation of $6\text{Li}, 15\text{N}$ and $6\text{Li}, 13\text{C}$

Couplings Due to Both C^α-Li and N^α-Li Contacts. *Journal of the American Chemical Society* **2004**, 126, (21), 6798-6805.

58. Strzalko, T.; Seyden-Penne, J.; Wartski, L.; Corset, J.; Castella-Ventura, M.; Froment, F. o., 1,2- vs 1,4-Regioselectivity of Lithiated Phenylacetonitrile toward \hat{I}^{\pm}, \hat{I}^2 -Unsaturated Carbonyl Compounds. 1. Monomer \hat{I}^{\pm} -Dimer Equilibrium of Lithiated Phenylacetonitrile Ion Pairs in Solution and Structure Determination of the Species by Spectroscopic Methods and ab Initio Calculations. Evidence of a Lithium Bridged Monomeric Ion Pair. *The Journal of Organic Chemistry* **1998**, 63, (10), 3287-3294.

59. Sott, R.; Granander, J.; Hilmersson, G., Solvent-Dependent Mixed Complex Formation—NMR Studies and Asymmetric Addition Reactions of Lithioacetonitrile to Benzaldehyde Mediated by Chiral Lithium Amides. *Chemistry – A European Journal* **2002**, 8, (9), 2081-2087.

60. Dayal, S. K.; Ehrenson, S.; Taft, R. W., Substituent effects, electronic transmission, and structural dependence of π delocalization as studied with the p-fluorophenyl tag. *Journal of the American Chemical Society* **1972**, 94, (26), 9113-9122.

61. Richard, J. P.; Williams, G.; Gao, J., Experimental and Computational Determination of the Effect of the Cyano Group on Carbon Acidity in Water. *Journal of the American Chemical Society* **1999**, 121, (4), 715-726.

62. Le Questel, J.-Y.; Berthelot, M.; Laurence, C., Hydrogen-bond acceptor properties of nitriles: a combined crystallographic and ab initio theoretical investigation. *Journal of Physical Organic Chemistry* **2000**, 13, (6), 347-358.

63. Sheppard, W. A., In *The Chemistry of the Cyano Group*, Rappoport, Z., Ed. 1970.

64. Curran, D. P.; Seong, C. M., Radical annulation reactions of allyl iodomalnonitriles. *Tetrahedron* **1992**, 48, (11), 2175-2190.
65. Curran, D. P.; Thoma, G., Additions of malononitrile radicals to alkenes: new examples of 1,2-asymmetric induction in iodine and phenylselenium transfer reactions. *Journal of the American Chemical Society* **1992**, 114, (11), 4436-4437.
66. Creary, X., Electronegatively substituted carbocations. *Chemical Reviews* **1991**, 91, (8), 1625-1678.
67. Takeuchi, K.; Kitagawa, T.; Ohga, Y.; Nakakimura, A.; Munakata, M., Effects of [gamma]-cyano substituent in allylic bridgehead solvolyses: evidence for cyano [pi] conjugation in carbocations. *Tetrahedron* **1997**, 53, (24), 8155-8164.
68. Fleming, F. F.; Shook, B. C., Nitrile Anions: Solvent-Dependent Cyclizations. *The Journal of Organic Chemistry* **2002**, 67, (9), 2885-2888.
69. Kujime, M.; Hikichi, S.; Akita, M., N/O- and C-Bound (Enolato)palladium Complexes with Hydrotris(pyrazolyl)borato Ligands (TpR: R = iPr₂, Me₂) Obtained via Dehydrative Condensation between the Hydroxo Complexes TpRPd(Py)OH and Active Methylene Compounds: Factors Determining the Isomer Distribution and Dimerization of Cyano Compounds. *Organometallics* **2001**, 20, (19), 4049-4060.
70. Naota, T.; Tanna, A.; Murahashi, S.-I., Synthesis and Characterization of C- and N-Bound Isomers of Transition Metal $\hat{\pm}$ -Cyanocarbanions. *Journal of the American Chemical Society* **2000**, 122, (12), 2960-2961.
71. Naota, T.; Tanna, A.; Murahashi, S.-I., Carbon-carbon bond forming reactions of α -bound transition metal [small alpha]-cyanocarbanions: a mechanistic probe for catalytic Michael reactions of nitriles. *Chemical Communications* **2001**, (1), 63-64.

72. Thibonnet, J.; Anh Vu, V.; Bérillon, L.; Knochel, P., Preparation of [alpha]-functionalized alkenylmagnesium reagents via a halide-magnesium exchange.

Tetrahedron **2002**, 58, (24), 4787-4799.

73. Thibonnet, J.; Knochel, P., Preparation of functionalized alkenylmagnesium bromides via a bromine-magnesium exchange. *Tetrahedron Letters* **2000**, 41, (18), 3319-3322.

2 Cation / Solvent Complexes

The first step of this this dissertation investigation is to first understand the nature of cation-ether complexes and to evaluate the accuracy and efficiency of several model chemistries in modeling these complexes. The electronic structure techniques used in this initial investigation were Hartree-Fock (HF), Second-order Møller-Plesset perturbation theory (MP2), the Becke three-parameter exchange functional coupled with the nonlocal correlation functional of Lee, Yang, and Parr (B3LYP). The complexes studied were the tetrahydrofuran (THF) and dimethyl ether (DME) solvation complexes of Li^+ , Na^+ , K^+ , Cu^+ , and MgCl^+ . The values calculated for DME ether complexes were compared with existing experimentally determined data. The B3LYP/6-31+G* model chemistry was found to be the most accurate and efficient method of modeling cation-DME molecular system.

2.1 Introduction

The properties of non-aqueous solutions of metal cations, in particular lithium, have been extensively studied in recent years, due in part to the importance of these solutions in the manufacture of batteries.¹⁻²⁵ Both experimental measurements^{1, 3-13, 15-18, 20-24} and computational techniques^{1, 2, 14, 19, 23, 25, 26} have been used to investigate these systems; however, little of this work has focused on the nature of the solution in the immediate vicinity of the cation. It was the aim of the project described in this chapter to investigate the structure and binding energies of the first solvation sphere of several metal

cations (Li^+ , Na^+ , K^+ , and Cu^+) in solutions of tetrahydrofuran (THF) and dimethyl ether (DME). In addition to the direct interest in this data, the work also provides a systematic foundation for further investigations on the influence of solvated ions in non-aqueous media on the thermodynamics and selectivity of synthetic reactions, particularly those involving nitrile anions. The solvated cations will be studied using electronic structure modeling techniques. A comparison to the explicit solvation of the cations, with the more common, but potentially less accurate continuum approximation of solvation²⁷ will be made. It is of particular interest to determine which computational model chemistry or chemistries provide the best agreement, at the lowest computational cost, with experimental measured results, and establish a protocol which could be used to efficiently build upon this work by exploring larger and more complicated systems.

Ab initio and Density Functional Theory (DFT) calculations are increasingly used to study the properties of molecules, such as organolithium compounds.^{20, 21, 28} It has been shown that for these types of systems, calculated structures and energies agree well with experimental results when the Hartree-Fock (HF) model chemistry²⁹⁻³⁴ is employed, even with a relatively small basis set²⁸. For this reason, HF/6-31⁺G(d) model chemistry, as well as Second-order Møller-Plesset perturbation theory (MP2) with the 6-31⁺G(d) basis set, and the Becke three-parameter exchange functional coupled with the nonlocal correlation functional of Lee, Yang, and Parr (B3LYP) with the 6-31⁺G(d) basis set, have been used to generate the computed results reported in this work.

The first key challenges that must be faced in the determination of the accuracy of a theoretical study of many atom systems, such as these, is the construction of a reliable “test set” of experimental data against which computational models can be compared and

evaluated. A limited amount of structural and binding energy data exists for THF solutions of several metal cations such as $\text{Li}^{+22, 35, 36}$, $\text{Na}^{+22, 37}$, and Cu^{+38} . Recently, several thorough experimental and computational studies of the gas phase binding of dimethyl ether (DME) and various crown ethers to metal cations have been reported^{2, 39-43}. Due to the similarity of DME and THF, these studies offer the opportunity to compare the usefulness of several different theoretical methods and techniques for modeling oxygenated, non-aqueous solvation of metal cations.

2.2 Computational Methods

All geometry optimizations and frequency calculations were performed using Gaussian 03.⁴⁴ The explicit, continuum, and explicit-continuum solvation models^{26, 45} were used to study the structure of DME and THF cation complexes. Geometry optimizations and frequency calculations were performed using either Hartree-Fock (HF), frozen-core, second-order Møller-Plesset perturbation theory⁴⁶⁻⁴⁸ (MP2) or the Becke three-parameter exchange functional⁴⁹ and the nonlocal correlation functional of Lee, Yang, and Parr⁵⁰ (B3LYP). These optimization and frequency calculations were carried out using the 6-31+G(d) basis set. For the sake of comparison, single point energy calculations were performed using a much larger basis set (6-311++G(d,p)). These single point energy calculations were performed on the optimized structure calculated with the corresponding level theory using the smaller basis set. Continuum and explicit-continuum solvation single point energy calculations were carried out using the polarizable continuum model (PCM) which has been previously described in detail^{27, 51}.

A brief description of the method is that the solute is represented by a charge distribution in a cavity which is surrounded by an infinite polarizable dielectric medium. The cavity shape is obtained from the van der Waals radii of the atoms of the solute. The solvents and dielectric constants used in this study are DME ($\epsilon=5.0$), and THF ($\epsilon=7.2$). Again, these single point energy calculations were carried out using the optimized structure calculated at the corresponding level theory with the 6-31+G(d) and no solvent continuum. All optimized geometries were confirmed to be energy minima by vibrational frequency analysis, in which no imaginary vibrational frequencies were observed. All thermodynamic data was calculated at standard temperature and pressure, and all experimental data was measured under the same conditions.

2.3 Results and Discussions

2.3.1 Explicit DME Solvation

Three model chemistries, HF, MP2, and B3LYP, were used to calculate the optimized geometries and thermochemical properties of $(M^+)DME_n$ complexes, where $M^+ = Li^+, Na^+, K^+, \text{ or } Cu^+$, and $n = 1, 2, 3, \text{ or } 4$. This data is summarized in Tables 2.1 and 2.2. From these thermochemical results, sequential bond dissociation energies of DME from $Li^+, Na^+, K^+, \text{ and } Cu^+$ were calculated and compared to experimentally measured values⁴⁰⁻⁴³, in Table 2.3. The sequential bond dissociation of DME from the cation is defined in Figure 2.1.

M ⁺	Theory	M ⁺ (DME) ₁	M ⁺ (DME) ₂		M ⁺ (DME) ₃		M ⁺ (DME) ₄	
		M ⁺ -O Bond Length (Å)	M ⁺ -O Bond Length (Å)	O-M ⁺ -O bond angle (degrees)	M ⁺ -O Bond Length (Å)	O-M ⁺ -O bond angle (degrees)	M ⁺ -O Bond Length (Å)	O-M ⁺ -O bond angle (degrees)
Li	HF	1.814	1.847	179.1	1.901	120.0	1.985	109.5
	MP2	1.789	1.817	179.2	1.844	120.0	1.896	109.5
	B3LYP	1.811	1.838	179.1	1.893	120.0	1.974	110.3
Na	HF	2.206	2.236	179.2	2.271	120.0	2.315	109.5
	MP2	2.180	2.214	180.0	2.250	107.7	2.272	108.7
	B3LYP	2.186	2.218	180.0	2.257	120.0	2.302	109.5
K	HF	2.656	2.696	145.6	2.726	120.0	2.760	109.5
	MP2	2.607	2.637	179.0	2.648	120.0	2.659	105.7
	B3LYP	2.620	2.659	141.0	2.693	120.0	2.725	109.2
Cu	HF	2.029	2.009	179.2	2.143	120.0	2.235	109.5
	MP2	1.891	1.840	178.1	1.998	120.0	2.080	107.7
	B3LYP	1.911	1.894	178.0	2.060	120.0	2.150	108.9

Table 2.1. Calculated values for selected structural features of DME-cation complexes.

M ⁺	Theory	M ⁺ (DME) ₁				M ⁺ (DME) ₂				M ⁺ (DME) ₃				M ⁺ (DME) ₄			
		Zero Point Energy	Electronic Energy	Enthalpy	Free Energy	Zero Point Energy	Electronic Energy	Enthalpy	Free Energy	Zero Point Energy	Electronic Energy	Enthalpy	Free Energy	Zero Point Energy	Electronic Energy	Enthalpy	Free Energy
Li	HF	0.088	-161.274	-161.273	-161.307	0.176	-315.303	-315.302	-315.355	0.265	-469.316	-469.315	-469.379	0.352	-623.314	-623.313	-623.392
	MP2	0.084	-161.741	-161.740	-161.774	0.169	-316.240	-316.239	-316.291	0.252	-470.724	-470.723	-470.789	0.336	-625.200	-625.199	-625.278
	B3LYP	0.083	-162.293	-162.292	-162.326	0.165	-317.292	-317.291	-317.344	0.247	-472.273	-472.272	-472.340	0.329	-627.241	-627.240	-627.320
Na	HF	0.087	-315.678	-315.677	-315.713	0.175	-469.691	-469.690	-469.747	0.262	-623.697	-623.696	-623.767	0.349	-777.697	-777.696	-777.783
	MP2	0.083	-316.144	-316.143	-316.180	0.166	-470.624	-470.623	-470.680	0.249	-625.098	-625.097	-625.168	0.332	-779.570	-779.569	-779.657
	B3LYP	0.082	-317.071	-317.070	-317.106	0.163	-472.054	-472.053	-472.110	0.245	-627.029	-627.028	-627.100	0.326	-781.997	-781.996	-782.085
K	HF	0.087	-752.977	-752.976	-753.013	0.174	-906.978	-906.977	-907.038	0.261	-1060.976	-1060.975	-1061.052	0.348	-1214.971	-1214.970	-1215.069
	MP2	0.083	-753.459	-753.458	-753.019	0.166	-907.927	-907.926	-907.984	0.249	-1062.393	-1062.392	-1062.466	0.332	-1216.859	-1216.858	-1216.947
	B3LYP	0.081	-754.700	-754.699	-754.737	0.163	-909.672	-909.671	-909.730	0.244	-1064.640	-1064.639	-1064.716	0.325	-1219.604	-1219.603	-1219.729
Cu	HF	0.087	-1792.488	-1792.487	-1792.525	0.175	-1946.515	-1946.514	-1946.569	0.262	-2100.516	-2100.515	-2100.587	0.349	-2254.511	-2254.510	-2254.599
	MP2	0.083	-1793.413	-1793.412	-1793.450	0.168	-1947.938	-1947.937	-1947.989	0.251	-2102.408	-2102.408	-2102.473	0.334	-2256.876	-2256.875	-2256.959
	B3LYP	0.082	-1795.042	-1795.041	-1795.079	0.165	-1950.062	-1950.061	-1950.114	0.246	-2105.026	-2105.025	-2105.095	0.327	-2259.987	-2259.986	-2260.071

Table 2.2. Thermochemical values calculated at standard pressure and 298 °K (all values are given in Hartrees).

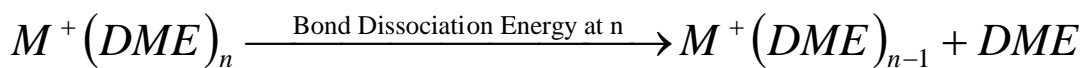


Figure 2.1. Dimethyl ether bond dissociation energy

M ⁺	Theory	M ⁺ (DME) ₁			M ⁺ (DME) ₂			M ⁺ (DME) ₃			M ⁺ (DME) ₄		
		ΔE	ΔH	ΔG	ΔE	ΔH	ΔG	ΔE	ΔH	ΔG	ΔE	ΔH	ΔG
Li	HF	156	156	167	130	133	104	88	91	43	51	53	12
	MP2	167	167	177	154	156	124	113	115	74	92	95	50
	B3LYP	155	155	166	130	133	103	85	87	46	49	51	5
	Experimental		167 ± 10			118 ± 6			87 ± 7			66 ± 10	
Na	HF	103	103	119	90	92	68	70	73	32	53	55	21
	MP2	112	112	128	100	103	80	87	90	47	81	83	51
	B3LYP	105	105	121	89	92	66	68	70	32	50	52	18
	Experimental		93 ± 5			79 ± 5			67 ± 5			58 ± 4	
K	HF	67	67	87	58	60	44	49	52	16	40	43	23
	MP2	78	78	98	69	72	47	66	69	31	67	69	29
	B3LYP	68	68	88	58	60	37	49	51	20	39	42	91
	Experimental		74 ± 4			65 ± 4			53 ± 7			46 ± 8	
Cu	HF	142	142	161	125	128	94	57	60	26	41	44	10
	MP2	214	214	235	222	225	182	77	79	36	69	72	42
	B3LYP	199	199	220	184	186	148	40	43	6	29	32	-4
	Experimental		185 ± 11			193 ± 8			55 ± 4			45 ± 10	

Table 2.3. Bond dissociation energies calculated at standard pressure and 298 °K (all values are given in kJ/mol)

Figures 2.2 – 2.5 show, graphically, the comparison of experimentally measured results with results calculated with the three model chemistries.

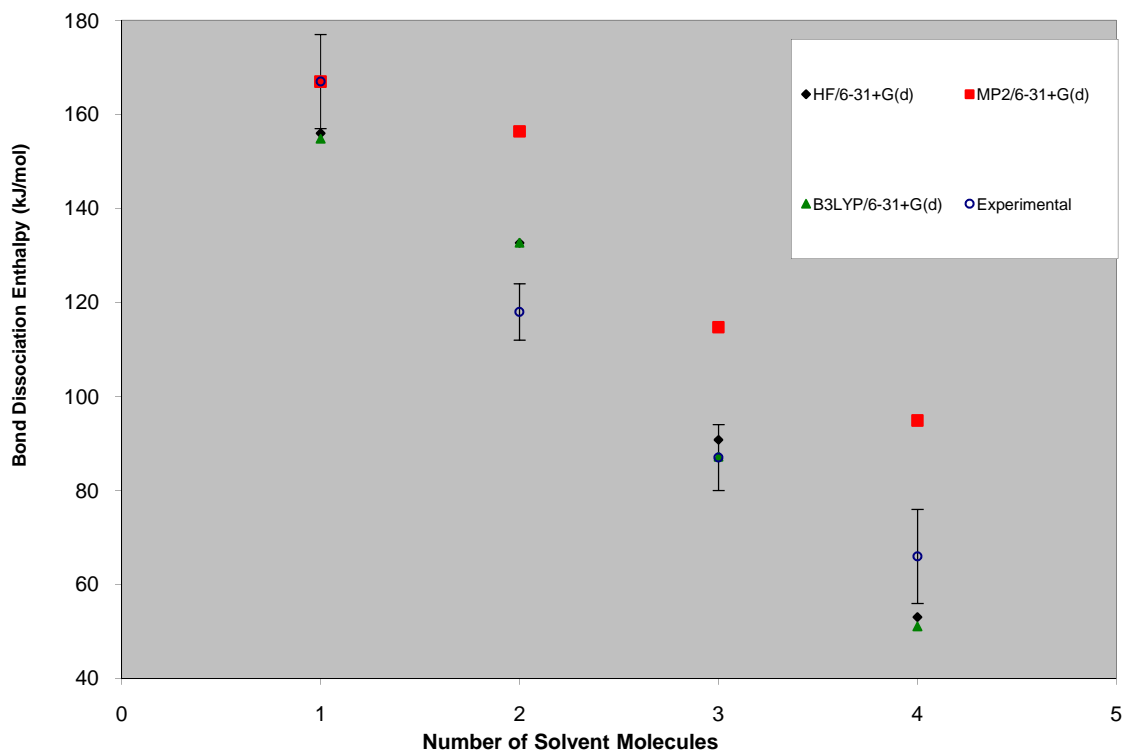


Figure 2.2. Comparison of Li⁺ - DME bond dissociation enthalpies calculated at HF/6-31+G(d),MP2/6-31+G(d), and B3LYP/6-31+G(d) with experimentally measured values.⁴¹

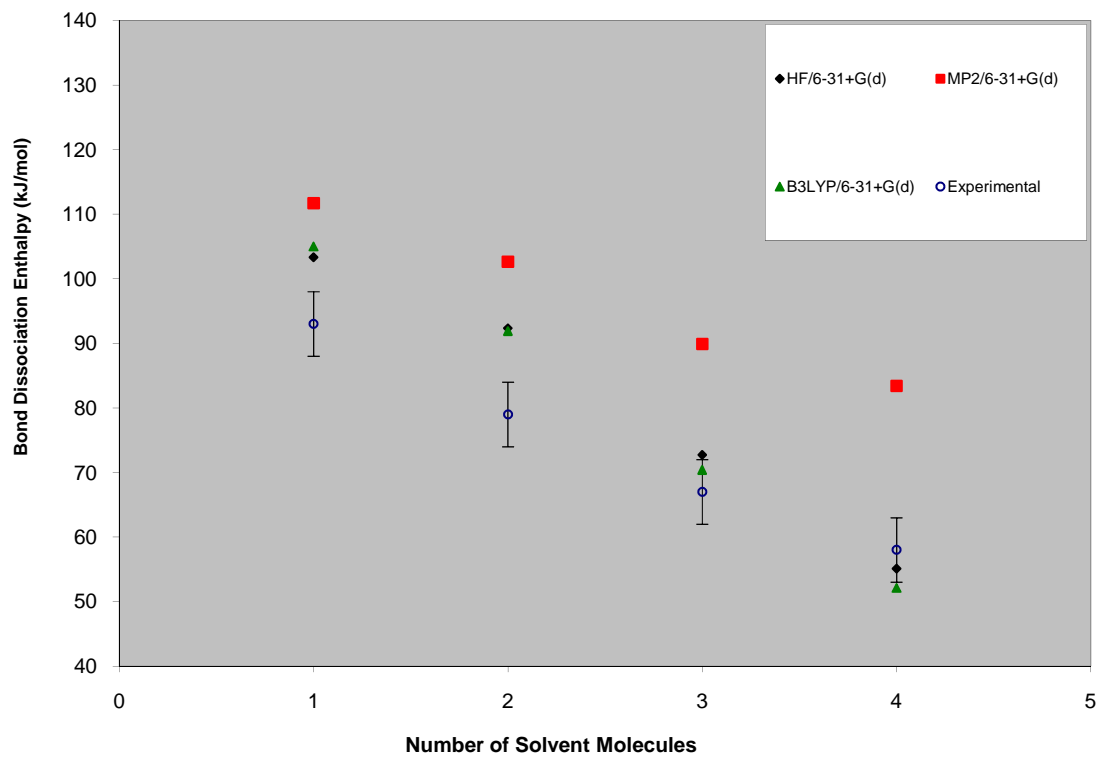


Figure 2.3. Comparison of NA^+ - DME bond dissociation enthalpies calculated at HF/6-31+G(d), MP2/6-31+G(d), and B3LYP/6-31+G(d) with experimentally measured values.⁴²

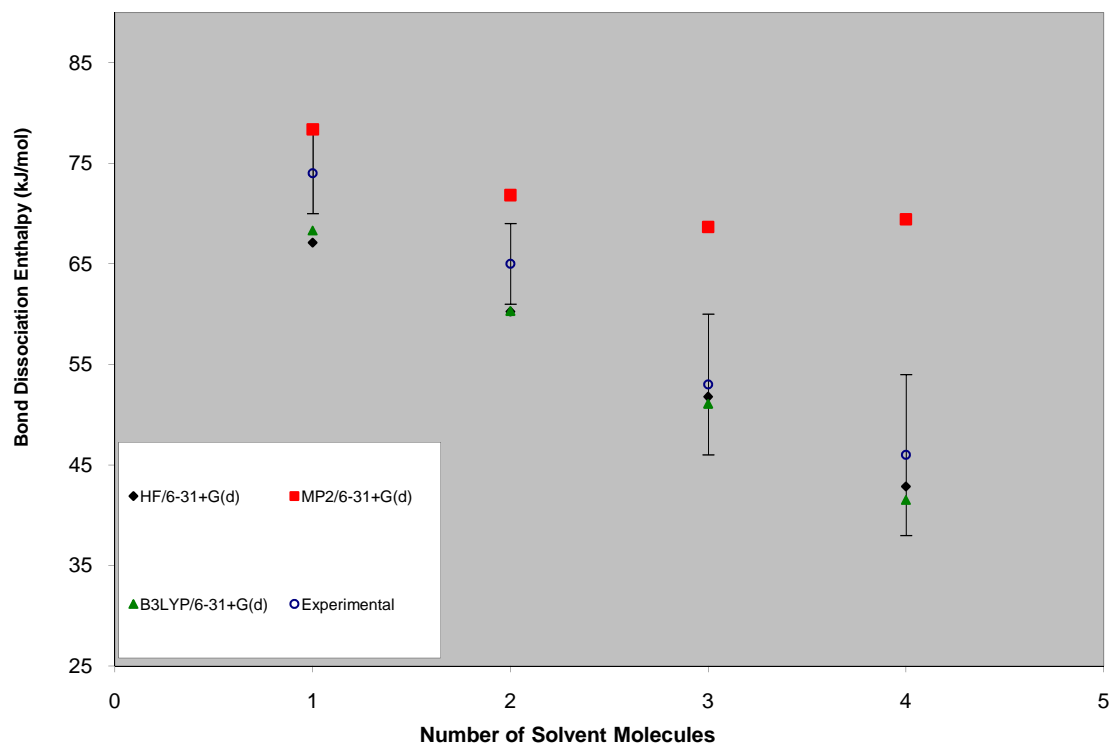


Figure 2.4. Comparison of K^+ - DME bond dissociation enthalpies calculated at HF/6-31+G(d), MP2/6-31+G(d), and B3LYP/6-31+G(d) with experimentally measured values⁴³

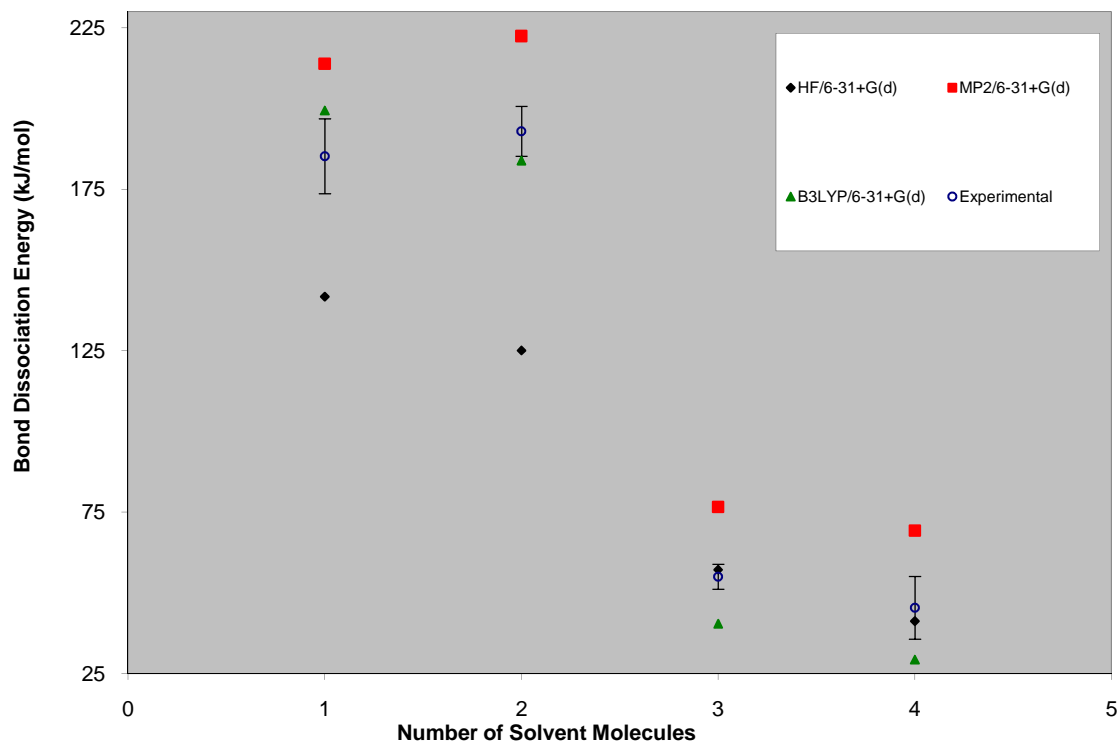


Figure 2.5. Comparison of Cu⁺ - DME bond dissociation energies calculated at HF/6-31+G(d), MP2/6-31+G(d), and B3LYP/6-31+G(d) with experimentally measured values⁴⁰

Comparison of the M⁺ - O distances in Table 2.1 with the bond dissociation energies in Table 2.3 shows the expected relationship between increasing and decreasing dissociation energy. Additionally, inspection of Table 2.3 and Figures 2.2 – 2.5 shows that HF and B3LYP yield similar results which are in good agreement with the experimentally measured values, while the MP2 method consistently overestimates the value of the dissociation energy. This suggests that the influence of electron correlation is significantly exaggerated by the MP2 model chemistry.

Figure 8 shows the unique behavior of the Cu⁺ cation. As opposed to the other three cations, which show a nearly linear decrease in bond dissociation enthalpy as the

number of solvent molecules is increased, Cu^+ shows nearly equal bond dissociation energy for the removal of the 4th (i.e. going from a system containing 4 DME molecules to one containing 3 DME molecules) and 3rd solvent molecules followed by large increase in dissociation energy for the removal of the 2nd solvent molecule which in turn is nearly equal to the energy for the removal of the 1st solvent molecule to form the naked cation. Similar behavior for the dissociation of water molecules from Cu^+ was previously shown by Bauschlicher and co-workers to be a result of 4s-3d σ hybridization.⁵² It is safe to assume that this is also the explanation for why these results were seen with Cu^+ and DME. This behavior is accurately captured by the B3LYP and MP2 model chemistries; however the HF results show a linear decrease in bond dissociation energy, as would be expected if 4s-3d σ hybridization was not present.

In order to determine the limitations of the moderately sized basis set used in these calculations, the energies were corrected for basis set and single point energies were calculated using a larger basis set. Basis set supposition error was corrected using the Boys-Bernardi full counterpoise method⁵³ (CP). Single point energies were calculated using a the 6-311++G(d,p) basis set. These two data sets were then compared to the experimental values shown in Figures 2.2 – 2.5. The root mean squared error, relative to the experimental values, for the three data sets, uncorrected, CP corrected, and larger basis set corrected, are shown in Table 2.4.

	Li ⁺	Na ⁺	K ⁺	Cu ⁺	All Cations
HF / 6-31+G*	11.385	9.027	4.520	40.397	21.584
HF / 6-31+G* (CP Adjusted)	11.445	8.060	5.512	42.795	22.681
HF / 6-311++G**	10.894	8.705	3.682	43.668	22.994
MP2 / 6-31+G*	27.727	22.794	14.662	26.113	23.373
MP2 / 6-31+G* (CP Adjusted)	23.698	17.701	14.733	19.737	19.245
MP2 / 6-311++G**	163.308	163.466	156.751	150.919	158.696
B3LYP / 6-31+G*	12.105	9.452	4.431	13.741	10.539
B3LYP / 6-31+G* (CP Adjusted)	11.408	8.955	5.473	11.662	9.699
B3LYP / 6-311++G**	10.223	13.085	2.624	9.493	9.653

Table 2.4. Root mean squared differences between calculated and experimentally measured bond dissociation enthalpies (bond dissociation energy for Cu+) in kJ/mol

Based on an analysis of the data in Table 2.4 it is clear that the best overall agreement between calculated results and experimental results are obtained from the use of the B3LYP method, with the better accuracy of this model in comparison with the experimental data for Cu⁺ providing the majority of the differentiation between the HF and B3LYP. There is an improvement in the accuracy of the calculations when the CP correction or a larger basis set is used, but these improvements are of limited significance when compared to the difference in accuracy that is obtained by using the B3LYP density functional method.

It is somewhat surprising that the results obtained using the MP2 method are not as accurate as the results obtained using the HF method, due to the inclusion of electron-electron correlation in the MP2 model chemistry. It is possible that MP2 over estimates the contribution of electron-electron correlation leading to the increased inaccuracy observed, and that going to a higher order perturbation theory such as MP3 or MP4 would give more accurate data. However, due to the size of the systems under

investigation higher order Møller-Plesset perturbation theory was considered prohibitively expensive, in terms of computational resources, at this time.

2.3.2 Explicit – Continuum DME Solvation

The free energy of solvation for the four cations (Li^+ , Na^+ , K^+ , and Cu^+) were calculated using the same three model chemistries (HF, MP2, and B3LYP) that were used to calculate the bond dissociation energies of DME. Table 2.5 shows the single point energies of the various cation/solvent systems calculated using the optimized geometries found in the explicit solvation calculations described above and the PCM method for representing solvation as a continuum of a constant dielectric constant⁴⁵. In addition to these calculated values, the values for free energy of solvation as predicted by the Born Equation⁵⁴ are also included in Table 2.5 and Figures 2.6 – 2.9, which are graphical representations of the data for the four cations. Based on the work of Rashin and others⁵⁵,⁵⁶ the covalent radii of the cations were used to solve the Born Equation for free energy of solvation. The results shown in Table 2.5 indicate that as the number of solvent molecules is increased, most of the systems studied showed improved agreement between the calculated values and the theoretical values. In the case of Li^+ , two explicit solvent molecules are required to obtain a calculated result that captures the majority of the theoretical free energy change. For Na^+ , and K^+ , three explicit solvent molecules are required. In the case of Cu^+ , the behavior witnessed is very different from the behavior exhibited by the other cations; the calculated values of ΔG appear to be independent of the number of explicit solvent molecules used in the calculation. These results clearly demonstrate that the properties of the cations in the condensed phase cannot be fully

understood by considering only the continuum solvation of the cation. Explicit solvation or a combination of explicit and continuum solvation are needed to understand the true nature of the solvation of the cations.

M ⁺	Theory	0 DME	1 DME	2 DME	3 DME	4 DME	Theory
Li	HF	-559	-513	-425	-425	-436	-423
	MP2	-558	-507	-411	-427	-418	-423
	B3LYP	-560	-508	-412	-421	-408	-423
Na	HF	-460	-428	-388	-348	-340	-331
	MP2	-456	-417	-377	-349	-319	-331
	B3LYP	-460	-423	-376	-331	-316	-331
K	HF	-361	-338	-320	-284	-284	-256
	MP2	-319	-288	-259	-222	-188	-256
	B3LYP	-362	-333	-302	-264	-313	-256
Cu	HF	-401	-404	-406	-398	-390	-444
	MP2	741	757	789	819	819	-444
	B3LYP	-407	-446	-493	-470	-470	-444

Table 2.5. $\Delta G(\text{solvation})$ calculated with a continuum approximation of solvation and the number of explicit solvent molecules listed. Calculated at standard pressure and 298° K (all values are in kJ/mol)

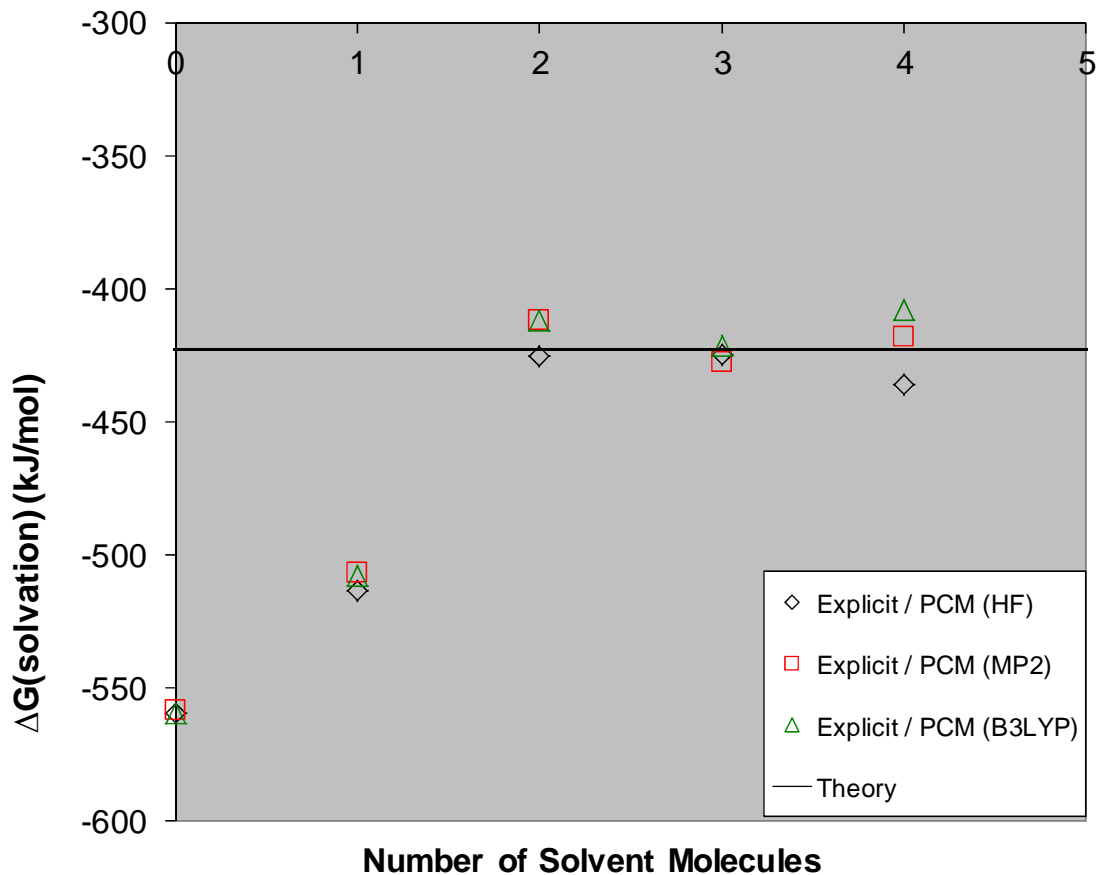


Figure 2.6. Comparison of Li⁺ - DME Gibbs Free Energy of Solvation calculated at HF/6-31+G(d),MP2/6-31+G(d), and B3LYP/6-31+G(d) using continuum solvation approximated by the PCM method and theoretical value calculated using the Born Equation

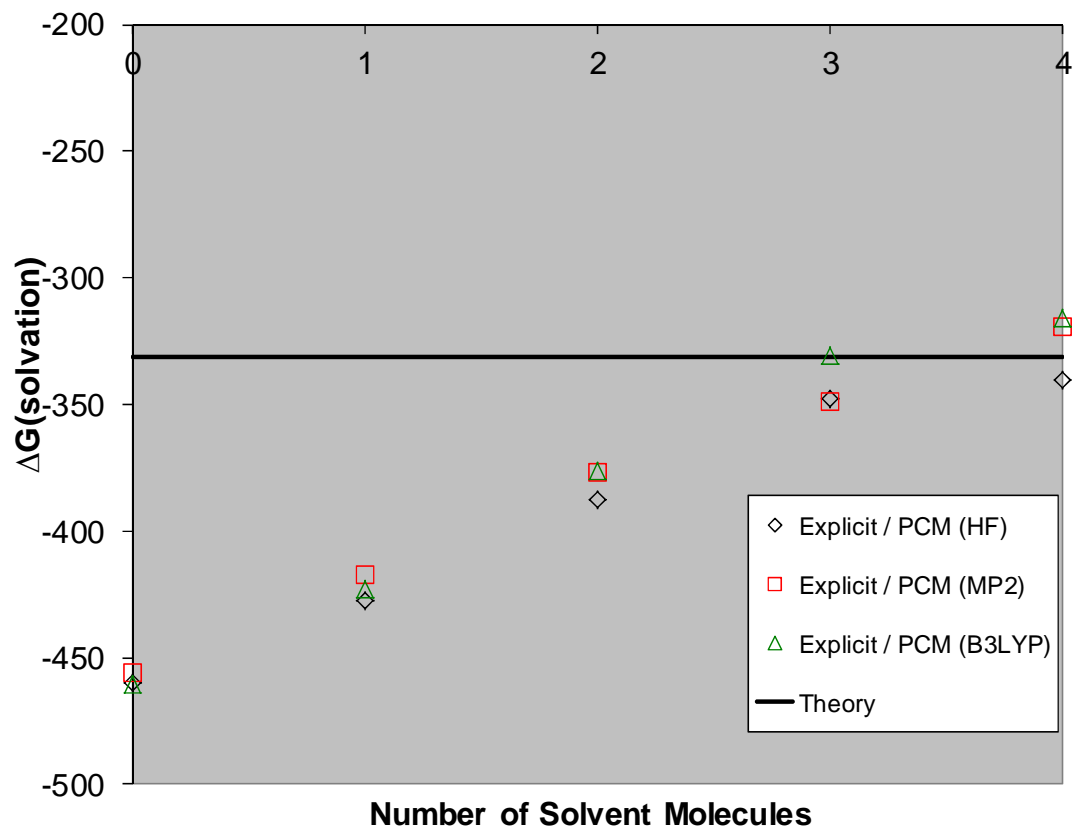


Figure 2.7. Comparison of Na⁺ - DME Gibbs Free Energy of Solvation calculated at HF/6-31+G(d),MP2/6-31+G(d), and B3LYP/6-31+G(d) using continuum solvation approximated by the PCM method and theoretical value calculated using the Born Equation

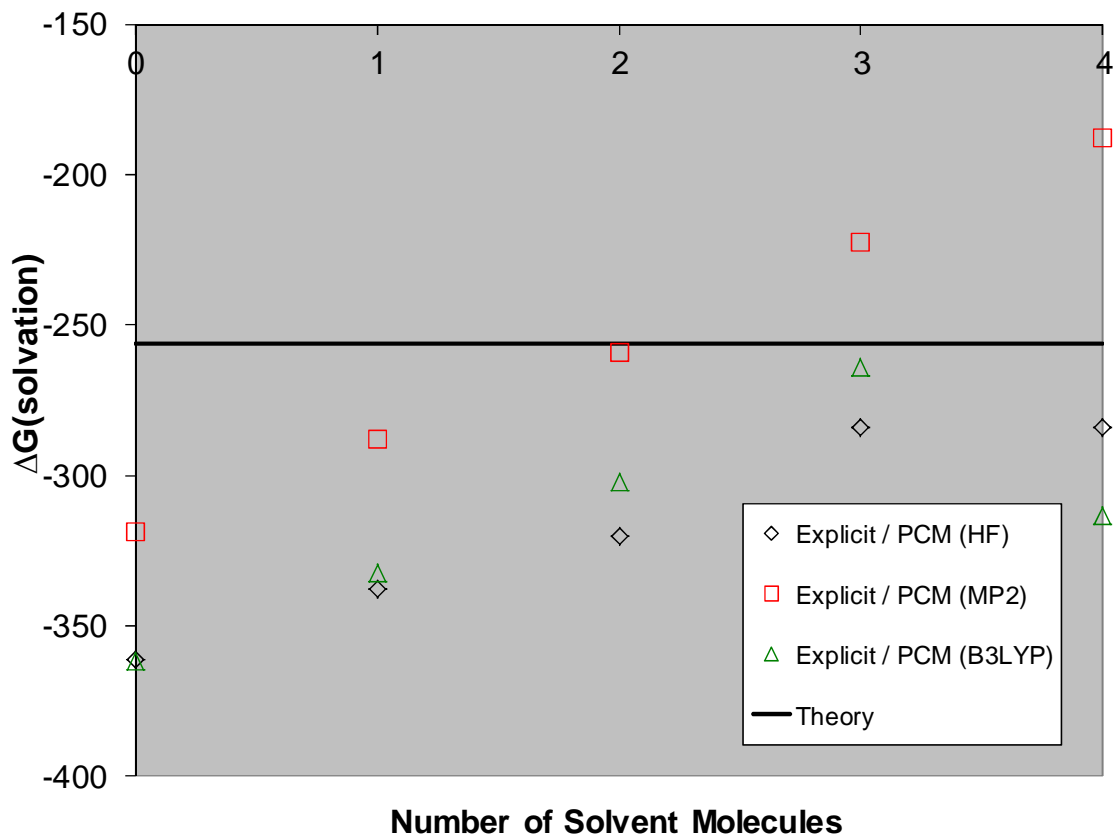


Figure 2.8. Comparison of K^+ - DME Gibbs Free Energy of Solvation calculated at HF/6-31+G(d), MP2/6-31+G(d), and B3LYP/6-31+G(d) using continuum solvation approximated by the PCM method and theoretical value calculated using the Born Equation

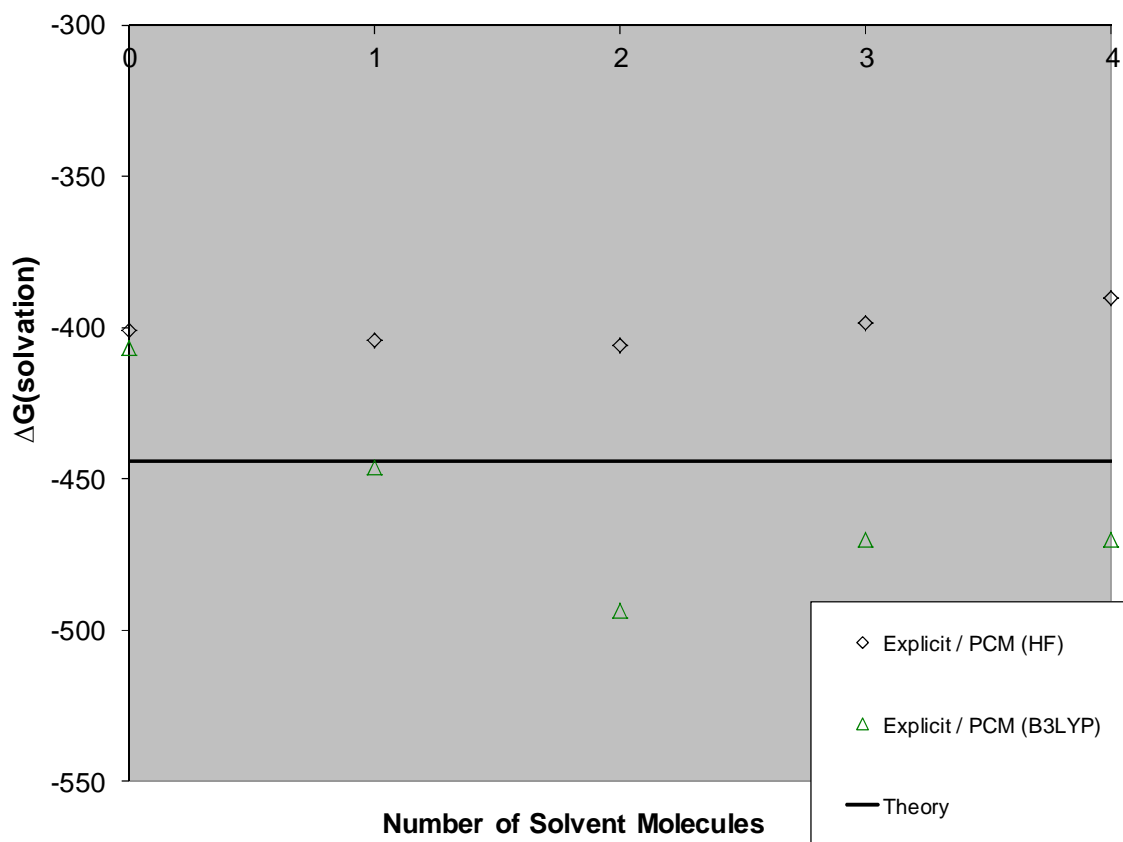


Figure 2.9. Comparison of Cu⁺ - DME Gibbs Free Energy of Solvation calculated at HF/6-31+G(d) and B3LYP/6-31+G(d) using continuum solvation approximated by the PCM method and theoretical value calculated using the Born Equation

Also of interest is the fact that, for Li⁺ and Na⁺, the calculations performed with all three model chemistries are in good agreement with one another. In the case of K⁺, the MP2 numbers are slightly but consistently higher than the values obtained with the other two levels of theory.

2.3.3 Explicit THF Solvation

The three model chemistries (HF, MP2, and B3LYP) used to model DME were also used to model THF. Due to limited amount of experimentally determined data available for the THF / cation systems, these results will be interpreted relative to the results for DME which in turn were evaluated against experimentally determined results.

Calculated structural and thermochemical properties of the optimized geometries of the solvent / cation complexes are reported in Tables 2.6 and 2.7. The definition sequential bond dissociation enthalpy of THF from the cation is analogous to definition for DME and is shown in Figure 2.10. A comparison of the calculated sequential bond dissociation energies of THF from Li^+ , Na^+ , K^+ , Cu^+ , and MgCl^+ is shown for all cations in Table 8 and is shown graphically in Figures 2.11 – 2.15.

M ⁺	Theory	M ⁺ (THF) ₁	M ⁺ (THF) ₂		M ⁺ (THF) ₃		M ⁺ (THF) ₄	
		M ⁺ -O Bond	M ⁺ -O Bond	O-M ⁺ -O	M ⁺ -O Bond	O-M ⁺ -O	M ⁺ -O Bond	O-M ⁺ -O
Li	HF	1.800	1.838	179.9	1.898	120.0	1.977	109.5
	MP2	1.783	1.818	180.0	1.853	120.0	1.886	109.4
	B3LYP	1.798	1.832	179.9	1.891	120.0	1.970	109.5
Na	HF	2.190	2.224	179.9	2.266	120.0	2.314	109.5
	MP2	2.164	2.198	180.0	2.241	120.0	2.263	107.7
	B3LYP	2.172	2.210	179.9	2.255	120.0	2.305	109.5
K	HF	2.634	2.682	158.5	2.718	120.2	2.755	109.8
	MP2	2.589	2.625	179.6	2.644	120.0	2.658	104.5
	B3LYP	2.602	2.652	180.0	2.685	119.9	2.722	109.5
Cu	HF	2.004	1.986	180.0	2.129	120.0	2.224	109.5
	MP2	1.866	1.817	179.9	1.980	120.0	2.064	106.8
	B3LYP	1.892	1.879	180.0	2.040	120.0	2.134	92.8
MgCl	HF	1.929	1.974	116.5	2.022	105.5	2.117	106.8
	MP2	1.943	1.975	114.0	2.004	103.7	2.084	105.0
	B3LYP	1.941	1.982	116.6	2.028	106.1	2.117	106.6

Table 2.6. Calculated values for selected structural features of cation / solvent complexes

M ⁺	Theory	M (TRF) ₁				M (TRF) ₂				M (TRF) ₃				M (TRF) ₄			
		Energy	Energy	Enthalpy	Free Energy	Energy	Energy	Enthalpy	Free Energy	Energy	Energy	Enthalpy	Free Energy	Energy	Energy	Enthalpy	Free Energy
Li	HF	0.128	-238.154	-238.153	-238.190	0.256	-469.060	-469.059	-469.117	0.384	-699.947	-699.946	-700.020	0.511	-930.818	-930.817	-930.908
	MP2	0.122	-238.891	-238.890	-238.927	0.244	-470.538	-470.537	-470.594	0.365	-702.167	-702.166	-702.241	0.486	-933.789	-933.787	-933.879
	B3LYP	0.120	-239.690	-239.689	-239.726	0.239	-472.082	-472.081	-472.138	0.358	-704.453	-704.452	-704.528	0.476	-936.809	-936.808	-936.901
Na	HF	0.127	-392.556	-392.555	-392.594	0.254	-623.446	-623.445	-623.507	0.381	-854.326	-854.325	-854.406	0.508	-1085.198	-1085.197	-1085.297
	MP2	0.121	-393.293	-393.292	-393.332	0.242	-624.919	-624.918	-624.981	0.362	-856.538	-856.537	-856.621	0.483	-1088.156	-1088.155	-1088.252
	B3LYP	0.119	-394.466	-394.465	-394.504	0.237	-626.842	-626.841	-626.902	0.356	-859.207	-859.206	-859.288	0.474	-1091.564	-1091.563	-1091.663
K	HF	0.127	-829.854	-829.853	-829.893	0.253	-1060.730	-1060.729	-1060.796	0.380	-1291.602	-1291.602	-1291.689	0.506	-1522.470	-1522.469	-1522.578
	MP2	0.121	-830.606	-830.605	-830.646	0.241	-1062.219	-1062.218	-1062.284	0.362	-1293.830	-1293.829	-1293.912	0.482	-1525.443	-1525.442	-1525.539
	B3LYP	0.118	-832.094	-832.093	-832.134	0.237	-1064.457	-1064.456	-1064.519	0.355	-1296.815	-1296.814	-1296.899	0.473	-1529.169	-1529.168	-1529.271
Cu	HF	0.127	-1869.369	-1869.368	-1869.408	0.255	-2100.275	-2100.274	-2100.332	0.381	-2331.148	-2331.147	-2331.227	0.508	-2562.015	-2562.014	-2562.113
	MP2	0.121	-1870.567	-1870.566	-1870.606	0.244	-2102.244	-2102.244	-2102.299	0.364	-2333.858	-2333.857	-2333.931	0.483	-2565.470	-2565.469	-2565.561
	B3LYP	0.119	-1872.442	-1872.441	-1872.481	0.239	-2104.857	-2104.856	-2104.913	0.357	-2337.210	-2337.209	-2337.286	0.474	-2569.557	-2569.556	-2569.655
MgCl	HF	0.129	-889.826	-889.825	-889.869	0.257	-1120.751	-1120.751	-1120.812	0.385	-1351.656	-1351.655	-1351.732	0.514	-1582.525	-1582.524	-1582.613
	MP2	0.123	-890.723	-890.722	-890.767	0.245	-1122.389	-1122.388	-1122.451	0.366	-1354.041	-1354.040	-1354.118	0.487	-1585.550	-1585.550	-1585.638
	B3LYP	0.121	-892.480	-892.479	-892.524	0.240	-1124.888	-1124.887	-1124.950	0.360	-1357.276	-1357.275	-1357.352	0.479	-1589.631	-1589.630	-1589.720

Table 2.7. Thermochemical values calculated at standard pressure and 298° K (all values are given in Hartrees)

M ⁺	Theory	M ⁺ (THF) ₁			M ⁺ (THF) ₂			M ⁺ (THF) ₃			M ⁺ (THF) ₄		
		ΔE	ΔH	ΔG	ΔE	ΔH	ΔG	ΔE	ΔH	ΔG	ΔE	ΔH	ΔG
Li	HF	178	178	186	144	147	113	92	95	51	53	55	9
	MP2	190	190	198	169	172	135	121	124	83	104	104	60
	B3LYP	177	177	185	144	147	109	89	91	50	49	51	5
Na	HF	120	120	134	102	104	75	76	78	41	55	57	19
	MP2	130	130	144	114	116	89	94	97	64	95	97	39
	B3LYP	123	123	137	102	105	70	73	76	40	51	54	11
K	HF	80	80	99	67	70	51	55	58	23	44	47	15
	MP2	92	92	110	80	82	59	74	76	32	81	84	29
	B3LYP	82	82	100	68	71	38	55	57	24	43	45	3
Cu	HF	166	166	181	143	145	106	59	61	30	41	43	6
	MP2	248	248	262	249	251	204	81	83	43	77	79	37
	B3LYP	230	230	246	203	206	160	40	43	4	28	30	-3
MgCl	HF	293	295	256	196	198	155	141	144	96	47	50	-9
	MP2	302	305	265	218	221	180	181	184	136	-192	-189	-250
	B3LYP	299	301	262	185	188	146	133	136	82	46	48	-9

Table 2.8. Bond dissociation energies and enthalpies calculated at standard pressure and 298° K (all values are in kJ/mol)

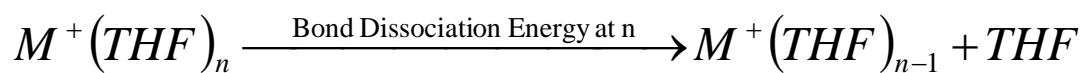


Figure 2.10. Tetrahydrofuran bond dissociation energy

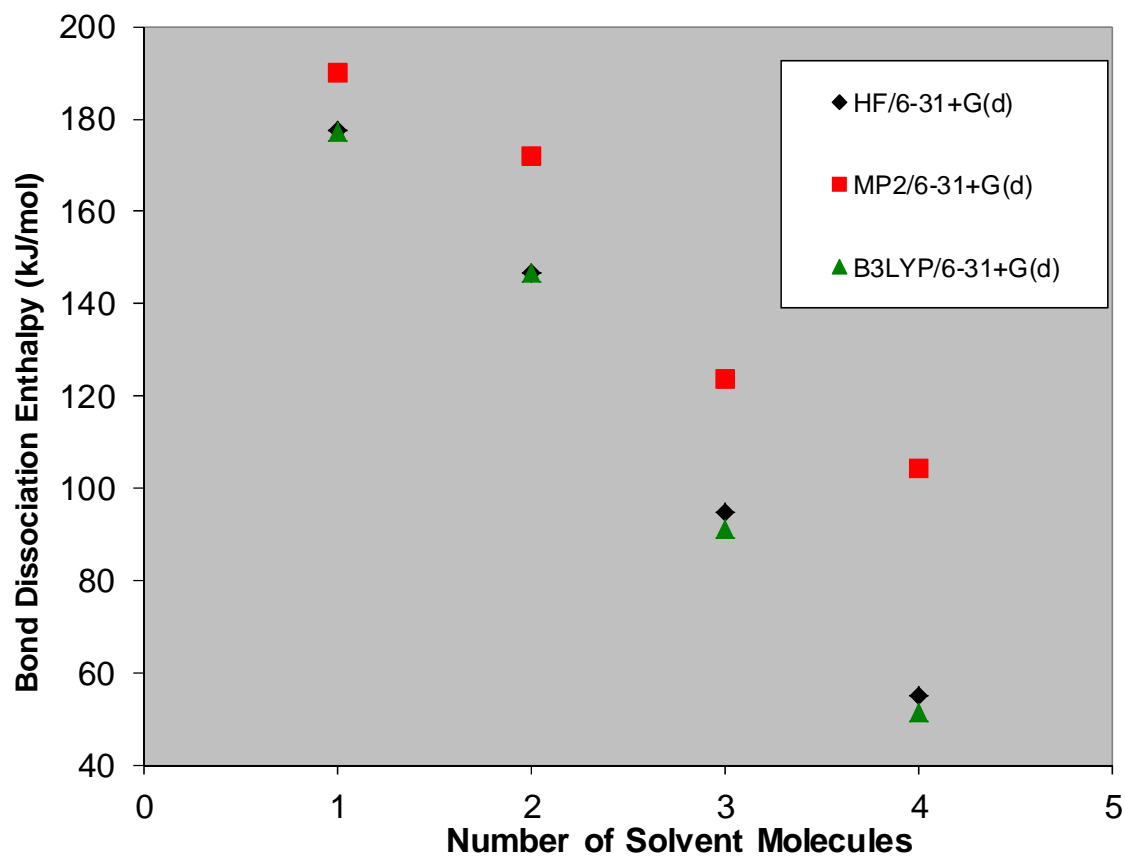


Figure 2.11. Comparison of Li⁺ - THF bond dissociation enthalpies calculated at HF/6-31+G(d), MP2/6-31+G(d), and B3LYP/6-31+G(d)

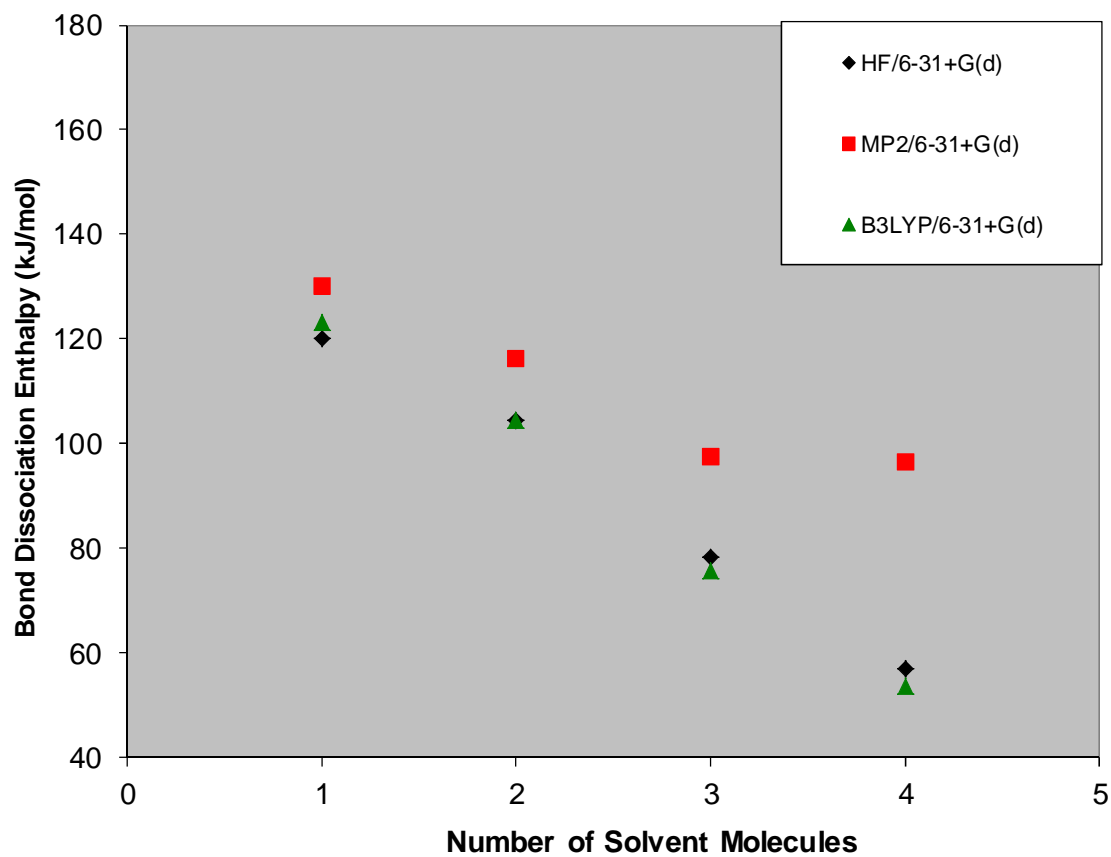


Figure 2.12. Comparison of Na⁺ - THF bond dissociation enthalpies calculated at HF/6-31+G(d),MP2/6-31+G(d), and B3LYP/6-31+G(d)

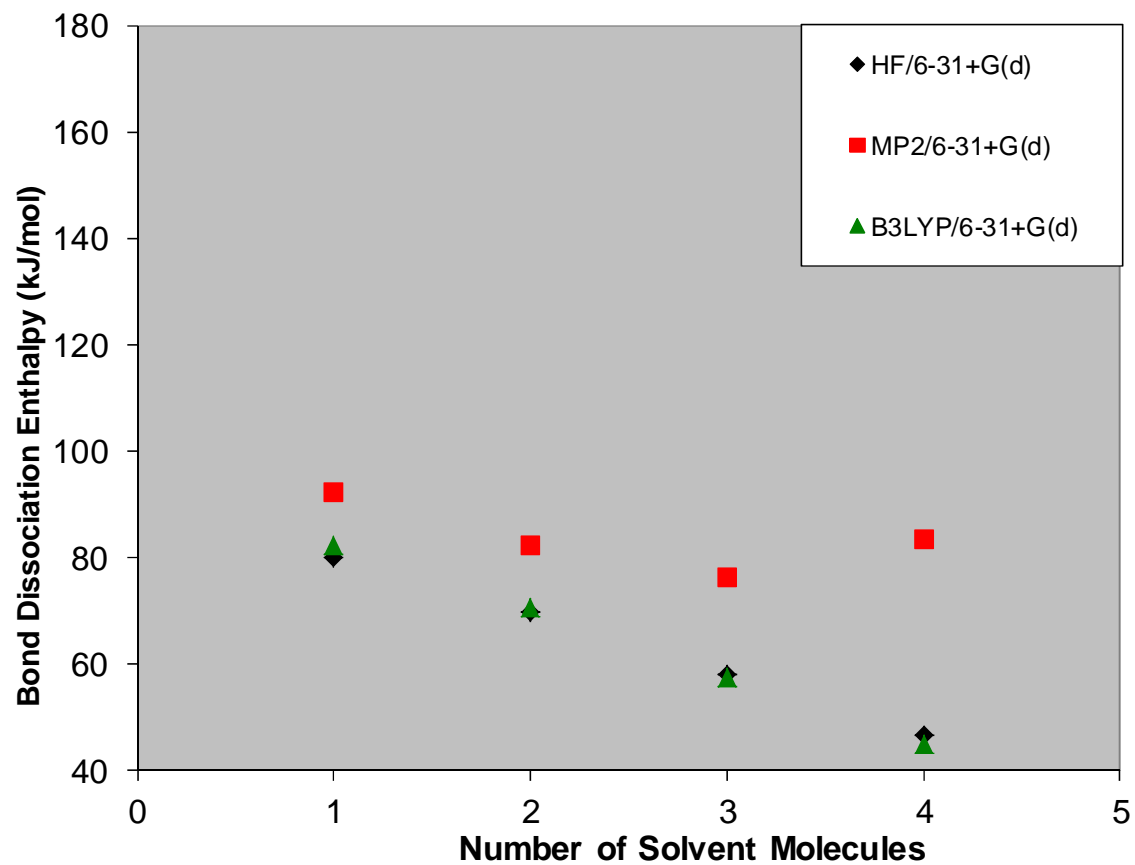


Figure 2.13. Comparison of K^+ - THF bond dissociation enthalpies calculated at HF/6-31+G(d),MP2/6-31+G(d), and B3LYP/6-31+G(d)

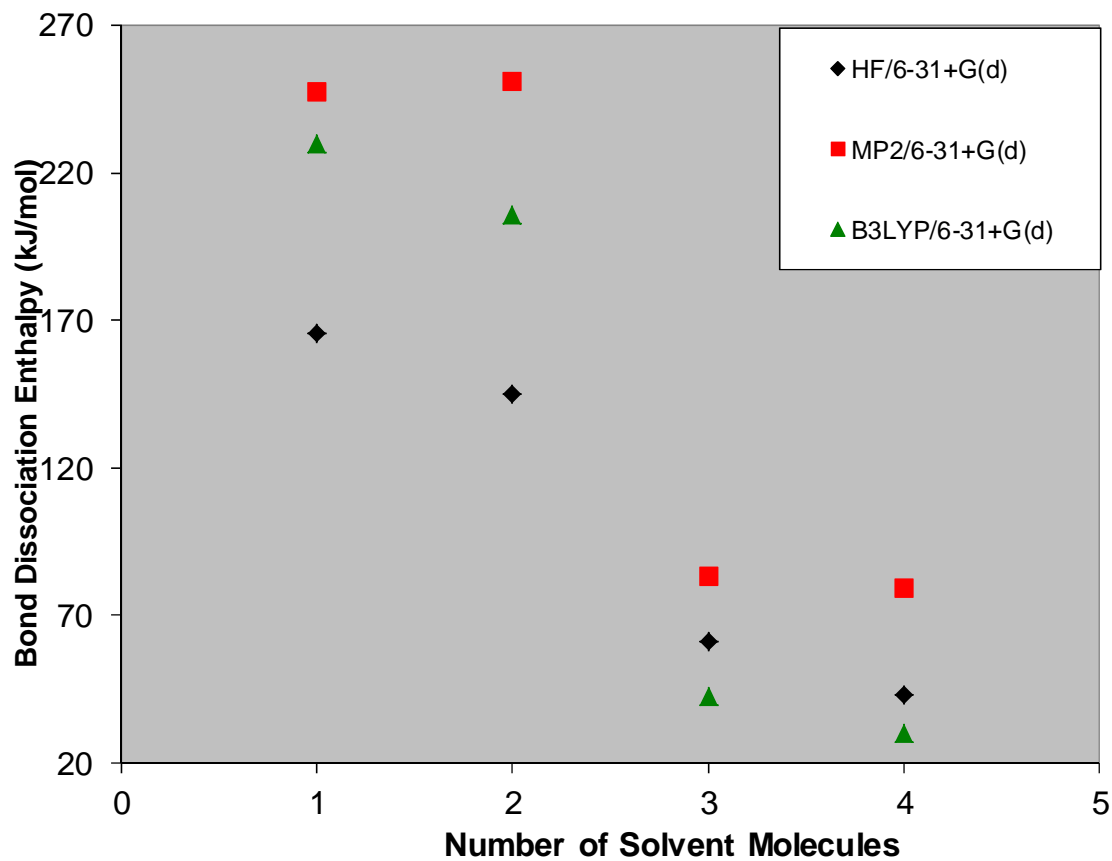


Figure 2.14. Comparison of Cu^+ - THF bond dissociation enthalpies calculated at HF/6-31+G(d), MP2/6-31+G(d), and B3LYP/6-31+G(d)

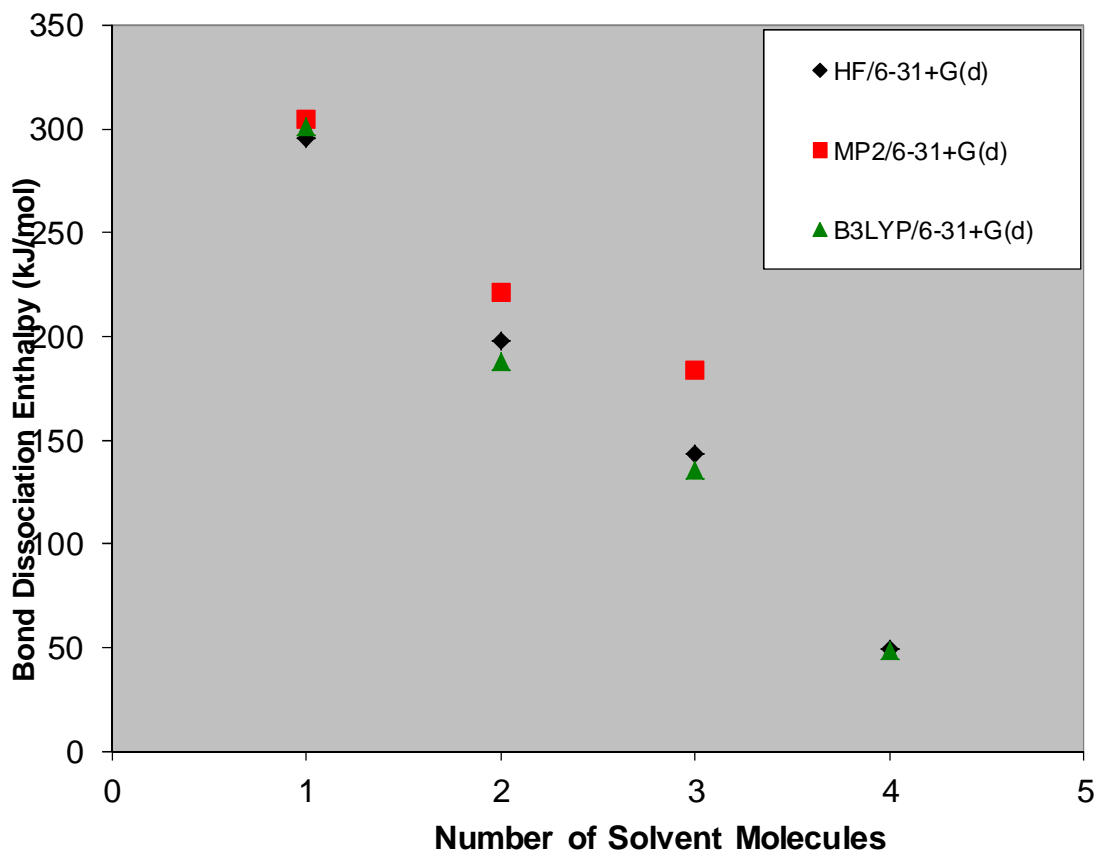


Figure 2.15. Comparison of MgCl⁺ - THF bond dissociation enthalpies calculated at HF/6-31+G(d),MP2/6-31+G(d), and B3LYP/6-31+G(d)

As in the case of DME, comparison of the values in Table 2.6 with those in Table 2.8 shows the expected relationship between increasing M⁺ - O distance and decreasing dissociation energy. The bond dissociation results seen in Table 2.8 and Figures 2.11 – 2.15 follow the same trends seen in the results calculated for the DME complexes. All of the cations, with the exception of Cu⁺, show the expected linear decrease in dissociation enthalpy with increasing number of solvent molecules. As in the case of DME, the results for the cations other than Cu⁺ show that HF and B3LYP give extremely similar results and that the MP2 calculations yield results that are consistently

and significantly higher than the bond dissociation results calculated using the other two model chemistries. The results for Cu^+ again show that the HF model chemistry gives bond dissociation energies with a more linear decrease whereas the MP2 and B3LYP show the anticipated “step-like” behavior caused by the previously discussed $4s-3d\sigma$ hybridization of Cu^+ .

2.3.4 Explicit – Continuum THF Solvation

The explicit – continuum modeling of solvation was also applied to the THF / cation systems. This was again accomplished using the optimized geometries found during the calculation of the bond dissociation energies of THF from Li^+ , Na^+ , K^+ , Cu^+ , and MgCl^+ coupled with the PCM method for approximating solvation using a dielectric constant continuum.

M ⁺	Theory	0 DME	1 DME	2 DME	3 DME	4 DME	Theory
Li	HF	-559	-514	-430	-427	-409	-458
	MP2	-558	-505	-414	-408	-380	-458
	B3LYP	-560	-513	-427	-423	-402	-458
Na	HF	-460	-424	-388	-338	-310	-359
	MP2	-456	-412	-372	-332	-256	-359
	B3LYP	-460	-425	-383	-337	-301	-359
K	HF	-361	-331	-306	-260	-223	-277
	MP2	-319	-279	-245	-191	-118	-277
	B3LYP	-362	-331	-295	-251	-204	-277
Cu	HF	-401	-403	-405	-385	-360	-481
	MP2	741	763	793	837	878	-481
	B3LYP	-407	-456	-513	-481	-449	-481
MgCl	HF	-764	-714	-685	-656	-622	
	MP2	-339	-283	-249	-5	-171	
	B3LYP	-743	-695	-668	-634	-602	

Table 2.9. $\Delta G(\text{solvation})$ calculated with a continuum approximation of solvation and the number of explicit solvent molecules listed. Calculated at standard pressure and 298° K (all values are in kJ/mol)

The results are shown in Table 2.9 for all cations and graphically in Figures 2.16 – 2.20 for the Li^+ cation. This data indicates that, as in the case of DME solvation, as the number of solvent molecules is increased, for most of the systems studied agreement between the calculated value and the theoretical value is improved. Again, in the cases of Li^+ , Na^+ , and K^+ , two to three explicit solvent molecules are required to obtain a result that captures the majority of the theoretical free energy change. In the case THF solvation of Cu^+ , the observed behavior is very similar to the behavior seen for the DME solvation of Cu^+ . In this case the results seem to indicate that there is not significant contribution to the total free energy change from the explicit solvation. It also appears however, that for the B3LYP model (which was shown in the DME investigation to give the most accurate agreement between experimental and calculated values) that the best agreement between the calculated results the theoretical values obtained from the Born equation is achieved when 2-3 explicit solvent molecules are included in the calculations. As in the case of DME these results suggest that the inclusion of explicit or explicit/continuum solvation of the cations is required to obtain a clearer, more accurate understand the true nature of the solvation of the cations than can be obtained with only a continuum model of solvation.

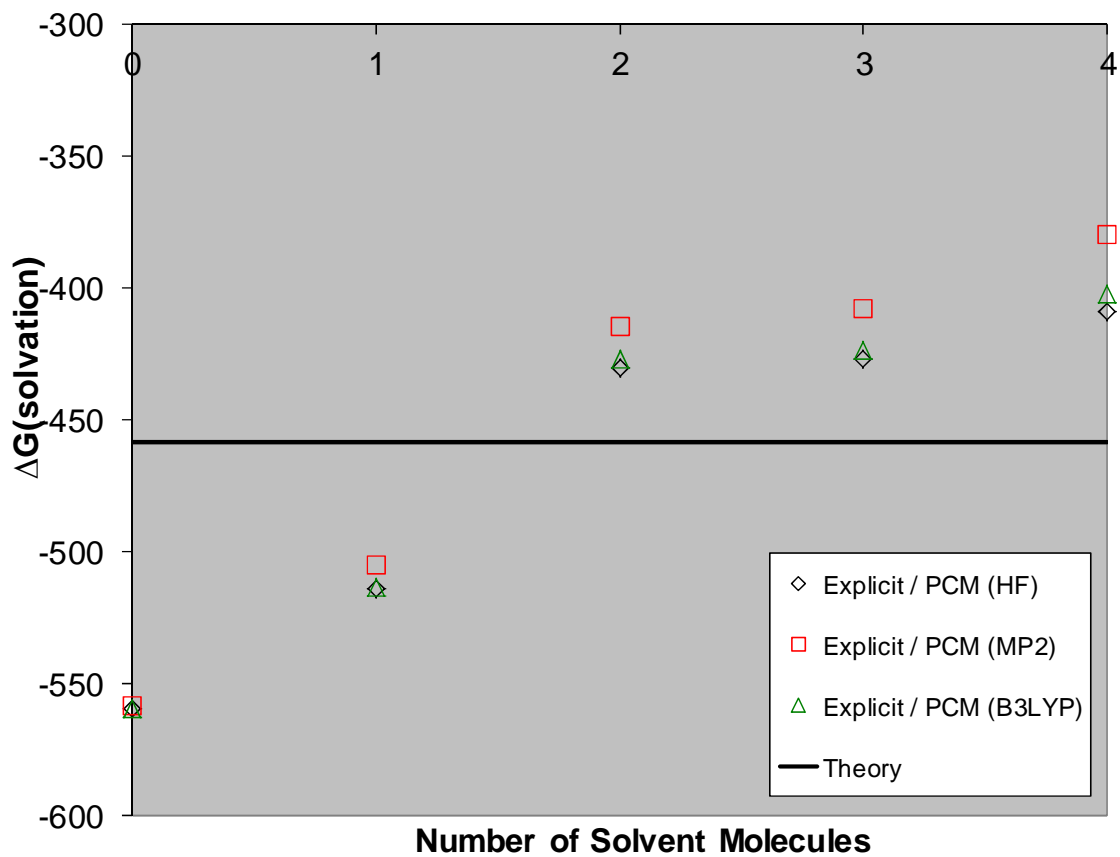


Figure 2.16. Comparison of Li⁺ - THF Gibbs Free Energy of Solvation calculated at HF/6-31+G(d),MP2/6-31+G(d), and B3LYP/6-31+G(d) using continuum solvation approximated by the PCM method and theoretical value calculated using the Born Equation

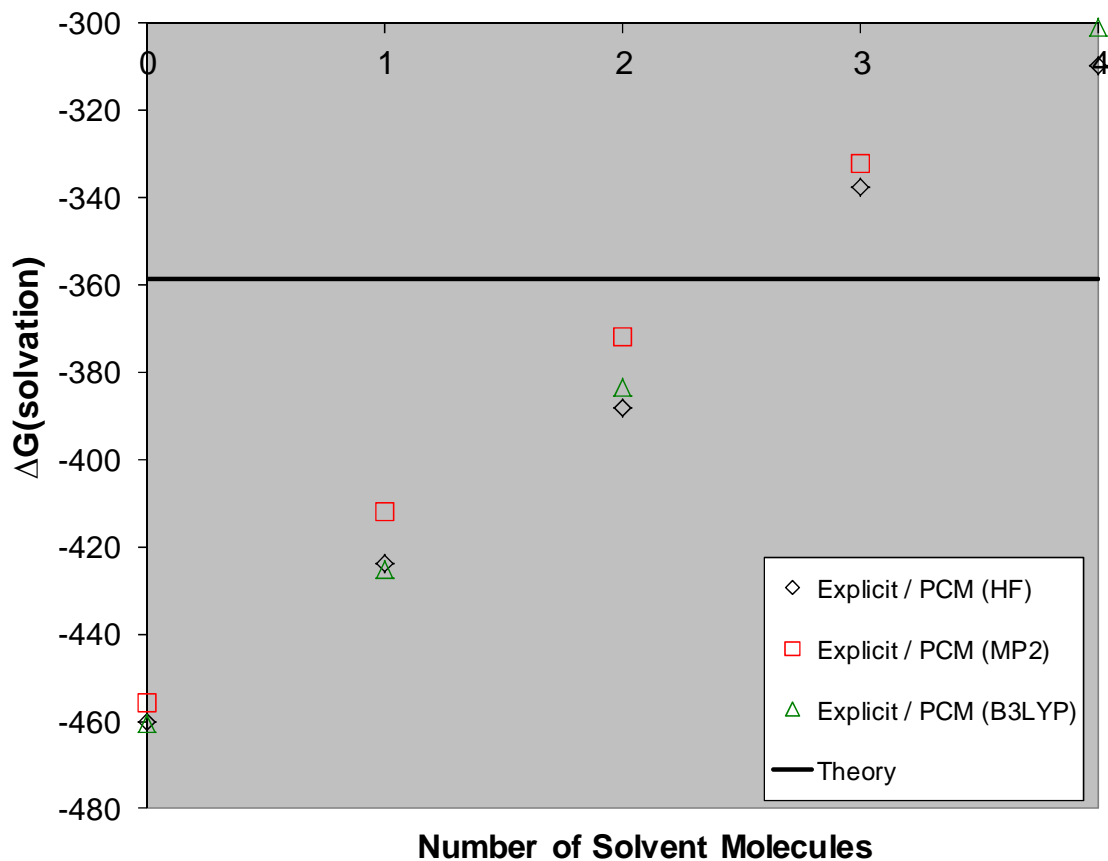


Figure 2.17. Comparison of Na⁺ - THF Gibbs Free Energy of Solvation calculated at HF/6-31+G(d),MP2/6-31+G(d), and B3LYP/6-31+G(d) using continuum solvation approximated by the PCM method and theoretical value calculated using the Born Equation

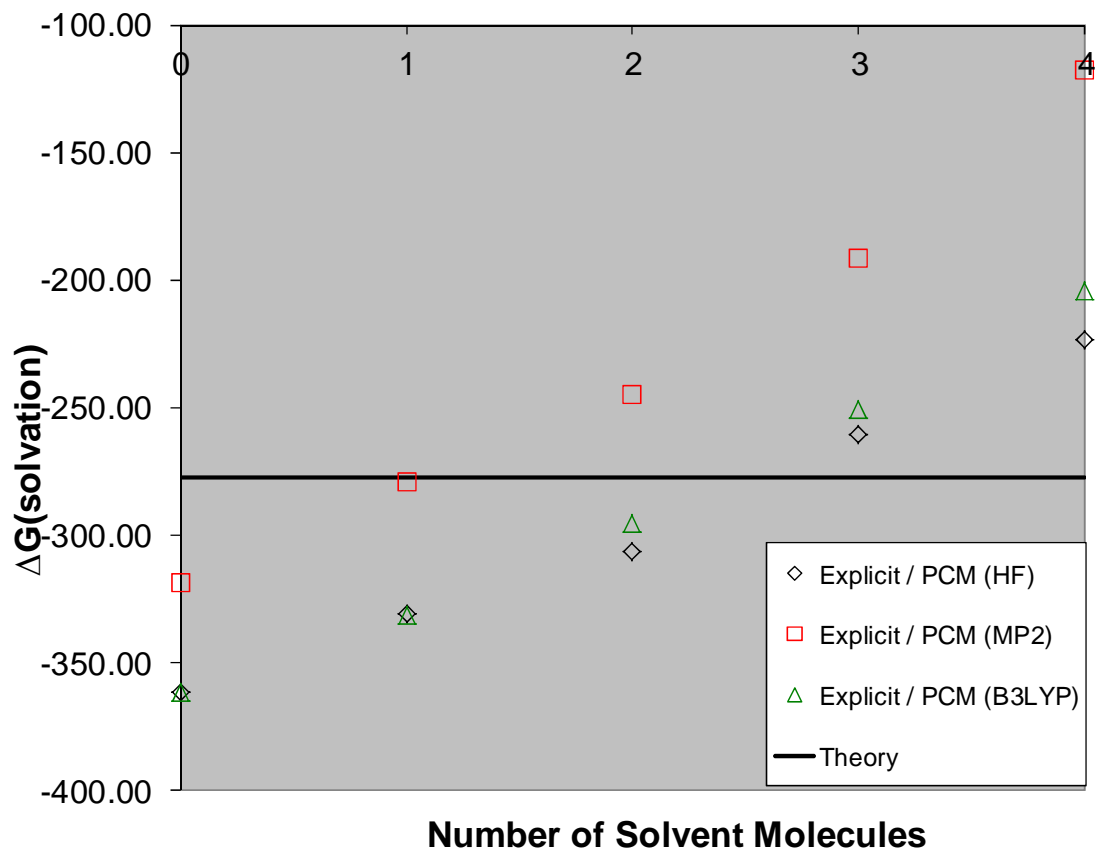


Figure 2.18. Comparison of K^+ - THF Gibbs Free Energy of Solvation calculated at HF/6-31+G(d), MP2/6-31+G(d), and B3LYP/6-31+G(d) using continuum solvation approximated by the PCM method and theoretical value calculated using the Born Equation

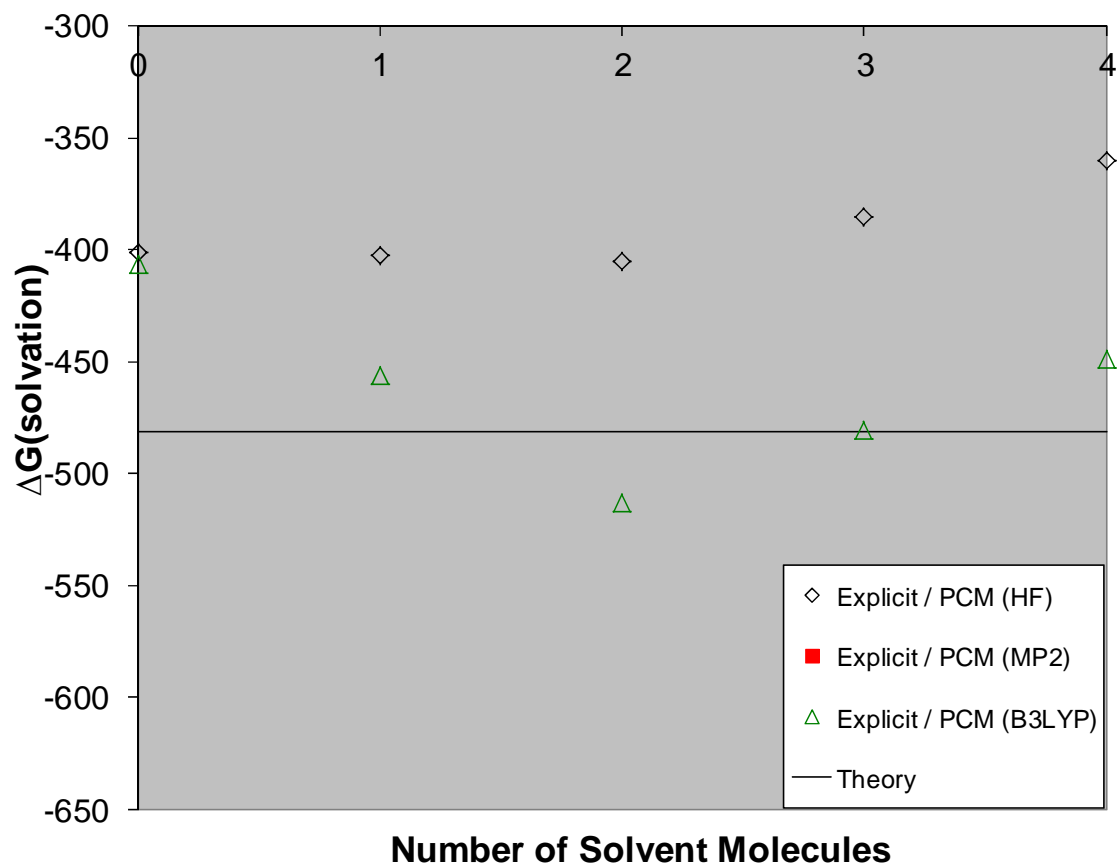


Figure 2.19. Comparison of Cu^+ - Gibbs Free Energy of Solvation calculated at HF/6-31+G(d), MP2/6-31+G(d), and B3LYP/6-31+G(d) using continuum solvation approximated by the PCM method and theoretical value calculated using the Born Equation

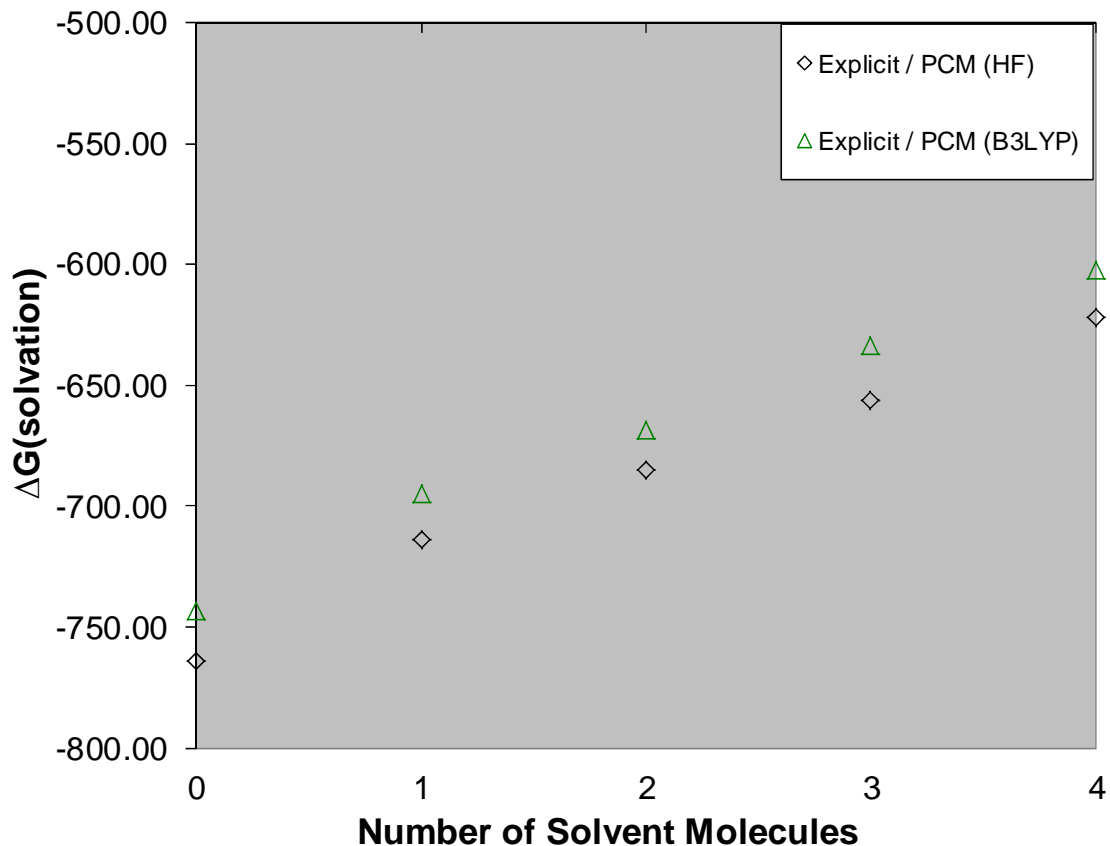


Figure 2.20. Comparison of MgCl^+ - Gibbs Free Energy of Solvation calculated at HF/6-31+G(d), MP2/6-31+G(d), and B3LYP/6-31+G(d) using continuum solvation approximated by the PCM method and theoretical value calculated using the Born Equation

The interesting and unexpected trends seen for the MP2 calculations of ΔG are also present in the THF investigation as well. The Li^+ and Na^+ MP2 values were in good agreement with the values obtained with the other two methods. The MP2 results began to diverge from those obtained from the other methods in the case of the K^+ , and very much higher for Cu^+ MgCl^+ . As discussed previously it is possible that the effect of electron correlation is overestimated by MP2, and may be more accurately addressed by higher order Møller-Plesset theory.

In non-aqueous liquids there are not only cations but also anions that may affect the conclusions and calculated values. These issues were not considered in this study; however, we anticipate the conclusions would remain the same while the calculated values would be different. For example in strong associating anions, e.g. with carbanions, one of the solvent molecules would be displaced and the cation – solvent interaction would be weaker. In other cases where the anion has similar intermolecular interactions with the solvent, e.g. halide anions, one would expect that the calculated results would be that same for the cations as reported here. In both cases the need for a mixed explicit/implicit ion – solvent model is necessary. These conclusions are consistent with the results for Diels-Alder reactions.⁴⁵

2.4 Conclusions

The principle objective of this work was to better understand how to accurately and efficiently model cations in solution in polar non-aqueous solvents. Of particular interest were THF due to its versatility as a reaction medium, and DME due to the thorough experimentally determined data available for this solvent with the cations of interest to the authors.

It has been determined that for DME, the use of Density Functional Theory, specifically B3LYP gives the best overall agreement between experimentally determined and calculated values for bond dissociation enthalpy or energy. For the majority of the cations studied, the results obtained with HF and B3LYP were very similar, however, of the two only the DFT method was accurately able to capture the effect of the $4s-3d\sigma$

hybridization of Cu^+ in the calculation of bond dissociation energy. For both model chemistries the use of the Boys-Bernardi full counterpoise method for correction of basis set supposition error slightly improved the accuracy of the calculated values, as did the use of the larger, 6-311++G(d,p), basis set. However the improvements obtained from these changes were small compared to the overall improvement in accuracy, relative to HF results, achieved by using B3LYP. In all cases the results obtained using the MP2 model chemistry were the least accurate and computationally the most expensive of the results of the three model chemistries.

The results of the THF investigation were not compared with experimentally determined data, but when compared with the results of the DME investigation the same trends in the data were observed, strongly suggesting the use of the B3LYP / 6-31+G(d) to be the most accurate and most efficient for those systems as well.

2.5 References

1. Kudo, H.; Hashimoto, M.; Yokoyama, K.; Wu, C. H.; Dorigo, A. E.; Bickelhaupt, F. M.; von Schleyer, P., Structure and Stability of the Li_2CN Molecule. An Experimental and ab Initio Study. *The Journal of Physical Chemistry* **1995**, 99, (17), 6477-6482.
2. Hill, S. E.; Glendening, E. D.; Feller, D., Theoretical Study of Cation/Ether Complexes: The Alkali Metals and Dimethyl Ether. *Journal of Physical Chemistry Part A* **1997**, 101, 6125-6131.

3. Alia, J. M.; Edwards, H. G. M., FT-Raman Study of Ionic Interactions in Lithium and Silver Tetrafluoroborate Solutions in Acrylonitrile. *Journal of Solution Chemistry* **2000**, 29, (9), 781-797.
4. Aroca, R.; Nazri, M.; Nazri, G. A.; Camargo, A. J.; Trsic, M., Vibrational Spectra and Ion-Pair Properties of Lithium Hexafluorophosphate in Ethylene Carbonate Based Mixed-Solvent Systems for Lithium Batteries. *Journal of Solution Chemistry* **2000**, 29, (10), 1047-1060.
5. Atkins, P.; Hefter, G. T.; Singh, P., Ion solvation in lithium battery electrolyte solutions. 1. Apparent molar volumes. *Journal of Solution Chemistry* **1991**, 20, (11), 1059-1078.
6. Barthel, J.; Buchner, R.; Wismeth, E., FTIR Spectroscopy of Ion Solvation of LiClO₄ and LiSCN in Acetonitrile, Benzonitrile, and Propylene Carbonate. *Journal of Solution Chemistry* **2000**, 29, (10), 937-954.
7. Barthel, J.; Deser, R., FTIR study of ion solvation and ion-pair formation in alkaline and alkaline earth metal salt solutions in acetonitrile. *Journal of Solution Chemistry* **1994**, 23, (10), 1133-1146.
8. Das, D., Ion Association and Solvation Behavior of Some Lithium Salts in Tetrahydrofuran. A Conductivity and Raman Spectroscopic Study. *Journal of Solution Chemistry* **2008**, 37, (7), 947-955.
9. Das, D.; Das, B.; Hazra, D. K., Electrical Conductance of Some Symmetrical Tetraalkylammonium and Alkali Salts in N,N-Dimethylacetamide at 25°C. *Journal of Solution Chemistry* **2003**, 32, (1), 77-83.

10. De, R.; Guha, C.; Das, B., Ion Association and Solvation Behavior of Some 1-1 Electrolytes in 2-Ethoxyethanol Probed by a Conductometric Study. *Journal of Solution Chemistry* **2006**, 35, (11), 1505-1514.
11. Hopkins, H.; Jahagirdar, D.; Norman, A., Conductance studies on lithium salt-acetonitrile solutions at 25°C. *Journal of Solution Chemistry* **1979**, 8, (2), 147-155.
12. Hourdakis, A.; Popov, A. I., Lithium-7, sodium-23, and cesium-133 NMR and far infrared study of alkali complexes with C222-dilactam in various solvents. *Journal of Solution Chemistry* **1977**, 6, (5), 299-307.
13. Kilroy, W. P., Solubility and solvate formation of lithium hexafluoroarsenate in acetonitrile. *Journal of Solution Chemistry* **1977**, 6, (7), 487-490.
14. Kunz, W.; Barthel, J.; Klein, L.; Cartailier, T.; Turq, P.; Reindl, B., Lithium bromide in acetonitrile: Thermodynamics, theory, and simulation. *Journal of Solution Chemistry* **1991**, 20, (9), 875-891.
15. Ohtaki, H.; Wada, H., Structure of solvated lithium and chloride ions in formamide. *Journal of Solution Chemistry* **1985**, 14, (3), 209-219.
16. Petrowsky, M.; Rhodes, C. P.; Frech, R., Vibrational Spectroscopic Study of 2-Methoxyethyl Ether Complexed with Lithium and Sodium Trifluoromethanesulfonate. *Journal of Solution Chemistry* **2001**, 30, (2), 171-181.
17. Reichstädter, L.; Fischerová, E.; Fischer, O., Conductance of Lithium and Sodium Perchlorates and Tetraphenylborates in 2-Butanone from -35 to 25°C. *Journal of Solution Chemistry* **1999**, 28, (1), 35-60.

18. Smetana, A. J.; Popov, A. I., Lithium-7 nuclear magnetic resonance and calorimetric study of lithium crown complexes in various solvents. *Journal of Solution Chemistry* **1980**, 9, (3), 183-196.
19. Abbotto, A.; Streitwieser, A.; Schleyer, P. v. R., Ab Initio and Semiempirical Study of the Effect of Ethereal Solvent on Aggregation of a Lithium Enolate. *Journal of the American Chemical Society* **1997**, 119, (46), 11255-11268.
20. Carlier, P. R.; Lo, C. W.-S., ⁷Li/³¹P NMR Studies of Lithiated Arylacetonitriles in THF-HMPA Solution: Characterization of HMPA-Solvated Monomers, Dimers, and Separated Ion Pairs. *Journal of The American Chemical Society* **2000**, 122, 12819-12823.
21. Carlier, P. R.; Lucht, B. L.; Collum, D. B., ⁶LiPN NMR-Based Solution Structural Determination of EtzO⁻ and TMEDA-Solvated Lithiophenylacetonitrile and a LiHMDS Mixed Aggregate. *Journal of The American Chemical Society* **1994**, 116, 11602-11603.
22. Erlich, R. H.; Roach, E.; Popov, A. I., Solvation Studies of Sodium and Lithium Ions by Sodium-23 and Lithium-7 Nuclear Magnetic Resonance *Journal of The American Chemical Society* **1970**, 92, 4889-4890.
23. Kaneti, J.; Schleyer, P. v. R.; Clark, T.; Kos, A. J.; Spitznagel, G. W.; Andrade, J. G.; Moffat, J. B., The structures and energies of the lithium, sodium, and magnesium derivatives of the anions CH₂CN⁻ and CH₂NC⁻. Solvation and aggregation of the lithium species. *Journal of the American Chemical Society* **1986**, 108, (7), 1481-1492.
24. O'Brien, D. H.; Russell, C. R.; Hart, A. J., Solvation of Alkali Metal Cations of Arylmethyl Anions by Ethereal Solvents. *Journal of The American Chemical Society* **1979**, 101, 633-639.

25. Kaufmann, E.; Gose, J.; Schleyer, P. v. R., Thermodynamics of Solvation of Lithium Compounds. A Combined MNDO and ab Initio Study. *Organometallics* **1989**, *8*, 2577-2584.
26. Westphal, E.; Pliego, J. R. J., Absolute solvation free energy of Li⁺ and Na⁺ ions in dimethyl sulfoxide solution: A theoretical ab initio and cluster-continuum model study. *The Journal of Chemical Physics* **2005**, *123*, 074508 - 7.
27. Tomasi, J.; Persico, M., Molecular Interactions in Solution: An Overview of Methods Based on Continuous Distributions of the Solvent. *Chemical Reviews* **1994**, *94*, 2027 - 2094.
28. Carlier, P. R.; Madura, J. D., Effective Computational Modeling of Constitutional Isomerism and Aggregation States of Explicit Solvates of Lithiated Phenylacetonitrile. *The Journal of Organic Chemistry* **2002**, *67*, 3832-3840.
29. Fock, V. A., Näherungsmethode zur Lösung des quantenmechanischen Mehrkörperproblems. *Zeitschrift für Physik* **1930**, *61*, 126-148.
30. Hartree, D. R., The Wave Mechanics of an Atom with a Non-Coulomb Central Field. Part I. Theory and Methods. *Proceedings of the Cambridge Philosophical Society* **1927**, *24*, 89-110.
31. Hartree, D. R., The Wave Mechanics of an Atom with a Non-Coulomb Central Field. Part II. Some Results and Discussion. *Proceedings of the Cambridge Philosophical Society* **1927**, *24*, 111-132.
32. Hartree, D. R., The Wave Mechanics of an Atom with a non-Coulomb Central Field. Part III. Term Values and Intensities in Series in Optical Spectra. *Proceedings of the Cambridge Philosophical Society* **1928**, *24*, 426-437.

33. Hartree, D. R., The Distribution of Charge and Current in an Atom consisting of many Electrons obeying Dirac's equations. *Proceedings of the Cambridge Philosophical Society* **1929**, 25, 225-236.
34. Hartree, D. R., The Wave Mechanics of an Atom with a Non-Coulomb Central Field. Part IV. Further Results relating to Terms of the Optical Spectrum. *Proceedings of the Cambridge Philosophical Society* **1929**, 25, 310-314.
35. Jarek, R. L.; Miles, T. D.; Trester, M. L.; Denson, S. C.; Shin, S. K., Solvation of Li⁺ by Acetone, THF, and Diethyl Ether in the Gas Phase and the Ion-Molecule Association Mechanism. *Journal of Physical Chemistry Part A* **2000**, 104, 2230-2237.
36. Jarek, R. L.; Shin, S. K., Solvation of the Li⁺-Br⁻-Li⁺ Triple Ion in the Gas Phase. *Journal of The American Chemical Society* **1997**, 119, 10501-10508.
37. Ohanessian, G.; McMahon, T. B., An Experimental and Ab Initio Study of the Nature of the Binding in Gas-Phase Complexes of Sodium Ions. *Chemistry - A European Journal* **2000**, 6, (16), 2931-2941.
38. Eriksson, H.; Hakansson, M.; Jagner, S., Pentamethylphenylcopper(I): a square-planar tetranuclear cluster. *Inorganica Chimica Acta* **1998**, 277, 233-236.
39. Katritzky, A. R.; Malhotra, N.; Ramanathan, R.; Kemerait, R. C. J.; Zimmerman, J. A.; Eyler, J. R., Measurement of gas-phase binding energies of crown ethers with metal ions by Fourier-transform ion cyclotron resonance mass Spectrometry. *Rapid Communications in Mass Spectrometry* **1992**, 6, (1), 25-27.
40. Koizumi, H.; Zhang, X.-G.; Armentrout, P. B., Collision-Induced Dissociation and Theoretical Studies of Cu⁺-Dimethyl Ether Complexes. *Journal of Physical Chemistry Part A* **2001**, 105, 2444-2452.

41. More, M. B.; Glendening, E. D.; Ray, D.; Feller, D.; Armentrout, P. B., Cation-Ether Complexes in the Gas Phase: Bond Dissociation Energies and Equilibrium Structures of $\text{Li}^+[\text{O}(\text{CH}_3)_2]_x$, $x = 1-4$. *Journal of Physical Chemistry* **1996**, 100, 1605-1614.
42. More, M. B.; Ray, D.; Armentrout, P. B., Cation-Ether Complexes in the Gas Phase: Bond Dissociation Energies of $\text{Na}^+(\text{dimethyl ether})_x$, $x = 1-4$; $\text{Na}^+(1,2\text{-dimethoxyethane})_x$, $x = 1$ and 2 ; and $\text{Na}^+(12\text{-crown-4})$. *Journal of Physical Chemistry Part A* **1997**, 101, 831-839.
43. More, M. B.; Ray, D.; Armentrout, P. B., Cation-Ether Complexes in the Gas Phase: Bond Dissociation Energies of $\text{K}^+(\text{dimethyl ether})_x$, $x = 1-4$; $\text{K}^+(1,2\text{-dimethoxyethane})_x$, $x = 1$ and 2 ; and $\text{K}^+(12\text{-crown-4})$. *Journal of Physical Chemistry Part A* **1997**, 101, 4254-4262.
44. Frisch, M. J.; Trucks, G. W.; Schlegel, H. B.; Scuseria, G. E.; Robb, M. A.; Cheeseman, J. R.; Montgomery, J. A., Jr.; Vreven, T.; Kudin, K. N.; Burant, J. C.; Millam, J. M.; Iyengar, S. S.; Tomasi, J.; V. B.; Mennucci, B.; Cossi, M.; Scalmani, G.; Rega, N.; Petersson, G. A.; Nakatsuji, H.; Hada, M.; Ehara, M.; Toyota, K.; Fukuda, R.; Hasegawa, J.; Ishida, M.; Nakajima, T.; Honda, Y.; Kitao, O.; Nakai, H.; Klene, M.; Li, X.; Knox, J. E.; Hratchian, H. P.; Cross, J. B.; Adamo, C.; Jaramillo, J.; Gomperts, R.; Stratmann, R. E.; Yazyev, O.; Austin, A. J.; Cammi, R.; Pomelli, C.; Ochterski, J. W.; Ayala, P. Y.; Morokuma, K.; Voth, G. A.; Salvador, P.; Dannenberg, J. J.; Zakrzewski, V. G.; Dapprich, S.; Daniels, A. D.; Strain, M. C.; Farkas, O.; Malick, D. K.; Rabuck, A. D.; Raghavachari, K.; Foresman, J. B.; Ortiz, J. V.; Cui, Q.; Baboul, A. G.; Clifford, S.; Cioslowski, J.; Stefanov, B. B.; Liu, G.; Liashenko, A.; Piskortz, P.; Komaromi, I.;

- Martin, R. L.; Fox, D. J.; Keith, T.; Al-Laham, M. A.; Peng, C. Y.; Nanayakkara, A.; Challacombe, M.; Gill, P. M. W.; Johnson, B.; Chen, W.; Wong, M. W.; Gonzalez, C.; Pople, J. A. *Gaussian 03, Revision D.01*, Gaussian, Inc.: Wallingford, CT, 2004.
45. Evanseck, J. D.; Kong, S., Density Functional Theory Study of Aqueous-Phase Rate Acceleration and Endo/Exo Selectivity of the Butadiene and Acrolein Diels-Alder Reaction. *Journal of The American Chemical Society* **2000**, 122, 10418-10427.
46. Krishnan, R.; Frisch, M. J.; Pople, J. A., Contribution of triple substitutions to the electron correlation energy in fourth order perturbation theory. *Journal of Chemical Physics* **1980**, 72, 4244-4245.
47. Krishnan, R.; Pople, J. A., Approximate fourth-order perturbation theory of the electron correlation energy. *Journal of Quantum Chemistry* **1978**, 14, 91-100.
48. Moller, C.; Plesset, M. S., Note on an Approximation Treatment for Many-Electron Systems. *Physical Review* **1934**, 46, 618-622.
49. Becke, A. D., Density-functional thermochemistry. III. The role of exact exchange. *Journal of Chemical Physics* **1993**, 98, (7), 5648-5662.
50. Lee, C.; Yang, W.; Parr, R. G., Development of the Colle-Salvetti correlation-energy formula into a functional of the electron density. *Physical Review B* **1988**, 37, (2), 785-789.
51. Cossi, M.; Barone, V.; Cammi, R.; Tomasi, J., Ab initio study of solvated molecules: a new implementation of the polarizable continuum model. *Chemical Physics Letters* **1996**, 255, (4-6), 327-335.

52. Bauschlicher, C. W. J.; Langhoff, S. R.; Partridge, H., The binding energies of $\text{Cu}^{+}(\text{H}_2\text{O})_n$ and $\text{Cu}^{+}(\text{NH}_3)_n$ ($n= 1-4$). *Journal of Chemical Physics* **1991**, 94, 2068-2072.
53. Boys, S. F.; Bernardi, F., The calculation of small molecular interactions by the differences of separate total energies. Some procedures with reduced errors *Molecular Physics* **1970**, 19, 553-566.
54. Born, M., Volumen und Hydratationswärme der Ionen *Zeitschrift für Physik* **1920**, 1, 45-48.
55. Latimer, W. M.; Pitzer, K. S.; Slansky, C. M., The Free Energy of Hydration of Gaseous Ions, and the Absolute Potential of the Normal Calomel Electrode. *Journal of Chemical Physics* **1939**, 7, 108-111.
56. Rashin, A. A.; Honig, B., Reevaluation of the Born Model of Ion Hydration. *Journal of Physical Chemistry* **1985**, 89, 5588-5593.

3 Effect of Solvent and Cation on the Structure of Acetonitrile Anion

Chapter 2 of this dissertation was the development of a more fundamental understanding of cation-ether complexes and to evaluate the accuracy and efficiency of several model chemistries in modeling these complexes. This chapter of the dissertation builds upon that work to include the acetonitrile anion in addition to the cation-ether complexes. The principle objective here is to answer the question of how cation and solvent variations affect the preference for carbon or nitrogen metalation of the acetonitrile anion. The electronic structure techniques used were Hartree-Fock (HF), Second-order Møller-Plesset perturbation theory (MP2), the Becke three-parameter exchange functional coupled with the nonlocal correlation functional of Lee, Yang, and Parr (B3LYP). The complexes studied were the tetrahydrofuran (THF) and dimethyl ether (DME) complexes of Li^+ , Na^+ , K^+ , Cu^+ , and MgCl^+ with acetonitrile anion. In general, it was found that metalation site which resulted in a minimized charge density on the cation was the energetically preferred structure.

3.1 Introduction

As shown in Chapter 1, in Figures 1.4 and 1.5, metalated nitrile stabilized carbanions are of significant interest for numerous reasons such as their usefulness in directing stereo- and regioselective in the synthesis of several types of biologically important molecules.¹⁻⁷ Spectroscopic techniques have been used to gain a limited understand of the solution phase properties of metalated nitrile anions.⁸⁻¹¹ An increased

understanding of the structure and reactivity of metalated nitrile anions would allow for the development of more powerful tools for controlling the synthesis of many types of molecules, in particular for directing the stereochemistry of decalin containing biologically active compounds.^{6, 12, 13} Recently, ab initio and density functional theory (DFT) calculations have been used to predict the properties of these difficult to study molecules and to eliminate gaps that exist in our understanding of the results from spectroscopic investigation.^{9, 10, 14-18}

The aim of this chapter is to expand on the understanding of how differences in solvent and cation affect the solution phase structure of acetonitrile anion complexes, through the use of electronic structure calculations. It is of particular interest to determine how apparent hybridization around the α -carbon changes as a function of solvent and cation. For the sake of this investigation the amount of deviation from the expected sp^2 hybridization will be quantified in terms of a deformation angle as shown in Figure 3.1. Based on this convention, a perfectly sp^2 hybridized molecule would have a deformation angle of 120° . As the molecule takes on more sp^3 character and deforms away from pure sp^2 hybridization the deformation angle will decrease toward the lower limit of 109.5° in the case of pure sp^3 hybridization.

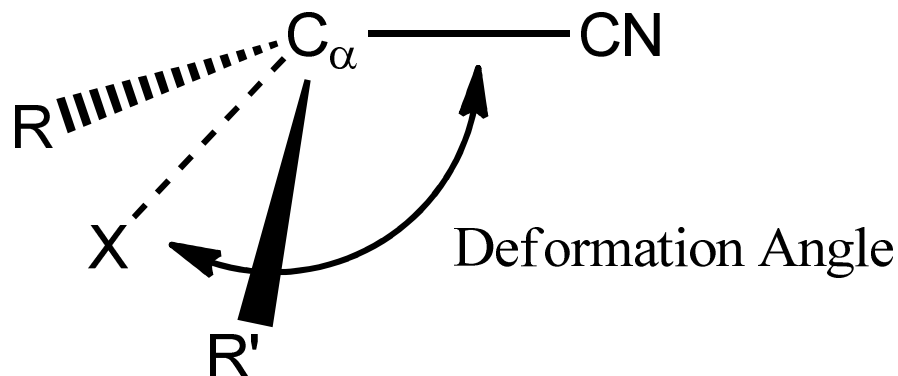


Figure 3.1. Deformation angle around the α -carbon of the nitrile anion

It is possible that the unexpected conservation of stereochemistry seen in some reactions involving nitrile anions⁷ could be attributable to distortion of the expected sp^2 hybridization of the negatively charged species. Fleming and coworkers have recently reported that cuprated nitrile anions showed significantly higher levels of stereoselectivity than analogous lithiated nitrile anions, which they pointed out could imply that the copper complexes were metalated at the carbon in the alpha position relative to the nitrile group, and the lithium complexes were metalated at the nitrile nitrogen.^{19, 20} These results further increase the desire to understand computationally both the preferred metalation point and degree of deformation from the expected sp^2 hybridization of the carbon adjacent to the nitrile group.

In order to maximize the effectiveness this investigation several factors were considered during the development of an appropriate computational protocol for these studies. Based on previously reported research²¹ a simple model chemistry based on Hartree-Fock (HF) theory²²⁻²⁷ with a relatively small basis set was able to generate structures which were in good agreement with experimentally determined structures. Additional studies on the structure of organometallic compounds have confirmed that the agreement of calculated and measured structure is not very sensitive to the size of the basis sets used in the computational treatment of the system^{28, 29}. For these reasons, the same model chemistries were used for this investigation as was used in a previous chapter of this dissertation which investigated the solvation of metal cations.³⁰ That work and the reports of others^{21, 30-33} have shown that in some cases it can be misleading to treat solvation as a continuum of polarity around a structure as opposed to explicitly modeling

the solvation and including those solvent molecules in the electronic structure calculations.

3.2 Computational Methods

All geometry optimizations, frequency, and natural bond order calculations were performed using Gaussian 03.³⁴ Geometry optimizations and frequency calculations were performed using either Hartree-Fock (HF), frozen-core, second-order Møller-Plesset perturbation theory³⁵⁻³⁷ (MP2) or the Becke three-parameter exchange functional³⁸ and the nonlocal correlation functional of Lee, Yang, and Parr³⁹ (B3LYP). These optimization and frequency calculations were carried out using the 6-31+G(d) basis set. For the sake of comparison a single optimization calculation was performed using MP2 with the much larger 6-311++G(d,p) basis, as was a single optimization calculation using third-order Møller-Plesset perturbation theory³⁵⁻³⁷ and the 6-31+G(d) basis set. All optimized geometries were confirmed to be energy minima by vibrational frequency analysis, in which no imaginary vibrational frequencies were observed. Continuum and explicit-continuum solvation single point energy calculations were carried out using the polarizable continuum model (PCM) which has been previously described in detail^{40, 41}. The solvents and dielectric constants used in this study are DME ($\epsilon=5.0$), and THF ($\epsilon=7.2$). Again, these single point energy calculations were carried out using the optimized structure calculated at the corresponding level theory with the 6-31+G(d) and no solvent continuum.

3.3 Results and Discussions

3.3.1 Comparison of Model Chemistries

As reported in Chapter 2, three model chemistries were used to calculate dissociation enthalpies for cation/ dimethyl ether (DME) complexes, and of the three, the B3LYP/6-31+G(d) model chemistry was found to give the better agreement with experimentally measured data, than the HF/6-31+G(d) or MP2/6-31+G(d) model chemistries.³⁰ Expanding upon those results, the calculated values for several key structural features of complexes of DME, one of five cations, Li⁺, Na⁺, K⁺, and Cu⁺ and an acetonitrile anion are shown in Table 3.1. The analogous THF complexes are shown in Table 3.2.

Species	Model Chemistry	Geometry around Cation	Average M+: O Distance	M+:AN- Distance	N:C(n) Bond Length	C(n):C(α) Bond Length	Average O : O Angle	Average O : N Angle	M+:N:C(n): Angle	Deformation Angle θ
AN ⁻	HF/6-31+G(d)	N/A			1.162	1.395				146.5
	MP2/6-31+G(d)	N/A			1.201	1.399				147.0
	B3LYP/6-31+G(d)	N/A			1.191	1.387				152.0
Li ⁺ / AN ⁻ (DME) ₃	HF/6-31+G(d)	Tetrahedral	2.024	1.889	1.173	1.353	107.9	112.4	168.4	172.5
	MP2/6-31+G(d)	Tetrahedral	1.925	1.936	1.210	1.373	107.0	114.4	105.6	152.2
	B3LYP/6-31+G(d)	Tetrahedral	2.015	1.876	1.200	1.354	108.5	111.2	170.7	172.4
Na ⁺ / AN ⁻ (DME) ₃	HF/6-31+G(d)	Tetrahedral	2.348	2.250	1.173	1.356	110.4	106.9	167.1	169.9
	MP2/6-31+G(d)	Tetrahedral	2.291	2.575	1.203	1.403	99.9	118.8	69.0	137.0
	B3LYP/6-31+G(d)	Tetrahedral	2.405	2.219	1.200	1.356	111.3	104.2	167.6	172.1
K ⁺ / AN ⁻ (DME) ₃	HF/6-31+G(d)	Tetrahedral	2.800	2.633	1.172	1.361	113.2	90.2	151.9	168.2
	MP2/6-31+G(d)	Tetrahedral	2.689	2.886	1.203	1.398	117.0	76.0	73.7	138.4
	B3LYP/6-31+G(d)	Tetrahedral	2.766	2.612	1.200	1.360	112.6	88.2	150.8	168.0
Cu ⁺ / AN ⁻ (DME) ₃	HF/6-31+G(d)	Tetrahedral	2.348	1.988	1.175	1.351	107.9	111.3	141.9	169.8
	MP2/6-31+G(d)	Tetrahedral	2.257	1.775	1.204	1.353	109.8	97.6	175.2	179.2
	B3LYP/6-31+G(d)	Planar	2.988	1.829	1.207	1.341	125.8	96.0	139.0	172.1

Table 3.1. Calculated values for selected structural features of cation / DME complexes using various model chemistries

Species	Model Chemistry	Geometry around Cation	Average M+: O Distance	M+:AN-Distance	N:C(n) Bond Length	C(n):C(o) Bond Length	Average O : O Angle	Average O : N Angle	M+:N:C(n): Angle	Deformation Angle θ
AN	HF/6-31+G(d)	N/A			1.162	1.395				146.5
	MP2/6-31+G(d)	N/A			1.201	1.399				147.0
	B3LYP/6-31+G(d)	N/A			1.191	1.387				152.0
Li ⁺ / AN ⁻ (THF) ₃	HF/6-31+G(d)	Tetrahedral	2.009	1.912	1.172	1.356	108.9	110.5	163.6	175.2
	MP2/6-31+G(d)	Tetrahedral	1.919	1.915	1.210	1.366	109.0	110.3	130.4	158.4
	B3LYP/6-31+G(d)	Tetrahedral	2.004	1.908	1.200	1.357	109.1	110.2	155.1	171.7
Na ⁺ / AN ⁻ (THF) ₃	HF/6-31+G(d)	Tetrahedral	2.335	2.256	1.172	1.359	110.8	106.3	151.5	171.6
	MP2/6-31+G(d)	Tetrahedral	2.311	2.626	1.204	1.399	109.8	92.6	68.1	138.9
	B3LYP/6-31+G(d)	Tetrahedral	2.323	2.259	1.199	1.361	111.2	105.0	138.1	166.9
K ⁺ / AN ⁻ (THF) ₃	HF/6-31+G(d)	Tetrahedral	2.781	2.659	1.171	1.364	112.6	94.6	143.6	166.7
	MP2/6-31+G(d)	Tetrahedral	2.638	2.832	1.203	1.353	120.0	99.8	78.2	138.3
	B3LYP/6-31+G(d)	Tetrahedral	2.741	2.646	1.198	1.365	112.2	93.8	131.3	163.0
Cu ⁺ / AN ⁻ (THF) ₃	HF/6-31+G(d)	Tetrahedral	2.310	2.014	1.174	1.352	105.7	116.1	140.0	172.2
	MP2/6-31+G(d)	Tetrahedral	2.320	1.769	1.203	1.353	90.5	124.1	178.4	170.0
	B3LYP/6-31+G(d)	Planar	3.009	1.830	1.206	1.342	83.0	142.4	138.9	176.9

Table 3.2. Calculated values for selected structural features of cation / THF complexes using various model chemistries

The results were generated using all three of the previously mentioned model chemistries, but as noted the results calculated using B3LYP/6-31+G(d) are likely to best represent the actual electronic and molecular structure of the complexes. The results obtained from calculations using the B3LYP/6-31+G(d) and HF/6-31+G(d) model chemistries showed good agreement with each other but very poor agreement with values calculated using the MP2/6-31+G(d) model chemistry. It is very likely that the deficiencies of the MP2/6-31+G(d) model chemistry in accurately modeling the cation / solvent systems are the same deficiencies that are causing these MP2/6-31+G(d) results to significantly disagree with the results from the other two model chemistries. This surprising deficiency of the MP2/6-31+G(d) system is likely explained by an overestimation of the contribution of electron-electron correlation. It is possible that the use of a higher order perturbation theory such as MP3 or MP4, or the use of a larger basis set, might overcome this overestimation. In order to gain insight into this possibility, the structure of the Na⁺ / Acetonitrile⁻ / (DME)₃ system was calculated using the MP3/6-31+G(d) model chemistry and the MP2/6-31++G(d,p) model chemistry. The results of

these calculations are shown in Table 3.3, and are very similar to the results obtained using the MP2/6-31+G(d) model chemistry, suggesting that this increase in the precision of the model chemistry is not sufficient to overcome the over overestimation of the contribution of electron-electron correlation. Further extension of this investigation to still higher order Møller-Plesset perturbation calculations, or still larger basis sets would be prohibitively expensive, in terms of computational resources.

Species	Model Chemistry	Average M+: O Distance	M+:AN- Distance	N:C(n) Bond Length	C(n):C(α) Bond Length	Average O : O Angle	Average O : N Angle	M+:N:C(n): Angle	N:C(n):C(α) Bond Angle	Deformation Angle θ
Na+An-	MP2/6-31+G(d)	2.291	2.575	1.203	1.403	99.9	118.8	69.0	167.4	137.0
	MP2/6-311++G(d,p)	2.327	2.770	1.195	1.407	94.0	113.0	62.8	168.4	135.9
	MP3/6-31+G(d)	2.414	2.751	1.183	1.408	94.8	116.3	64.4	168.3	137.7

Table 3.3. Calculated values for selected structural features of cation / THF complexes using various levels of Møller-Plesset perturbation theory and sizes of basis set

When viewing the data obtained from the HF/6-31+G(d), and most importantly the B3LYP/6-31+G(d) calculations, a trend clearly emerges showing a decrease in the deformation angle (in other words more deformation from the expected planar geometry) around the α -carbon of the nitrile anion as the size of the counter ion increases, with the largest angles being observed in the case of no cation being present. This behavior is shown in Figure 3.2 (DME solvation) and Figure 3.3 (THF solvation), and suggests that the proximity of the positively charged species to the nitrile anion is a key factor in determining how strongly the anion is deformed from the expected sp^2 hybridization of the α -carbon.

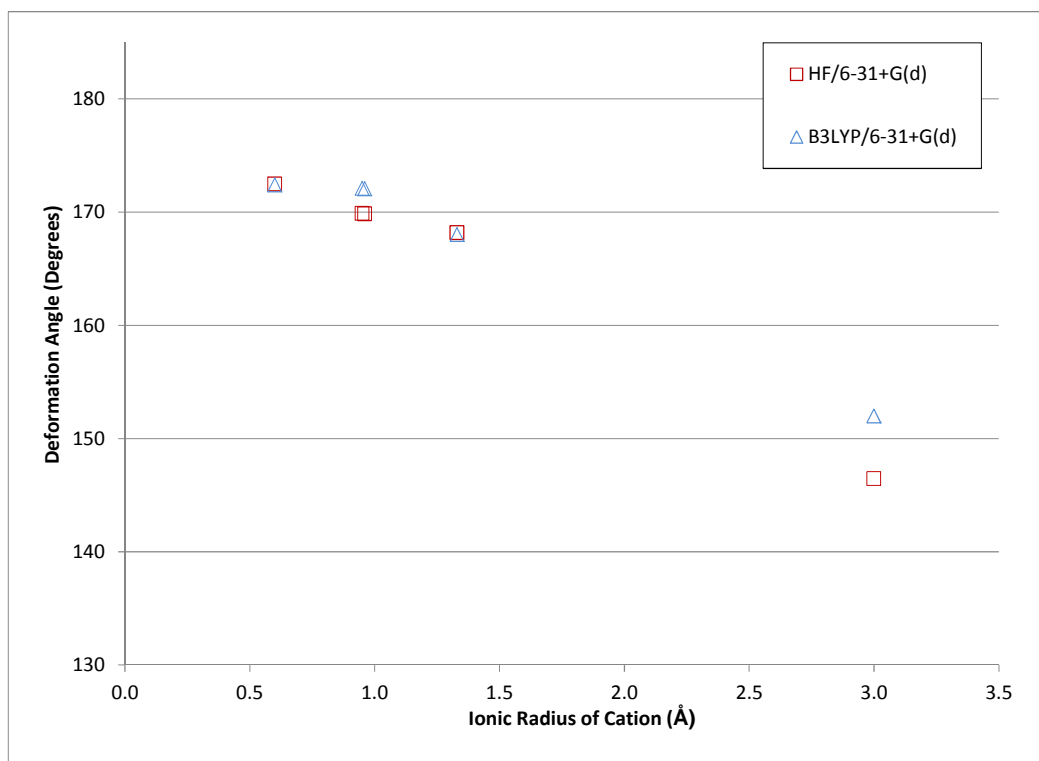


Figure 3.2. Deformation angle around the α -carbon of the nitrile anion (calculated at B3LYP/6-31+G(d) and HF/6-31+G(d)) as a function of the covalent radius of the counter ion present in the DME complex

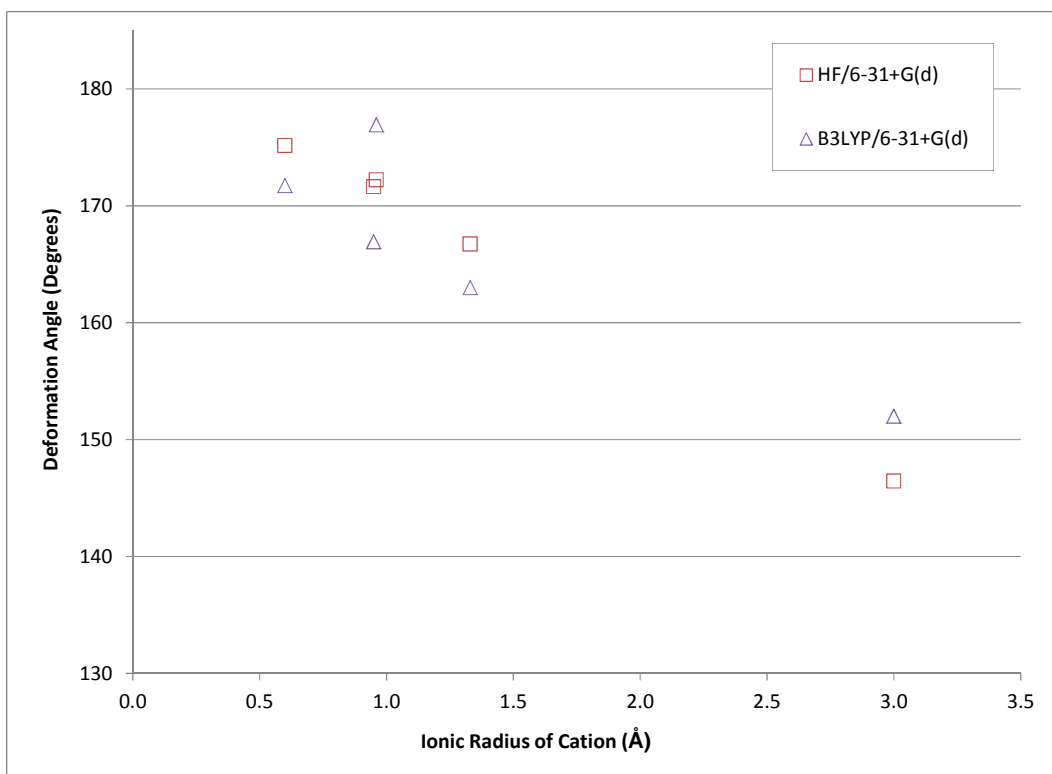


Figure 3.3. Deformation angle around the α -carbon of the nitrile anion (calculated at B3LYP/6-31+G(d) and HF/6-31+G(d)) as a function of the covalent radius of the counter ion present in the THF complex

Figures 3.2 and 3.3 show that deformation angle trends toward decreasing values as the size of the cation increases, continue to a minimum value in the case of infinite separation of the cation from the nitrile anion. The data points in these figures corresponding to the ionic radius Cu^+ shows a deviation from this trend, especially for the value calculated at B3LYP/6-31+G(d). It is likely that this behavior can be explained by the effects of $4s$ - $3d\sigma$ hybridization of copper ion as previously reported by Bauschlicher and co-workers⁴². This effect would be seen much more clearly in calculations using a model chemistry that includes electron correlation, such as B3LYP, than it would be in a

calculations a model chemistry which does not include electron correlation, such as HF, which is in agreement with the calculated results.

In the cases of both the DME and the THF calculations, the results obtained from the HF/6-31+G(d) and B3LYP/6-31+G(d) model chemistries agreed fairly well with each other. This is shown by combining and examining the deformation angles of all structures (regardless of cation) for each combination of solvent and theory. Figure 3.4 shows the result of this summary of the data. Figure 3.4 also shows that the average deformation angles were, overall, very similar for both the DME and THF complexes. The green lines in the figure show the mean value for the two different levels of theory, and indicate that there is no significant difference in the two sets of results. This could suggest that either the hybridization of the α -carbon in the nitrile anion is not affected by the nature of the solvent, or more likely it suggests that any effect on hybridization would be driven by the polarity of the solvent as opposed to the size of the solvent molecule. In this case the similarity of the polarities of THF and DME would explain the lack of an effect of solvent on deformation angle.

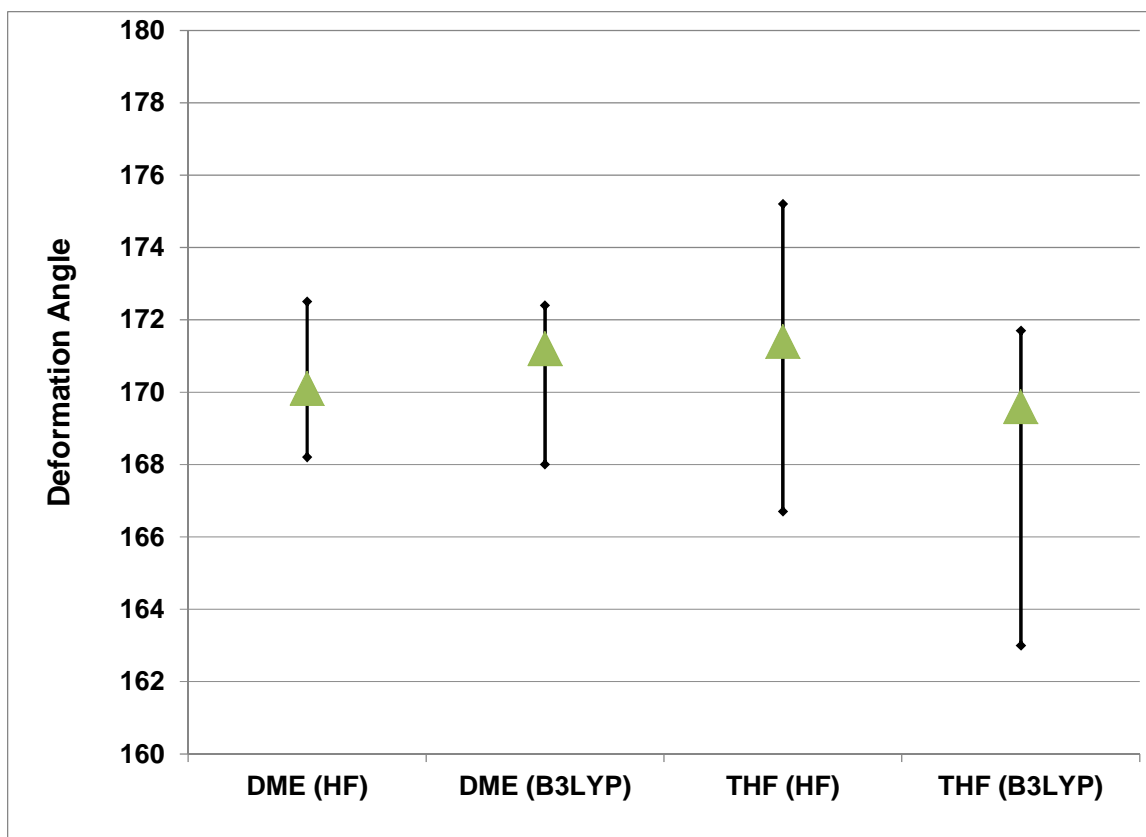


Figure 3.4. Deformation angle around the α -carbon of the nitrile anion (calculated at B3LYP/6-31+G(d) and HF/6-31+G(d)) as a function of model chemistry and solvent. The lines show the range of values, and the triangles show the mean values of deformation angle for all cations using that specific solvent and theory combination.

3.3.2 Determination of Carbon or Nitrogen Metalation for DME Complexes

One of the most interesting questions being probed by this work is which metalation site, nitrogen, as shown in Figure 3.5(a), or carbon, as shown in Figure 3.5(b), is energetically favored, and how does that preference vary as a function of the cation or solvent components of the solvation complex change.

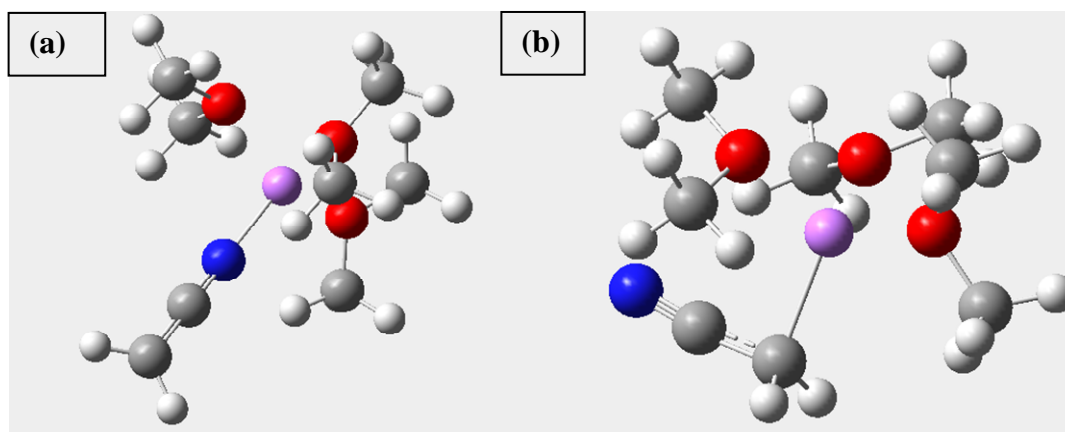


Figure 3.5. (a) Nitrogen metalated lithium / acetonitrile complex, explicitly solvated with DME. (b) Carbon metalated lithium / acetonitrile complex, explicitly solvated with DME. White spheres represent hydrogen atoms, gray spheres represent carbon atoms, red spheres represent oxygen atoms, the blue sphere represents a nitrogen atom, and the purple sphere represents a Li^+ cation.

The previously discussed results are all based on the starting point assumption that in all cases the metal cation is complexed to the nitrile anion at the nitrogen atom. In order to take a closer look at the question of metalation site the previous calculations on the DME solvated species were repeated using the preferred B3LYP/6-31+G(d) model chemistry, and the assumption that the cation was in fact complexed at that nitrile groups α -carbon atom. In addition to repeating these calculations, additional calculations were performed for both the carbon and nitrogen metalated starting points in which either just continuum solvation or continuum / explicit hybrid solvation used. The results of these calculations are compared with the original nitrogen metalated results in Table 3.4.

Species	Carbon or Nitrogen Metallated	Geometry around Cation	Electronic Energy (Hartrees)	C α - CN Bond Length	C-N Bond Length	Deformation Angle θ
Li ⁺ / AN ⁻	Nitrogen	N/A	-139.684	1.343	1.204	179.9
	Carbon	N/A	-139.687	1.393	1.192	145.1
Na ⁺ / AN ⁻	Nitrogen	N/A	-294.447	1.349	1.202	179.9
	Carbon	N/A	-294.449	1.404	1.187	141.1
K ⁺ / AN ⁻	Nitrogen	N/A	-732.056	1.354	1.202	180.0
	Carbon	N/A	-732.064	1.395	1.189	142.2
Cu ⁺ / AN ⁻	Nitrogen	N/A	-1772.472	1.336	1.213	178.9
	Carbon	N/A	-1772.493	1.444	1.166	129.0
MgCl ⁺ / AN ⁻	Nitrogen	N/A	-792.521	1.330	1.207	179.9
	Carbon	N/A	-792.521	1.446	1.167	126.5
Li ⁺ / AN ⁻ (DME) ₃	Nitrogen	Tetrahedral	-604.858	1.354	1.200	172.4
	Carbon	Tetrahedral	-604.854	1.415	1.180	131.6
Na ⁺ / AN ⁻ (DME) ₃	Nitrogen	Trig bipy	-759.606	1.356	1.200	172.1
	Carbon	Tetrahedral	-759.607	1.398	1.187	140.5
K ⁺ / AN ⁻ (DME) ₃	Nitrogen	Trig bipy	-1197.206	1.360	1.200	168.0
	Carbon	Tetrahedral	-1197.209	1.391	1.190	142.5
Cu ⁺ / AN ⁻ (DME) ₃	Nitrogen	Planar	-2237.628	1.341	1.207	172.1
	Carbon	Planar	-2237.644	1.445	1.169	124.9
MgCl ⁺ / AN ⁻ (DME) ₂	Nitrogen	Tetrahedral	-1102.660	1.341	1.202	175.0
	Carbon	Tetrahedral	-1102.661	1.433	1.172	126.7
Li ⁺ / AN ⁻ (PCM-DME)	Nitrogen	N/A	-139.744	1.343	1.204	179.9
	Carbon	N/A	-139.733	1.393	1.192	145.1
Na ⁺ / AN ⁻ (PCM-DME)	Nitrogen	N/A	-294.504	1.349	1.202	179.9
	Carbon	N/A	-294.498	1.404	1.187	141.1
K ⁺ / AN ⁻ (PCM-DME)	Nitrogen	N/A	-732.109	1.354	1.202	180.0
	Carbon	N/A	-732.107	1.395	1.189	142.2
Cu ⁺ / AN ⁻ (PCM-DME)	Nitrogen	N/A	-1772.489	1.336	1.213	178.9
	Carbon	N/A	-1772.513	1.444	1.166	129.0
MgCl ⁺ / AN ⁻ (PCM-DME)	Nitrogen	N/A	-792.578	1.330	1.207	179.9
	Carbon	N/A	-792.586	1.446	1.167	126.5
Li ⁺ / AN ⁻ (DME) ₃ / (PCM-DME)	Nitrogen	Tetrahedral	-604.878	1.354	1.200	172.4
	Carbon	Tetrahedral	-604.873	1.415	1.180	131.6
Na ⁺ / AN ⁻ (DME) ₃ / (PCM-DME)	Nitrogen	Trig bipy	-759.631	1.356	1.200	172.1
	Carbon	Tetrahedral	-759.626	1.398	1.187	140.5
K ⁺ / AN ⁻ (DME) ₃ / (PCM-DME)	Nitrogen	Trig bipy	-1197.232	1.360	1.200	168.0
	Carbon	Tetrahedral	-1197.231	1.391	1.190	142.5
Cu ⁺ / AN ⁻ (DME) ₃ / (PCM-DME)	Nitrogen	Planar	-2237.642	1.341	1.207	172.1
	Carbon	Planar	-2237.659	1.445	1.169	124.9
MgCl ⁺ / AN ⁻ (DME) ₂ / (PCM-DME)	Nitrogen	Tetrahedral	-1102.686	1.341	1.202	175.0
	Carbon	Tetrahedral	-1102.687	1.433	1.172	126.7

Table 3.4. Calculated values for selected structural features and electronic energy of cation / DME complexes using various types of solvation models and the B3LYP/6-31+G(d) model chemistry

Regardless of solvation model used, significantly more deviation from planar geometry around the α -carbon is shown for the carbon metallated complexes. When no

solvation at all was used, the results strongly favored carbon metalated structures over the nitrogen metalated structures. In the case of the explicit solvation, only the smallest cation (Li^+) showed an energetic preference for the nitrogen metalated geometry. Interestingly the continuum only solvation calculations showed a preference for nitrogen metalated structures for the lithium, sodium, and potassium cation based systems. This trend in the results is also seen exactly in the continuum / explicit hybrid solvation calculations, suggesting that the contribution of the continuum solvation strongly outweighs the contribution of the more realistic explicit solvation model. In terms of the explicit solvation only calculations, the calculated preference of the lithium cation for nitrogen metalation and of the larger cations for carbon metalation strongly supports the experimental data reported by Fleming and Carlier.^{19, 20, 43} Given the stronger preference for carbon metalation in non-lithium systems, and the higher degree of deformation in those carbon metalated systems, it naturally follows that, as observed by Fleming, copper based complexes would show a greater retention of stereochemistry than the analogous nitrogen metalated lithium based complexes.

As has been observed in numerous instances during this dissertation investigation, copper cation complexes have shown significantly different behavior from the other cations being studied. These results continue that trend, with the notable difference in the behavior of the copper complexes being the differences in optimized geometry. The other cation complexes show tetrahedral, or distorted tetrahedral geometries. The copper complexes, however, invariably show square planar geometries as shown in Figure 3.6.

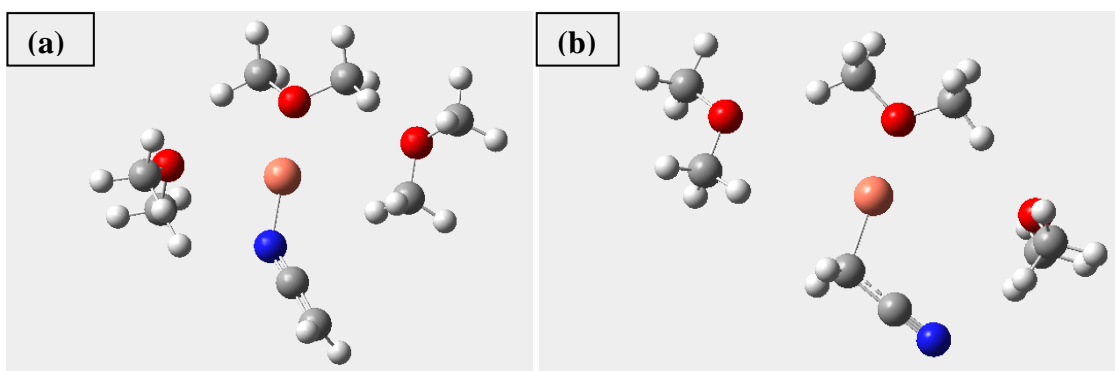


Figure 3.6. (a) Nitrogen metalated copper / acetonitrile complex, explicitly solvated with DME. (b) Carbon metalated copper / acetonitrile complex, explicitly solvated with DME. White spheres represent hydrogen atoms, gray spheres represent carbon atoms, red spheres represent oxygen atoms, the blue sphere represents a nitrogen atom, and the pink sphere represents a Cu^+ cation.

3.3.3 Determination of Carbon or Nitrogen Metalation for THF Complexes

The THF calculations that are analogous to the DME results reported in previous section are shown in Table 3.5.

Species	Carbon or Nitrogen Metallated	Geometry around Cation	Electronic Energy (Hartrees)	C α - CN Bond Length	C-N Bond Length	Deformation Angle θ
Li ⁺ / AN ⁻	Nitrogen	N/A	-139.684	1.343	1.204	179.9
	Carbon	N/A	-139.687	1.393	1.192	145.1
Na ⁺ / AN ⁻	Nitrogen	N/A	-294.447	1.349	1.202	179.9
	Carbon	N/A	-294.449	1.404	1.187	141.1
K ⁺ / AN ⁻	Nitrogen	N/A	-732.056	1.354	1.202	180.0
	Carbon	N/A	-732.064	1.395	1.189	142.2
Cu ⁺ / AN ⁻	Nitrogen	N/A	-1772.472	1.336	1.213	178.9
	Carbon	N/A	-1772.493	1.444	1.166	129.0
MgCl ⁺ / AN ⁻	Nitrogen	N/A	-792.521	1.330	1.207	179.9
	Carbon	N/A	-792.521	1.446	1.167	126.5
Li ⁺ / AN ⁻ (THF) ₃	Nitrogen	Tetrahedral	-837.142	1.357	1.200	171.7
	Carbon	Only 2 THF	-837.128	1.396	1.187	N/A
Na ⁺ / AN ⁻ (THF) ₃	Nitrogen	Tetrahedral	-991.890	1.361	1.199	166.9
	Carbon	Only 2 THF	-991.877	1.413	1.181	N/A
K ⁺ / AN ⁻ (THF) ₃	Nitrogen	Tetrahedral	-1429.488	1.365	1.198	163.0
	Carbon	Tetrahedral	-1429.489	1.390	1.190	144.8
Cu ⁺ / AN ⁻ (THF) ₃	Nitrogen	Planar	-2469.911	1.342	1.206	176.9
	Carbon	Planar	-2469.927	1.445	1.169	125.0
MgCl ⁺ / AN ⁻ (THF) ₂	Nitrogen	Tetrahedral	-1257.519	1.343	1.202	175.9
	Carbon	Tetrahedral	-1257.520	1.434	1.172	127.1
Li ⁺ / AN ⁻ (PCM-THF)	Nitrogen	N/A	-139.744	1.343	1.204	179.9
	Carbon	N/A	-139.733	1.393	1.192	145.1
Na ⁺ / AN ⁻ (PCM-THF)	Nitrogen	N/A	-294.504	1.349	1.202	179.9
	Carbon	N/A	-294.498	1.404	1.187	141.1
K ⁺ / AN ⁻ (PCM-THF)	Nitrogen	N/A	-732.109	1.354	1.202	180.0
	Carbon	N/A	-732.107	1.395	1.189	142.2
Cu ⁺ / AN ⁻ (PCM-THF)	Nitrogen	N/A	-1772.489	1.336	1.213	178.9
	Carbon	N/A	-1772.513	1.444	1.166	129.0
MgCl ⁺ / AN ⁻ (PCM-THF)	Nitrogen	N/A	-792.578	1.330	1.207	179.9
	Carbon	N/A	-792.586	1.446	1.167	126.5
Li ⁺ / AN ⁻ (THF) ₃ / (PCM-THF)	Nitrogen	Tetrahedral	-837.159	1.357	1.200	171.7
	Carbon	Only 2 THF	-837.146	1.396	1.187	N/A
Na ⁺ / AN ⁻ (THF) ₃ / (PCM-THF)	Nitrogen	Tetrahedral	-991.913	1.361	1.199	166.9
	Carbon	Only 2 THF	-991.904	1.413	1.181	N/A
K ⁺ / AN ⁻ (THF) ₃ / (PCM-THF)	Nitrogen	Tetrahedral	-1429.513	1.365	1.198	163.0
	Carbon	Tetrahedral	-1429.511	1.390	1.190	144.8
Cu ⁺ / AN ⁻ (THF) ₃ / (PCM-THF)	Nitrogen	Planar	-2469.925	1.342	1.206	176.9
	Carbon	Planar	-2469.942	1.445	1.169	125.0
MgCl ⁺ / AN ⁻ (THF) ₂ / (PCM-THF)	Nitrogen	Tetrahedral	-1257.545	1.343	1.202	175.9
	Carbon	Tetrahedral	-1257.547	1.434	1.172	127.1

Table 3.5. Calculated values for selected structural features and electronic energy of cation / THF complexes using various types of solvation models and the B3LYP/6-31+G(d) model chemistry.

As in the case of DME, all THF calculations, regardless of solvation model used, showed significantly more deviation from planar geometry around the α -carbon is shown

for the carbon metalated complexes than for the nitrogen metalated complexes. In the case of the explicit solvation, the two smallest cations (Li^+ and Na^+) showed an energetic preference for the nitrogen metalated geometry which is strongly influenced by the fact that the optimization calculations indicated that in the case of the carbon metalated complexes the first solvation sphere around the cation decreased from four ligands to three, as shown in Figure 3.7. This reduction of the number of ligands decreases the overall stabilization of the complex by solvation, resulting in strongly, energetically unfavored carbon metalated complexes. This behavior was not seen in the case of DME solvation due to the small size of that solvent molecule relative to the THF solvent molecule. It is also interesting to note that this behavior is seen only in the case of carbon metalation and not in the case of nitrogen metalation. This reinforces the fact that in the carbon metalated structures the cation interacts with not just the α -carbon, but also the nitrile carbon and nitrogen, resulting in a significant larger volume of interaction between the cation and the nitrile anion in the case of carbon metalation.

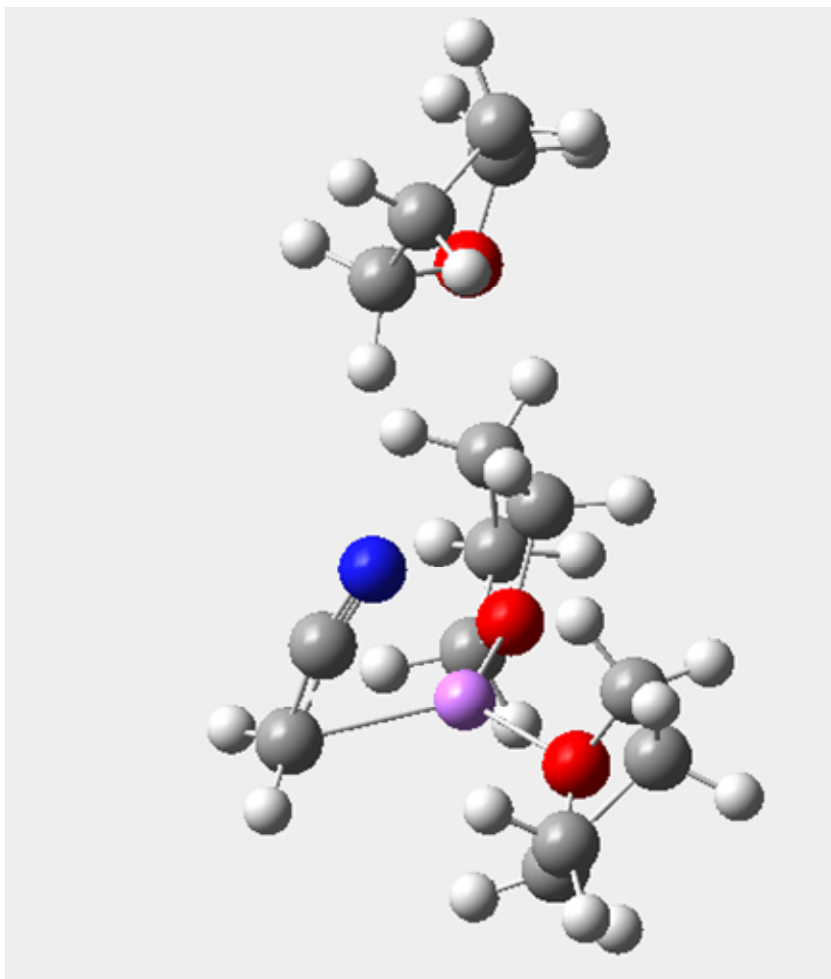


Figure 3.7. Carbon metalated lithium / acetonitrile complex, explicitly solvated with THF. White spheres represent hydrogen atoms, gray spheres represents carbon atoms, red spheres represent oxygen atoms, the blue sphere represents a nitrogen atom, and the purple sphere represents a Li^+ cation.

As in the case of the DME calculations, the continuum only solvation calculations showed a preference for nitrogen metalated structures for the lithium, sodium, and potassium cation based systems. An interesting artifact of the Gaussian Program Suite³⁴ can be seen in this data. The continuum only solvation calculations yielded the exact same results for both DME and THF solvation. Despite the fact that two different dielectric constants were used for these calculations, 5.0 for DME and 7.52

for THF, the small difference in the two values was not large enough to impact the results of the calculation. This strongly reinforces the conclusion reached in Chapter 2 that continuum only solvation is insufficient to appropriately study systems such as these, and explicit solvation must be employed to produce meaningful results. Again as in the case of DME the trend for the continuum only calculations is repeated in the continuum / explicit hybrid solvation calculations. However, by building a hybrid system which includes a contribution from the explicit solvation model the data is distinct between the DME and THF calculations using the hybrid system. This not only suggests that the contribution of the continuum solvation contributes significantly to hybrid system, but it also suggests that the hybrid system may in fact be less accurate than the explicit only model, based on the significant influence of the much less realistic and inaccurate continuum solvation model. It again is clear from this data that the stronger preference for carbon metalation in copper and magnesium chloride systems, and the higher degree of deformation in those carbon metalated systems, it naturally follows that, as observed by Fleming, copper based complexes would show a greater retention of stereochemistry than the analogous nitrogen metalated lithium based complexes.

3.3.4 Natural Bond Order Analysis

A summary of the results discussed in sections 3.3.2 and 3.3.3 is provided in Table 3.6 below.

Cation	No solvation	DME			THF		
		<u>Continuum Only</u>	<u>Explicit Only</u>	<u>Explicit / Continuum</u>	<u>Continuum Only</u>	<u>Explicit Only</u>	<u>Explicit / Continuum</u>
Li	Carbon	Nitrogen	Nitrogen	Nitrogen	Nitrogen	Nitrogen	Nitrogen
Na	Carbon	Nitrogen	Carbon	Nitrogen	Nitrogen	Nitrogen	Nitrogen
K	Carbon	Nitrogen	Carbon	Nitrogen	Nitrogen	Carbon	Nitrogen
Cu	Carbon	Carbon	Carbon	Carbon	Carbon	Carbon	Carbon
MgCl	Carbon	Carbon	Carbon	Carbon	Carbon	Carbon	Carbon

Table 3.6. Energetically favored metalation site for each cation under various solvation conditions.

There is an obvious trend in the data that suggests that the smaller the cation, the more likely the resulting complex is to adopt a nitrogen metalated structure. However, the fact that the compact Cu(I) cation shows an exclusive preference for carbon metalation cast substantial doubt on the accuracy of the trend. In addition, this observation does not provide significant insight into why the smaller cations show a preference for nitrogen metalation. In an effort to address these two issues, Natural Bond Order Analysis⁴⁴ (NBO) was used to further explore this data. A key observation that was made in the review the NBO data was the difference in natural charge on the various atoms of the cation/anion complexes depending on the metalation point of the cation. This data is summarized for DME complexes in Table 3.7 and for THF complexes in Table 3.8. The natural charges on the cation in each calculation was used along with the calculated volume of each of the cations to calculate the natural charge density on each of the cations. This data is also shown in Tables 3.8 and 3.9.

Species	Carbon or Nitrogen Metallated	Electronic Energy (Hartrees)	Natural Charge				Calculated Charge Density on Cation
			Metal Ion	Nitrile Nitrogen	Nitrile Carbon	α -Carbon	
Li ⁺ / AN ⁻	Nitrogen	-139.684	0.894	-0.935	0.388	-0.837	0.094
	Carbon	-139.687	0.843	-0.577	0.193	-0.971	0.088
Na ⁺ / AN ⁻	Nitrogen	-294.447	0.942	-0.905	0.358	-0.874	0.047
	Carbon	-294.449	0.900	-0.570	0.205	-1.030	0.045
K ⁺ / AN ⁻	Nitrogen	-732.056	0.968	-0.887	0.345	-0.896	0.023
	Carbon	-732.064	0.937	-0.619	0.224	-1.022	0.022
Cu ⁺ / AN ⁻	Nitrogen	-1772.472	0.597	-0.732	0.335	-0.708	0.073
	Carbon	-1772.493	0.523	-0.365	0.247	-0.952	0.064
MgCl ⁺ / AN ⁻	Nitrogen	-792.521	1.506	-0.982	0.439	-0.781	0.018
	Carbon	-792.521	1.418	-0.372	0.242	-1.156	0.016
Li ⁺ / AN ⁻ (DME) ₃	Nitrogen	-604.858	0.610	-0.757	0.340	-0.896	0.064
	Carbon	-604.854	0.646	-0.532	0.262	-1.068	0.068
Na ⁺ / AN ⁻ (DME) ₃	Nitrogen	-759.606	0.785	-0.783	0.317	-0.907	0.040
	Carbon	-759.607	0.748	-0.574	0.229	-0.998	0.038
K ⁺ / AN ⁻ (DME) ₃	Nitrogen	-1197.206	0.875	-0.782	0.298	-0.919	0.020
	Carbon	-1197.209	0.828	-0.620	0.246	-0.988	0.019
Cu ⁺ / AN ⁻ (DME) ₃	Nitrogen	-2237.628	0.633	-0.782	0.356	-0.826	0.077
	Carbon	-2237.644	0.545	-0.439	0.287	-1.022	0.066
MgCl ⁺ / AN ⁻ (DME) ₂	Nitrogen	-1102.660	1.376	-0.871	0.395	-0.834	0.015
	Carbon	-1102.661	1.352	-0.464	0.276	-1.135	0.014
Li ⁺ / AN ⁻ (PCM-DME)	Nitrogen	-139.744	0.949	-0.840	0.328	-0.922	0.099
	Carbon	-139.733	0.906	-0.640	0.199	-0.963	0.095
Na ⁺ / AN ⁻ (PCM-DME)	Nitrogen	-294.504	0.977	-0.808	0.304	-0.950	0.049
	Carbon	-294.498	0.953	-0.641	0.221	-1.017	0.048
K ⁺ / AN ⁻ (PCM-DME)	Nitrogen	-732.109	0.983	-0.788	0.291	-0.962	0.023
	Carbon	-732.107	0.963	-0.671	0.237	-1.004	0.022
Cu ⁺ / AN ⁻ (PCM-DME)	Nitrogen	-1772.489	0.788	-0.815	0.332	-0.813	0.096
	Carbon	-1772.513	0.660	-0.494	0.302	-1.024	0.080
MgCl ⁺ / AN ⁻ (PCM-DME)	Nitrogen	-792.578	1.687	-0.913	0.393	-0.864	0.020
	Carbon	-792.586	1.640	-0.524	0.309	-1.165	0.019
Li ⁺ / AN ⁻ (DME) ₃ / (PCM-DME)	Nitrogen	-604.878	0.620	-0.706	0.315	-0.947	0.065
	Carbon	-604.873	0.664	-0.602	0.281	-1.050	0.070
Na ⁺ / AN ⁻ (DME) ₃ / (PCM-DME)	Nitrogen	-759.631	0.803	-0.718	0.284	-0.962	0.040
	Carbon	-759.626	0.770	-0.614	0.230	-0.986	0.039
K ⁺ / AN ⁻ (DME) ₃ / (PCM-DME)	Nitrogen	-1197.232	0.886	-0.717	0.272	-0.974	0.021
	Carbon	-1197.231	0.845	-0.649	0.242	-0.978	0.020
Cu ⁺ / AN ⁻ (DME) ₃ / (PCM-DME)	Nitrogen	-2237.642	0.666	-0.775	0.341	-0.866	0.081
	Carbon	-2237.659	0.577	-0.512	0.316	-1.033	0.070
MgCl ⁺ / AN ⁻ (DME) ₂ / (PCM-DME)	Nitrogen	-1102.686	1.435	-0.829	0.375	-0.883	0.015
	Carbon	-1102.687	1.416	-0.536	0.310	-1.129	0.015

Table 3.7. Electronic energies, natural charges, and cation natural charge densities for DME solvated complexes using various solvation models.

Species	Carbon or Nitrogen Metallated	Electronic Energy (Hartrees)	Natural Charge				Calculated Charge Density on Cation
			Metal Ion	Nitrile Nitrogen	Nitrile Carbon	α -Carbon	
Li ⁺ / AN ⁻	Nitrogen	-139.684	0.894	-0.935	0.388	-0.837	0.094
	Carbon	-139.687	0.843	-0.577	0.193	-0.971	0.088
Na ⁺ / AN ⁻	Nitrogen	-294.447	0.942	-0.905	0.358	-0.874	0.047
	Carbon	-294.449	0.900	-0.570	0.205	-1.030	0.045
K ⁺ / AN ⁻	Nitrogen	-732.056	0.968	-0.887	0.345	-0.896	0.023
	Carbon	-732.064	0.937	-0.619	0.224	-1.022	0.022
Cu ⁺ / AN ⁻	Nitrogen	-1772.472	0.597	-0.732	0.335	-0.708	0.073
	Carbon	-1772.493	0.523	-0.365	0.247	-0.952	0.064
MgCl ⁺ / AN ⁻	Nitrogen	-792.521	1.506	-0.982	0.439	-0.781	0.018
	Carbon	-792.521	1.418	-0.372	0.242	-1.156	0.016
Li ⁺ / AN ⁻ (THF) ₃	Nitrogen	-837.142	0.859	-0.817	0.323	-0.905	0.090
	Carbon	-837.128	0.878	-0.593	0.212	-1.025	0.092
Na ⁺ / AN ⁻ (THF) ₃	Nitrogen	-991.890	0.921	-0.794	0.300	-0.920	0.046
	Carbon	-991.877	0.906	-0.550	0.238	-1.084	0.046
K ⁺ / AN ⁻ (THF) ₃	Nitrogen	-1429.488	0.952	-0.768	0.294	-0.935	0.022
	Carbon	-1429.489	0.935	-0.635	0.227	-1.005	0.022
Cu ⁺ / AN ⁻ (THF) ₃	Nitrogen	-2469.911	0.727	-0.810	0.350	-0.833	0.089
	Carbon	-2469.927	0.591	-0.446	0.284	-1.032	0.072
MgCl ⁺ / AN ⁻ (THF) ₂	Nitrogen	-1257.519	1.709	-0.938	0.381	-0.848	0.019
	Carbon	-1257.520	1.644	-0.473	0.271	-1.177	0.018
Li ⁺ / AN ⁻ (PCM-THF)	Nitrogen	-139.744	0.949	-0.840	0.328	-0.922	0.099
	Carbon	-139.733	0.906	-0.640	0.199	-0.963	0.095
Na ⁺ / AN ⁻ (PCM-THF)	Nitrogen	-294.504	0.977	-0.808	0.304	-0.950	0.049
	Carbon	-294.498	0.953	-0.641	0.221	-1.017	0.048
K ⁺ / AN ⁻ (PCM-THF)	Nitrogen	-732.109	0.986	-0.788	0.291	-0.962	0.023
	Carbon	-732.107	0.963	-0.671	0.237	-1.004	0.022
Cu ⁺ / AN ⁻ (PCM-THF)	Nitrogen	-1772.489	0.788	-0.815	0.332	-0.813	0.096
	Carbon	-1772.513	0.660	-0.494	0.302	-1.024	0.080
MgCl ⁺ / AN ⁻ (PCM-THF)	Nitrogen	-792.578	1.687	-0.913	0.393	-0.864	0.020
	Carbon	-792.586	1.640	-0.524	0.309	-1.165	0.019
Li ⁺ / AN ⁻ (THF) ₃ / (PCM-THF)	Nitrogen	-837.159	0.635	-0.706	0.312	-0.949	0.067
	Carbon	-837.146	0.681	-0.583	0.222	-0.970	0.071
Na ⁺ / AN ⁻ (THF) ₃ / (PCM-THF)	Nitrogen	-991.913	0.817	-0.722	0.281	-0.960	0.041
	Carbon	-991.904	0.869	-0.606	0.255	-1.054	0.044
K ⁺ / AN ⁻ (THF) ₃ / (PCM-THF)	Nitrogen	-1429.513	0.889	-0.716	0.276	-0.972	0.021
	Carbon	-1429.511	0.833	-0.637	0.239	-0.990	0.019
Cu ⁺ / AN ⁻ (THF) ₃ / (PCM-THF)	Nitrogen	-2469.925	0.672	-0.774	0.341	-0.873	0.082
	Carbon	-2469.942	0.582	-0.513	0.316	-1.034	0.071
MgCl ⁺ / AN ⁻ (THF) ₂ / (PCM-THF)	Nitrogen	-1257.545	1.441	-0.821	0.368	-0.886	0.015
	Carbon	-1257.547	1.426	-0.539	0.310	-1.128	0.015

Table 3.8. Electronic energies, natural charges, and cation natural charge densities for THF solvated complexes using various solvation models.

As seen in these two tables a strong relationship between cation charge density and favored structure exists. For the calculations on the gas phase, unsolvated complexes, all of the cations show an energetic preference for carbon metalation. In

addition, these complexes all show that the carbon metalated structure exhibits a lower charge density on the cation than does the analogous nitrogen metalated structure. This is true even for the copper complexes which do not follow the previously mentioned size based trend. The explicit only solvation using both DME and THF also shows this same relationship between energetic preference and charge density. For all cations, the metalation site with the lower charge density on the cation is also the energetically preferred metalation site. DME solvated complex calculations show that only lithium cation favors nitrogen metalation, and has lower charge density when nitrogen metalated, and that the sodium, potassium, copper and magnesium chloride cations favor carbon metalation, and have lower charge density when carbon metalated. For THF solvated complexes, the sodium cation changes its preference from carbon to nitrogen metalation, and displays the same change in lowest charge density from the carbon to nitrogen metalated structure. As discussed in section 3.3.3, this difference between the results for DME and THF solvated sodium cation complexes is likely due to the increased size of the THF molecules and the contraction of the primary solvation sphere from three solvent ligands to only two, and not likely due to the small difference in polarity of the two solvents.

Unfortunately, the situation becomes more complicated and less definitive when continuum solvation is introduced to the system. Following the previously observed trends for continuum only solvation of the cations, the results of the DME and THF solvated systems are the same and it is noted that the sodium and potassium complexes are now shown to have an energetic preference for the nitrogen metalated structure, despite having lower charge densities in the cases of the carbon metalated structure. As

seen in the previous section, the hybrid explicit / continuum model yields the same results as the continuum only model. These results clearly call into question the validity of the charge density / energetic preference relationship. However, as shown in Chapter 2 of this dissertation and in previous sections of this chapter, continuum solvation has significant disadvantages and limitations relative the explicit solvation model such as insufficiently capture the total free energy of the system and being unable to distinguish between the two similar solvents used in this investigation. It also appears that the contributions of continuum model in the hybrid model are inappropriately, strongly weighted, overshadowing the results of the more accurate and realistic explicit solvation model results. Finally, it is seen that in at least the case of sodium and lithium there is a strong steric component in the energetic preference of the system. This steric component is, by definition, completely ignored in the continuum model of solvation. Based on these limitations and problems with the continuum model, the relationship between the cation charge density and the energetic preference of the solvated complexes which is strongly seen in the explicit only solvent modeled systems and the gas phase systems may be the rule and not the exception, or it may be possible that the observed behavior is an indicator of significant changes in nature of these complexes as they go from the gas phase to the condensed phase.

3.4 Conclusions

In an effort to better understand the role that cation and solvation play in the experimentally observed behavior of nitrile anions, electronic structure calculations were

carried out on a series of acetonitrile complexes using several different model chemistries and solvation models. As in the previous chapter, the results of calculations using B3LYP and HF model chemistries were in good agreement with one another, and MP2 based calculations gave out-lying results. The results obtained for the two solvents showed only small dependencies on the type solvent employed, and the differences that were seen were related to steric considerations and not polarity or electrostatic considerations. The way in which solvation was modeled, however, proved to have a significant effect on the results obtained, and the interpretation of those results. As seen in previous sections, and the reports of other authors, the use of explicit solvation proves to be more informative and likely more accurate than models which employ continuum approximations of solvation. The various cations used in the studies were found to have a strong influence on the structure of the complexes. In general, as the size of the cation increased the preference for carbon metalation also increased. The notable exception to this trend was the copper cation, however, that observation led to an NBO population analysis of the calculated structures which resulted in the identification of a critical and more definitive relationship between cation charge density minimization and metalation site preference. An initial practical consequence of these observations is the possibility that the stereoselectivity of a reaction involving a nitrile anion could be tuned by manipulating the sp^3 character of the α -carbon. The sp^3 character of the α -carbon is significantly higher for carbon metalated complexes which is likely to result in a high conservation of stereochemistry in reactions taking place at that atom. Further, these results show that the carbon versus nitrogen metalation of a complex can be driven by minimizing the charge density of the cation in the complex. An obvious way to drive the

minimization of charge density is by employing larger cations while maintain a singularly positive charge on the cation. These observation are, for the most part, in good agreement with previously reported experimental results.^{19, 20}

3.5 References

1. Stork, G.; Boeckman, R. K., Mechanism and stereochemical control in the .alpha.-haloketal cyclization. Remarkable effect of metal cations. *Journal of the American Chemical Society* **1973**, 95, (6), 2016-2017.
2. Stork, G.; Gardner, J. O.; Beckman, R. K.; Parker, K. A., Haloketal cyclization. General method for the synthesis of functionalized cis bicyclic ketones. *Journal of the American Chemical Society* **1973**, 95, (6), 2014-2016.
3. Carlier, P. R.; Lo, K. M., 2,3-Anti Selective Aldol Reaction of Phenylacetonitrile. *The Journal of Organic Chemistry* **1994**, 59, (15), 4053-4055.
4. Rychnovsky, S. D.; Griesgraber, G.; Kim, J., Rapid Construction of the Roflamycoin System. *Journal of the American Chemical Society* **1994**, 116, (6), 2621-2622.
5. Rychnovsky, S. D.; Swenson, S. S., Alkylation and Reductive Decyanation of 4-Cyano-2,2-dimethyl-1,3-dioxanes (Cyanohydrin Acetonides). *The Journal of Organic Chemistry* **1997**, 62, (5), 1333-1340.
6. Fleming, F. F.; Shook, B. C.; Jiang, T.; Steward, O. W., Î²-Siloxy Unsaturated Nitriles: Stereoselective Cyclizations to cis- and trans-Decalins. *Organic Letters* **1999**, 1, (10), 1547-1550.

7. Arseniyadis, S.; Kyler, K. S.; Watt, D. S., *Organic Reactions* **1984**, 31, 1-364.
8. Abbotto, A.; Bradamante, S.; Pagani, G. A., Charge mapping in carbanions. Weak charge demand of the cyano group as assessed from a carbon-13 NMR study of carbanions of .alpha.-activated acetonitriles and phenylacetonitriles: breakdown of a myth. *The Journal of Organic Chemistry* **1993**, 58, (2), 449-455.
9. Carlier, P. R.; Lucht, B. L.; Collum, D. B., ⁶Li/³¹P NMR-Based Solution Structural Determination of EtzO⁻ and TMEDA-Solvated Lithiophenylacetonitrile and a LiHMDS Mixed Aggregate. *Journal of The American Chemical Society* **1994**, 116, 11602-11603.
10. Carlier, P. R.; Lo, C. W.-S., ⁷Li/³¹P NMR Studies of Lithiated Arylacetonitriles in THF-HMPA Solution: Characterization of HMPA-Solvated Monomers, Dimers, and Separated Ion Pairs. *Journal of The American Chemical Society* **2000**, 122, 12819-12823.
11. Hilmersson, G.; Sott, R.; Granander, J., Mixed Complexes Formed by Lithioacetonitrile and Chiral Lithium Amides: Observation of ⁶Li,¹⁵N and ⁶Li,¹³C Couplings Due to Both C-Li and N-Li Contacts. *Journal of The American Chemical Society* **2004**, 126, 6798-6805.
12. Fleming, F. F.; Zhang, Z., Cyclic nitriles: tactical advantages in synthesis. *Tetrahedron* **2005**, 61, 747-789.
13. Singh, V.; Iyer, S. R.; Pal, S., Recent approaches towards synthesis of *cis*-decalins. *Tetrahedron* **2005**, 61, 9197-9231.
14. Carlier, P. R.; Madura, J. D., Effective Computational Modeling of Constitutional Isomerism and Aggregation States of Explicit Solvates of Lithiated

Phenylacetonitrile. *Journal of Organic Chemistry* **2002**, 67, 3822-3840.

15. Abbotto, A.; Streitwieser, A.; Schleyer, P. v. R., Ab Initio and Semiempirical Study of the Effect of Ethereal Solvent on Aggregation of a Lithium Enolate. *Journal of the American Chemical Society* **1997**, 119, (46), 11255-11268.
16. Kaneti, J.; Schleyer, P. v. R.; Clark, T.; Kos, A. J.; Spitznagel, G. W.; Andrade, J. G.; Moffat, J. B., The structures and energies of the lithium, sodium, and magnesium derivatives of the anions CH₂CN⁻ and CH₂NC⁻. Solvation and aggregation of the lithium species. *Journal of the American Chemical Society* **1986**, 108, (7), 1481-1492.
17. Kaufmann, E.; Gose, J.; Schleyer, P. v. R., Thermodynamics of Solvation of Lithium Compounds. A Combined MNDO and ab Initio Study. *Organometallics* **1989**, 8, 2577-2584.
18. Sannigrahi, A. B.; Nandi, P. K.; Schleyer, P. v. R., Ab Initio Study of Cation-Dipole Interactions. Proton, Lithium, and Sodium Affinities of Hydrogen and Alkali Halides and Natural Orbital Study of Bonding. *Journal of the American Chemical Society* **1994**, 116, (16), 7225-7232.
19. Fleming, F. F.; Gudipati, S.; Zhang, Z.; Liu, W.; Steward, O. W., Cyclic Nitriles: Diastereoselective Alkylations. *The Journal of Organic Chemistry* **2005**, 70, (10), 3845-3849.
20. Fleming, F. F.; Zhang, Z.; Liu, W.; Knochel, P., Metalated Nitriles: Organolithium, -magnesium, and -copper Exchange of \hat{I}^{\pm} -Halonitriles. *The Journal of Organic Chemistry* **2005**, 70, (6), 2200-2205.

21. Carlier, P. R.; Madura, J. D., Effective Computational Modeling of Constitutional Isomerism and Aggregation States of Explicit Solvates of Lithiated Phenylacetonitrile. *The Journal of Organic Chemistry* **2002**, *67*, 3832-3840.
22. Fock, V. A., Näherungsmethode zur Lösung des quantenmechanischen Mehrkörperproblems. *Zeitschrift für Physik* **1930**, *61*, 126-148.
23. Hartree, D. R., The Wave Mechanics of an Atom with a Non-Coulomb Central Field. Part I. Theory and Methods. *Proceedings of the Cambridge Philosophical Society* **1927**, *24*, 89-110.
24. Hartree, D. R., The Wave Mechanics of an Atom with a Non-Coulomb Central Field. Part II. Some Results and Discussion. *Proceedings of the Cambridge Philosophical Society* **1927**, *24*, 111-132.
25. Hartree, D. R., The Wave Mechanics of an Atom with a non-Coulomb Central Field. Part III. Term Values and Intensities in Series in Optical Spectra. *Proceedings of the Cambridge Philosophical Society* **1928**, *24*, 426-437.
26. Hartree, D. R., The Distribution of Charge and Current in an Atom consisting of many Electrons obeying Dirac's equations. *Proceedings of the Cambridge Philosophical Society* **1929**, *25*, 225-236.
27. Hartree, D. R., The Wave Mechanics of an Atom with a Non-Coulomb Central Field. Part IV. Further Results relating to Terms of the Optical Spectrum. *Proceedings of the Cambridge Philosophical Society* **1929**, *25*, 310-314.
28. Pratt, L. M., A Computational Study of Lithium Dialkylamide Mixed Aggregates with Lithium Chloride. *Bulletin of The Chemical Society of Japan* **2005**, *78*, 890-895.

29. Pratt, L. M.; Phan, D. H. T.; Tran, P. T. T.; Nguyen, N. V., Basis Set and Electron Correlation Effects on Lithium Carbenoid Dimerization Energies. *Bulletin of The Chemical Society of Japan* **2007**, 80, (8).
30. Ziegler, M. J.; Madura, J. D., Solvation of Metal Cations. *Journal of Solution Chemistry* **2009**, In Press.
31. Blake, J. F.; Jorgensen, W. L., Solvent effects on a Diels-Alder reaction from computer simulations. *Journal of the American Chemical Society* **1991**, 113, (19), 7430-7432.
32. Ruiz-Lopez, M. F.; Assfeld, X.; Garcia, J. I.; Mayoral, J. A.; Salvatella, L., Solvent effects on the mechanism and selectivities of asymmetric Diels-Alder reactions. *Journal of the American Chemical Society* **1993**, 115, (19), 8780-8787.
33. Evanseck, J. D.; Kong, S., Density Functional Theory Study of Aqueous-Phase Rate Acceleration and Endo/Exo Selectivity of the Butadiene and Acrolein Diels-Alder Reaction. *Journal of The American Chemical Society* **2000**, 122, 10418-10427.
34. Frisch, M. J.; Trucks, G. W.; Schlegel, H. B.; Scuseria, G. E.; Robb, M. A.; Cheeseman, J. R.; Montgomery, J. A., Jr.; Vreven, T.; Kudin, K. N.; Burant, J. C.; Millam, J. M.; Iyengar, S. S.; Tomasi, J.; V., B.; Mennucci, B.; Cossi, M.; Scalmani, G.; Rega, N.; Petersson, G. A.; Nakatsuji, H.; Hada, M.; Ehara, M.; Toyota, K.; Fukuda, R.; Hasegawa, J.; Ishida, M.; Nakajima, T.; Honda, Y.; Kitao, O.; Nakai, H.; Klene, M.; Li, X.; Knox, J. E.; Hratchian, H. P.; Cross, J. B.; Adamo, C.; Jaramillo, J.; Gomperts, R.; Stratmann, R. E.; Yazyev, O.; Austin, A. J.; Cammi, R.; Pomelli, C.; Ochterski, J. W.; Ayala, P. Y.; Morokuma, K.; Voth, G. A.; Salvador, P.; Dannenberg, J. J.; Zakrzewski, V. G.; Dapprich, S.; Daniels, A. D.; Strain, M. C.; Farkas, O.; Malick, D. K.; Rabuck, A.

D.; Raghavachari, K.; Foresman, J. B.; Ortiz, J. V.; Cui, Q.; Baboul, A. G.; Clifford, S.; Cioslowski, J.; Stefanov, B. B.; Liu, G.; Liashenko, A.; Piskortz, P.; Komaromi, I.; Martin, R. L.; Fox, D. J.; Keith, T.; Al-Laham, M. A.; Peng, C. Y.; Nanayakkara, A.; Challacombe, M.; Gill, P. M. W.; Johnson, B.; Chen, W.; Wong, M. W.; Gonzalez, C.; Pople, J. A. *Gaussian 03, Revision D.01*, Gaussian, Inc.: Wallingford, CT, 2004.

35. Krishnan, R.; Frisch, M. J.; Pople, J. A., Contribution of triple substitutions to the electron correlation energy in fourth order perturbation theory. *Journal of Chemical Physics* **1980**, 72, 4244-4245.

36. Krishnan, R.; Pople, J. A., Approximate fourth-order perturbation theory of the electron correlation energy. *Journal of Quantum Chemistry* **1978**, 14, 91-100.

37. Moller, C.; Plesset, M. S., Note on an Approximation Treatment for Many-Electron Systems. *Physical Review* **1934**, 46, 618-622.

38. Becke, A. D., Density-functional thermochemistry. III. The role of exact exchange. *Journal of Chemical Physics* **1993**, 98, (7), 5648-5662.

39. Lee, C.; Yang, W.; Parr, R. G., Development of the Colle-Salvetti correlation-energy formula into a functional of the electron density. *Physical Review B* **1988**, 37, (2), 785-789.

40. Tomasi, J.; Persico, M., Molecular Interactions in Solution: An Overview of Methods Based on Continuous Distributions of the Solvent. *Chemical Reviews* **1994**, 94, 2027 - 2094.

41. Cossi, M.; Barone, V.; Cammi, R.; Tomasi, J., Ab initio study of solvated molecules: a new implementation of the polarizable continuum model. *Chemical Physics Letters* **1996**, 255, (4-6), 327-335.

42. Bauschlicher, C. W. J.; Langhoff, S. R.; Partridge, H., The binding energies of $\text{Cu}^{+}(\text{H}-\text{O})^{-}$ and $\text{Cu}^{+}(\text{NH})^{-}$ ($n=1-4$). *Journal of Chemical Physics* **1991**, 94, 2068-2072.
43. Carlier, P. R.; Zhang, Y., The First Enantioenriched Metalated Nitrile Possessing Macroscopic Configurational Stability. *Organic Letters* **2007**, 9, (7), 1319-1322.
44. Reed, A. E.; Curtiss, L. A.; Weinhold, F., Intermolecular interactions from a natural bond orbital, donor-acceptor viewpoint. *Chemical Reviews* **1988**, 88, (6), 899-926.

4 Selectivity of Substitution Reactions Involving Nitrile Anion Containing Molecules

The next logical step in this dissertation is to apply the lessons learned from the study of simple cation – solvent complexes and acetonitrile anion complexes to large molecules and reactions involving those larger nitrile anion containing molecules. The principle aim of this portion of the investigation was to determine the reaction path and energy profile for a pair of simple S_N2 reactions. Meeting this aim would help to understand how variations in cation or solvation would affect those reaction coordinates and in turn if those reaction coordinate changes would explain experimentally observed selectivity results. The reactions studied were the addition of a methyl group to a five or six membered cycloaliphatic ring functionalized with a nitrile anion group. Based on the results presented in the previous chapters, the principle electronic structure technique used in this portion of the investigation was a density functional theory model chemistry using the Becke three-parameter exchange functional coupled with the nonlocal correlation functional of Lee, Yang, and Parr (B3LYP). The complexes were studied in the gas phase and in the condensed phase solvated by tetrahydrofuran (THF). The cations studied were Li^+ , Na^+ , K^+ , and Cu^+ .

4.1 Introduction

As previously discussed, and shown in Figures 1.4 and 1.5, metalated nitrile stabilized carbanions are of significant interest for numerous reasons such as their usefulness in directing stereo- and regioselective in the synthesis of several types of

biologically important molecules.¹⁻¹¹ The research reported in the previous two chapters of this dissertation have focused on the study of molecular complexes with a constant composition. The next step of this investigation is to begin probing the nature of simple reactions involving nitrile anion containing molecules. In keeping with the overall strategy of this dissertation, a simple starting point was chosen to begin building a systematic understanding of how cation and solvation affects selectivity. The ultimate objective of this work would be to lay the foundations for the later development of a predictive model which would allow the user to computationally manipulate reaction conditions in order to drive the selectivity of a specific reaction to yield the desired product while minimizing the formation of undesired side products.

To begin the extension of this investigation to simple substitution reactions, two reactions were chosen which would have the possibility of yielding two different stereoisomers. Those two reactions, which are the basis of the work described in this chapter, are shown in Figures 4.1 and 4.2.

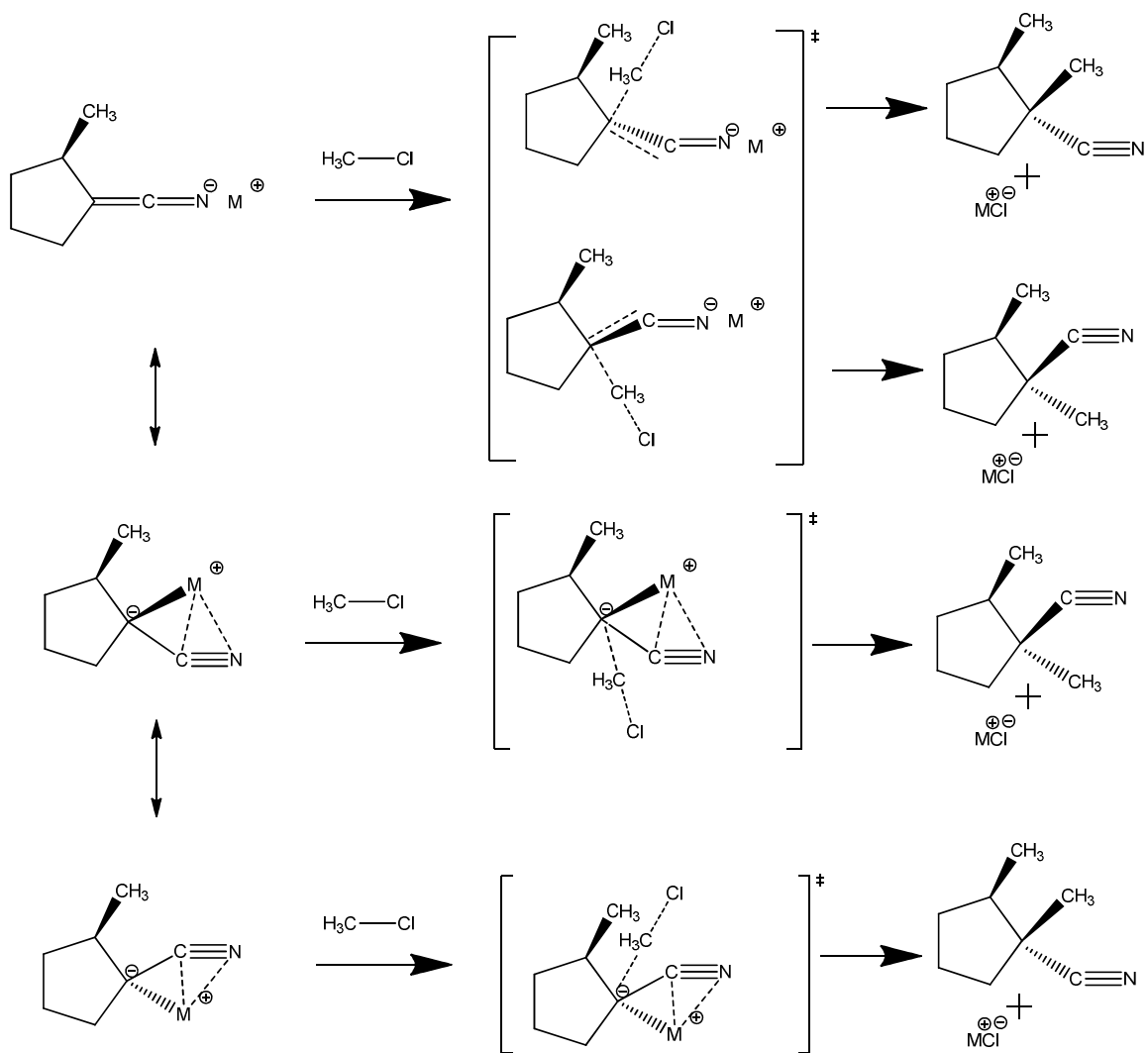


Figure 4.1. Reaction scheme for 5 membered ring, where M is Li, Na, K, or Cu, showing first the nitrogen metalated reactant going through the two possible transition structures to two possible products, followed by the two different carbon metalated starting points each going through a single transition structure to a single product.

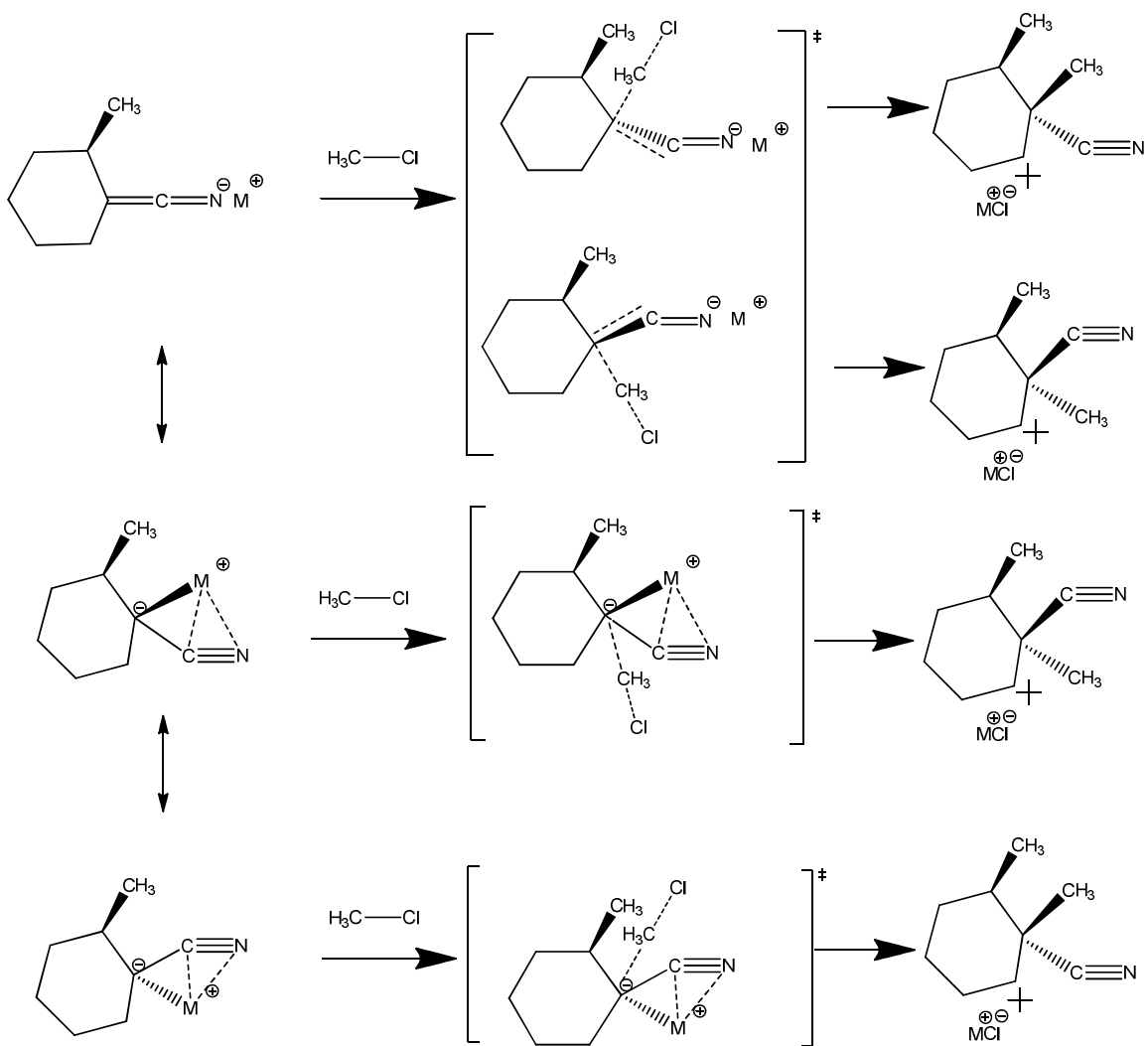


Figure 4.2. Reaction scheme for 6 membered ring, where M is Li, Na, K, or Cu, showing first the nitrogen metalated reactant going through the two possible transition structures to two possible products, followed by the two different carbon metalated starting points each going through a single transition structure to a single product.

The two reactions differ in the amount of strain on the α -carbon of the cycloaliphatic. Studying both of these reactions will provide some insight into the impact of the higher ring strain associated with the five membered ring relative to the six membered ring on the level of pyramidization of the α -carbon.

Experimental studies of either of these two reactions have not been reported in the literature, but several examples of substitution reactions involving nitrile anion functionalized rings have been reported in which varying the nature of the cation effects the selectivity of the reaction¹²⁻²⁰.

One example of this is shown in Figure 32 below.

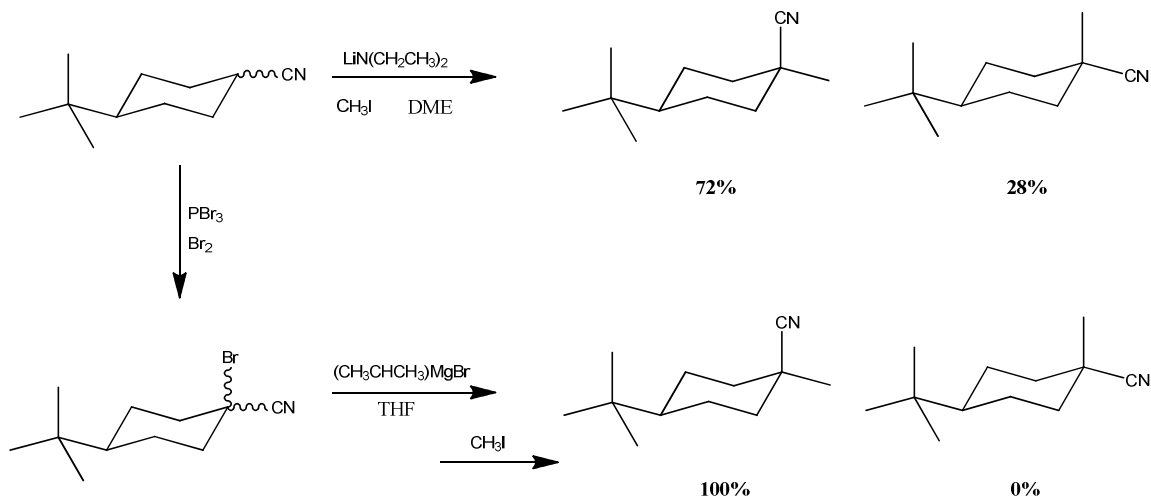


Figure 4.3. An experimental example of a cation influenced alkylation reaction.^{16, 17, 20}

In the case of the lithium metalated reaction, there is a preference for equatorial alkylation, but there is not exclusivity of that product. As shown in experimentally and computationally in this dissertation and other reports, lithium cation has a strong preference for nitrogen metalation. This preference for nitrogen metalation would result in a transition structure in which the methyl iodide could approach from either face of the ring. The preference for equatorial alkylation would then be a result of the slight penalty associated with the steric interaction that would occur between the axial hydrogen at the β -carbon position and the approaching methyl group if it were to add at the axial position on the nitrile carbon. On the other hand, when a Grignard type reaction is carried out the

equatorial product is exclusively formed. This is consistent with a reaction pathway in which the nitrile is magnesiated at the α -carbon as opposed to the nitrogen. This type of transition structure would force the methyl iodide to approach from one direction, leading to exclusively one product, in this case the equatorial product. This is consistent with the work discussed in the previous chapter which showed the strong preference for α -carbon metalation with magnesium-halide cations.¹⁶

It is the nature of these reactants, transition structures, and products that are studied in greater detail in this chapter of the dissertation.

4.2 Computational Methods

All geometry optimizations, frequency, and natural bond order calculations were performed using Gaussian 09²¹ or MOPAC²² as specified in the body of the text. Unless otherwise noted, all geometry optimizations and frequency calculations were performed using the Becke three-parameter exchange functional²³ and the nonlocal correlation functional of Lee, Yang, and Parr²⁴ (B3LYP). The optimization and frequency calculations were carried out using the 6-31+G(d) basis set. All optimized geometries were either confirmed to be energy minima by vibrational frequency analysis, in which no imaginary vibrational frequencies were observed, or confirmed to transition structure by vibrational frequency analysis in which a single imaginary vibrational frequency was observed which corresponded to the pathway of the reaction being studied. As noted in the body of the text, several additional geometry optimizations were carried out using the AM1²⁵, PM3^{26, 27}, and PM6²⁸ semi-empirical model chemistries. Continuum and

explicit-continuum solvation single point energy calculations were carried out using the polarizable continuum model (PCM) which has been previously described in detail^{29, 30}. The solvent and dielectric constant used in this study was THF ($\epsilon=7.2$). All thermodynamic data was calculated at standard temperature and pressure, and all experimental data was measured under the same conditions.

4.3 Results and Discussions

Based on the principle aims of this work, as discussed in the introduction to this chapter, the preliminary work on this portion of the investigation was focused on building reaction coordinate profiles for the two reactions in question. However, that initial work was focused only on the reaction path way from the nitrogen metalated starting point to the two different final products. Based on the results of the work in the previous two chapters, however, it was realized that there were numerous deficiencies in that treatment of this subject. Key among those deficiencies were the lack of solvation, either explicit or continuum based solvation, the use of two model chemistries which were shown to be less accurate for this type of system than the preferred density functional method, and most importantly, the lack of consideration given to the possibility of carbon metalated starting points.

Given these concerns, the original research plan was significantly modified to focus only on the reaction with either gas phase explicit THF solvation or explicit THF solvation coupled with THF continuum solvation, and to expand the view of the reaction to include both possible carbon metalated starting points in addition to the nitrogen

metalated starting points. The principle model chemistry used for these calculations was also shifted from HF and MP2 to the preferred B3LYP model chemistry.

Determination of the electronic energies of the reactants and the products of the 5 and 6 membered rings was relatively straightforward and the results of those calculations are discussed in sections 4.3.1 and 4.3.2. However, finding the transition structures for these large molecular systems has proven to be extremely challenging. The work done on that aspect of this investigation is discussed in section 4.3.3. Despite the fact that the transition structure calculations have not been as successful as was originally hoped, it is still possible to gain insight into the nature of the selectivity of these reactions based on the calculated data in this portion of the dissertation investigation. In particular it is useful to understand the role of energetic preference for nitrogen versus carbon metalation in the starting reactants and what influence that may have on the selectivity of the reaction.

4.3.1 Reactant and Product Energies for the Reaction of the Five Membered Ring

The first step in understanding the reaction pathway for substitution reaction shown in Figure 4.1 is to calculate the energy of the two possible products. Those two products only differ in terms of the placement of the newly added methyl group relative to the methyl group that is present in the unreacted starting material. The added methyl group can be visualized as adding as either cis or trans to the methyl group already on the ring. For the sake of simplicity and for comparison of the five and six membered rings, the five membered ring product in which the second methyl group has added in a cis

fashion will be referred to as the equatorial product and the product in which the second methyl group has added in a trans fashion will be referred to as the axial position, in the context of this dissertation. The two products possible from the reaction in Figure 4.1 are shown below in Figure 4.4 along with the relative electronic energies of the two potential products.

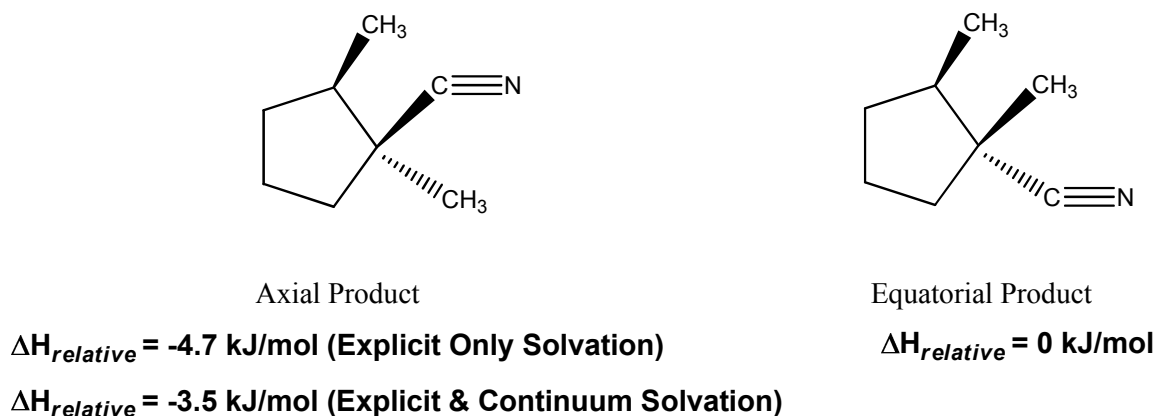


Figure 4.4. Structures and relative enthalpies of the two products of the 5 membered ring reaction.

As seen in Figure 4.4, there is an energetic preference for the axial product, in both the case of explicit only solvation and explicit/continuum hybrid solvation. This is very likely due to the steric repulsion in the equatorial product where the two methyl groups are closer together and can interact more easily.

Table 4.1 shows the relative energies of the three different conformations of the reactant for each of the four cations being studied in both an explicit only and explicit/continuum solvation scheme. As expected, the copper cation showed a very strong preference for carbon metalation, however, somewhat surprisingly; the potassium cation is the only cation which shows a preference for nitrogen metalation. Based on previous results it was expected that the lithium cation and possibly the sodium cation

would have favored nitrogen metalation, but this behavior was not observed. Further inspection of the lithium complexes shows that the energetically preferred carbon metalated species adopt a structure in which the lithium cation is in fact interacting with both the α -carbon and nitrogen atoms as shown in the reactants section of Figure 4.1, but that the cation is actually significantly closer (1.9\AA versus 4.4\AA) to the nitrogen atom than the α -carbon. Combining this observation with the experimental structural data of Carlier and Hilmersson³¹⁻³⁵, leads to a potential explanation of this behavior based on the preference for lithiated nitrile anions to exist as dimers in the condensed phase. Since these calculations have artificially imposed the requirement that the complexes must exist as monomers, it is possible that the slight preference for carbon metalation, which has unexpectedly been observed, could be attributable to the increased stabilization provided by interaction with the α -carbon as a replacement for the stabilization that would come from the bridged dimer conformation that would very likely exist in a real world solution.

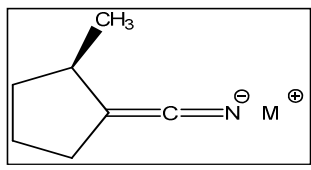
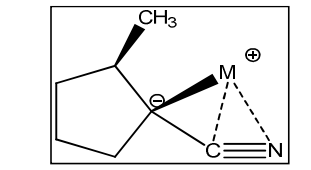
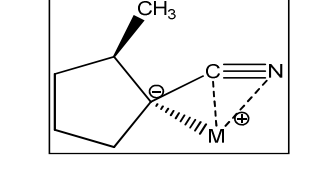
Reactant	Explicit THF Solvation				Explicit and Continuum THF Solvation			
	M = Li	M = Na	M = K	M = Cu	M = Li	M = Na	M = K	M = Cu
	1.5	1.3	0	21.5	1.7	9.5	0	25.1
	0	0	4.4	4.3	0	0	3.7	5.5
	3.1	2.4	9.6	0	3.1	2.3	3.3	0

Table 4.1. Relative enthalpies, in kJ/mol, for the three possible conformations of the reactant of the 5 membered ring reaction calculated with the B3LYP/6-31⁺G(d) model chemistry.

The same trends exist in both the explicit and explicit/continuum, however the magnitudes of the energetic changes amongst the three conformations does change based on the solvation model employed. In order to better understand this observation, the dipole moments of the complexes are shown in Table 4.2. Based on a comparison of the data in Tables 4.1 and 4.2 it seems that there is a loose relationship with the size of the dipole moment of the explicitly solvated complex and how significantly the relative energies of those complexes change when a solvation continuum is applied to the complex. Specifically, copper and lithium which have the smallest dipole moments have also the smallest changes in magnitude of the relative energies of the three conformations.

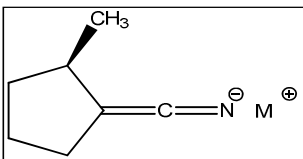
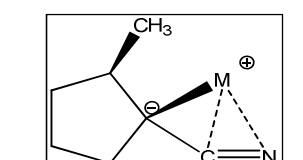
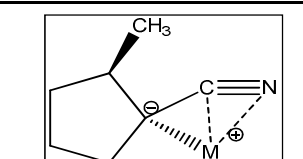
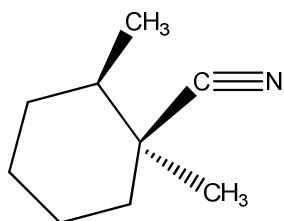
Reactant	Explicit THF Solvation				Explicit and Continuum THF Solvation			
	M = Li	M = Na	M = K	M = Cu	M = Li	M = Na	M = K	M = Cu
	8.81	9.41	9.57	6.60	10.38	11.01	11.55	7.69
	9.03	9.56	8.81	4.83	10.56	11.14	10.60	6.24
	8.91	9.65	9.33	5.01	10.40	11.20	11.10	6.61

Table 4.2. Dipole moments, in Debyes, for the three possible conformations of the reactant of the 5 membered ring reaction.

4.3.2 Reactant and Product Energies for the Reaction of the Six Membered Ring

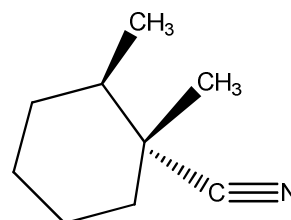
The same process used to study the reactants and products of the 5 membered ring reaction was applied to the 6 membered ring reaction's reactants and products. As in the previous section, the first step of this process is to calculate the relative energies of the two products possible from the reaction in Figure 4.2. These are shown below in Figure 4.5 along with the naming conventions used for the two products and the relative electronic energies of the two potential products, both in an explicit only solvation scheme and explicit/continuum hybrid solvation scheme. As seen was the case for the 5 membered ring products, there is an energetic preference for the axial product in the case of either solvation scheme. This is very likely due to the steric repulsion in the equatorial product where the two methyl groups are closer together and can interact more easily.



Axial Product

$$\Delta H_{relative} = -6.3 \text{ kJ/mol (Explicit Only Solvation)}$$

$$\Delta H_{relative} = -5.2 \text{ kJ/mol (Explicit \& Continuum Solvation)}$$



Equatorial Product

$$\Delta H_{relative} = 0 \text{ kJ/mol}$$

Figure 4.5. Structures and relative enthalpies of the two products of the 6 membered ring reaction.

Table 4.3 shows the relative energies of the three different conformations of the reactant for each of the four cations being studied in both an explicit only and explicit/continuum solvation scheme. As expected, the copper cation again showed a very strong preference for carbon metalation, however, in the case of the 6 membered ring the preference was for the metalation to occur on the same face as the existing methyl group. This would lead to the expected, lower energy product. As in the case of the 5 membered ring, the potassium cation is, again, the only cation which shows a preference for nitrogen metalation in the explicit solvation only model. However, unlike the results for the 5 membered ring reactants, there was a change in the preferred conformation for the lithium and sodium cations when the THF solvent continuum was applied to the complex.

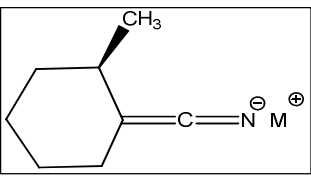
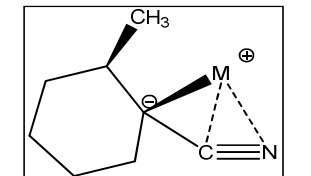
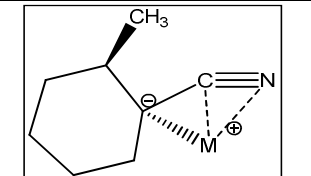
Reactant	Explicit THF Solvation				Explicit and Continuum THF Solvation			
	M = Li	M = Na	M = K	M = Cu	M = Li	M = Na	M = K	M = Cu
	0.5	2.4	0	27.1	0	0	0	25.9
	0	0	2.7	0	2.9	8.3	5.1	0
	6.1	26.9	11.8	10.2	7.7	26.1	7.2	7.1

Table 4.3. Relative enthalpies, in kJ/mol, for the three possible conformations of the reactant of the 6 membered ring reaction calculated with the B3LYP/6-31⁺G(d) model chemistry.

A comparison of the dipole moments of the complexes was again carried out in an effort to better understand why this change in energetic preference had occurred. This data is shown in Table 4.4, but unfortunately, there are no obvious differences in the conformations that would explain the change in preference based on application of a solvent continuum. It is possible that the known preference for lithium to form bridged dimers is again the key to understanding this data, in that the increased stabilization provided by solvent continuum could be acting as a replacement for the stabilization that would come from the bridged dimer conformation. It is also possible that the three explicit THF molecules used to provide a model of the primary solvation sphere is not sufficient to capture all of the stabilization energy coming from solvation. The addition of the solvent continuum would in that case, be providing the additional stabilization that would exist in a real world scenario, thus giving a more accurate description of the relative energies of the three conformations.

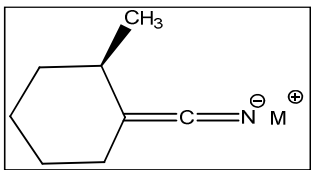
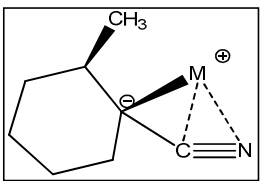
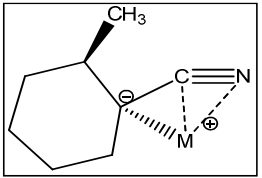
Reactant	Explicit THF Solvation				Explicit and Continuum THF Solvation			
	M = Li	M = Na	M = K	M = Cu	M = Li	M = Na	M = K	M = Cu
	9.09	9.91	10.22	6.96	10.51	11.34	12.06	8.03
	9.32	9.90	9.27	4.93	11.01	11.48	11.16	6.45
	9.16	8.17	9.46	4.78	10.72	9.82	11.37	6.31

Table 4.4. Dipole moments, in Debyes, for the three possible conformations of the reactant of the 6 membered ring reaction.

4.3.3 Transition State Calculations

The final aspect of these reactions that was studied were the two transition structures for the two reactions. These transition structures would be associated with the case of nitrogen metalated reactants. The transition structures for the carbon metalated reactants were not particularly interesting to this investigation since the reaction pathway and nature of the transition structure would be determined by which of the two starting point conformations the reaction began from. The energy differences associated with the structures would, however, be very relevant for the nitrogen metalated reactants as both structures and reaction pathways would be available when the starting from the nitrogen metalated reactant. The two transition structures associated with the nitrogen metalated reactants are shown in Figures 4.6 and 4.7.

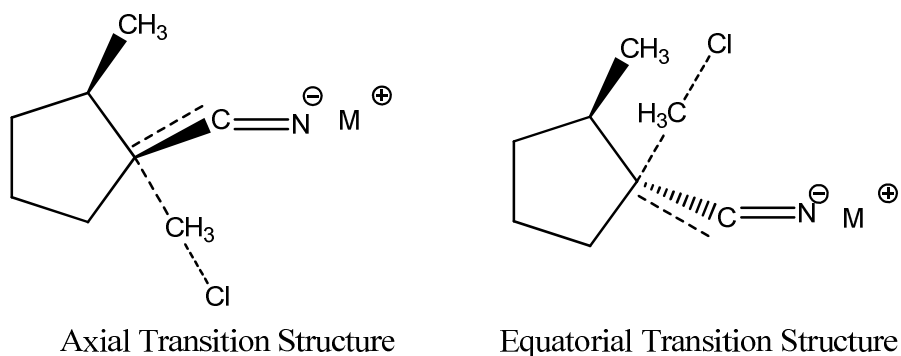


Figure 4.6. Two transition structures for the 5 membered ring reaction.

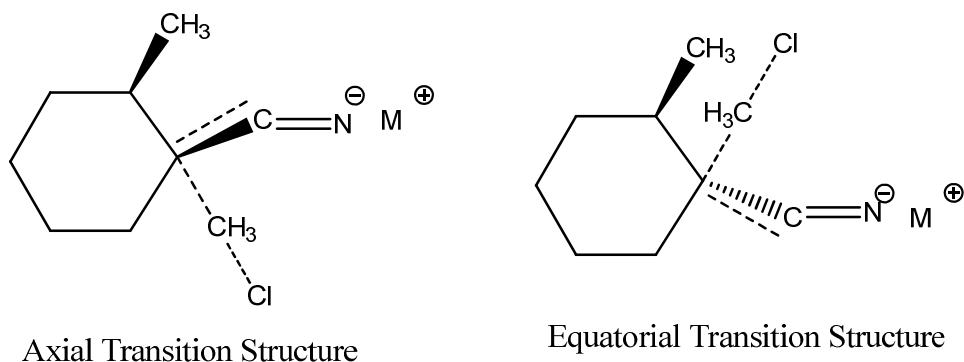


Figure 4.7. Two transition structures for the 6 membered ring reaction.

The initial strategy employed in studying these transition structures was to use the same B3LYP used to study the reactants and the products of the reactions. However, numerous difficulties and obstacles were found using this approach, and several other strategies were then used in an attempt to overcome these obstacles. The next several sections describe the results of the initial and subsequent strategies used to study these transition structures.

4.3.3.1 Density Functional Theory Calculations

The first attempts to find the two transition structures for the each of the reactant / cation compositions were carried out using the “opt=ts” function in the Gaussian software suite. However, it quickly became apparent that the size and complexity of the molecular systems being studied made it impossible to find the transition structure using this direct method. To overcome this, the computational strategy was changed to a two-stage approach. In the first stage, the atoms which made up the reaction axis, as shown highlighted in red in Figure 4.8, were frozen in position while the remainder of the

molecule was optimized normally to a geometry which represented an energy minimum with no imaginary vibrational frequencies. Once the bulk of the molecule was optimized the reaction axis was then unfrozen and the entire molecule was optimized to a transition structure.

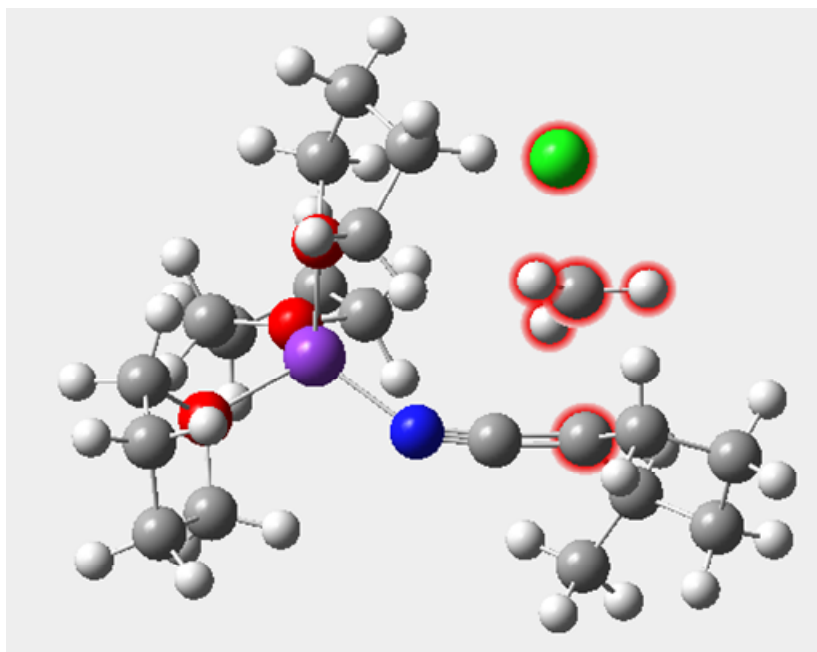


Figure 4.8. A starting point geometry showing the reaction axis highlighted in red. White spheres represent hydrogen atoms, gray spheres represent carbon atoms, red spheres represent oxygen atoms, the blue sphere represents a nitrogen atom, the green sphere represents a chlorine atom, and the purple sphere represents a K^+ cation.

After numerous iterations through this two staged process for the 16 possible structures, only three transition structures, the trans structure for the 5 membered ring with Li^+ , the cis structure for the 5 membered ring with Li^+ , and the trans structure for Cu^+ , were successfully obtained. For the 13 situations in which a transition structure was not successfully obtained, a common mode of failure existed. During the either the first or second stage of the calculation, depending on which molecule was being studied, a series of undesired imaginary vibrational frequencies would develop in the optimized

geometry. Detailed inspection of these vibrational frequencies showed the computational artifact which was wreaking havoc on the calculations. In all cases the imaginary frequencies corresponded to one or more of the following molecular motions:

- i. The movement of the reactant ring toward the metal center in such a way as to minimize the distance between the large positive charge center (the metal cation) and the large negative charge center (the chlorine ion)
- ii. The wobbling of the entire frozen reaction axis toward the cation, again suggesting the favorable shrinking of distance between charge centers
- iii. Ring twisting and ring torsion that occurred in the THF rings as they followed the cation toward the chlorine anion.

In all cases it seemed that the root cause of the failed calculations was the unanticipated and undesired interaction between the cation and the chlorine atom as it became an anion by taking on the electron density previously associated with nitrile group. An example of this behavior is shown in Figure 4.9. Figure 4.9a shows the starting point geometry for the trans transition structure of the 5 membered ring reaction with the sodium cation. In this structure the cation-chlorine distance is 5.0 Å, while in Figure 4.9b, which shows the geometry after approximately 3,000 SCF iterations, the cation-chlorine distance has shrunk to only 2.6 Å.

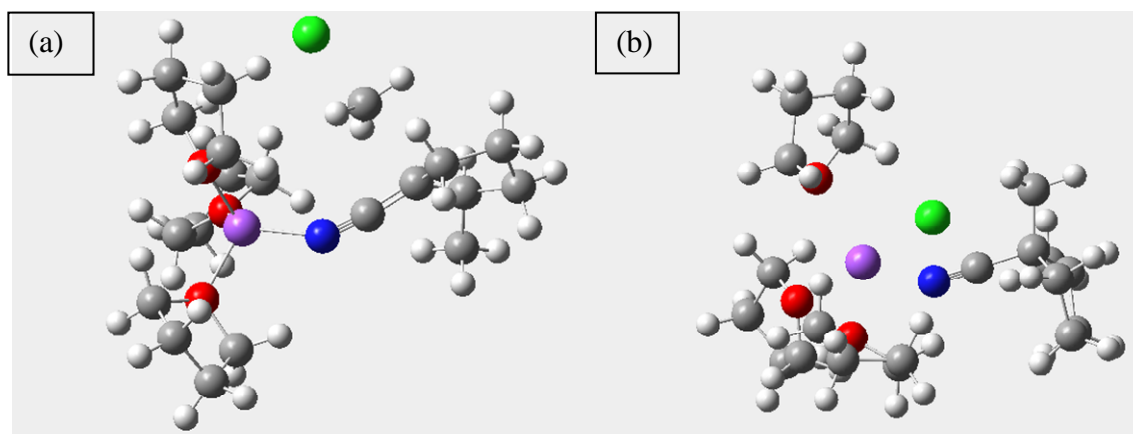


Figure 4.9. (a) Starting point geometry for the trans transition structure of the 5 membered ring reaction with the Na^+ . (b) Unoptimized geometry for the trans transition structure of the 5 membered ring reaction with the Na^+ after ~3,000 SCF iterations. White spheres represent hydrogen atoms, gray spheres represent carbon atoms, red spheres represent oxygen atoms, the blue sphere represents a nitrogen atom, the green sphere represents a chlorine atom, and the purple sphere represents a Na^+ cation.

Based on these observations, the calculations were repeated with the addition of the continuum solvation model. It was believed that this might help stabilize the growing negative charge on the chlorine atom and help minimize the interactions between that atom and the metal cation. Unfortunately however, the size of the molecules being studied combined with the use of continuum solvation during the optimization of the structure, as opposed to just modifying the results of a single point, proved to be more complex than software could handle.

Despite the numerous problems with this methodology, a full picture of the reaction coordinate for the 5 membered ring with Li^+ starting from the nitrogen metalated reactant was obtained and is shown in Figure 4.10. As shown in that figure, the axial transition structure is significantly lower in energy than that equatorial transition structure, which corresponds to the lower energy of the axial product than the equatorial product. Several key pieces of structural data from the two transition structures are

summarized in Table 4.5. Table 4.5 shows that the bond distances between the chlorine and the adding methyl group and α -carbon are significantly smaller for the axial transition structure. As expected, the distance between the two methyl groups is smaller for the lower energy axial transition structure it is possible that these results are the drivers for the higher energy of equatorial transition state and explain the unexpectedly large difference in the enthalpy of the two transition structures.

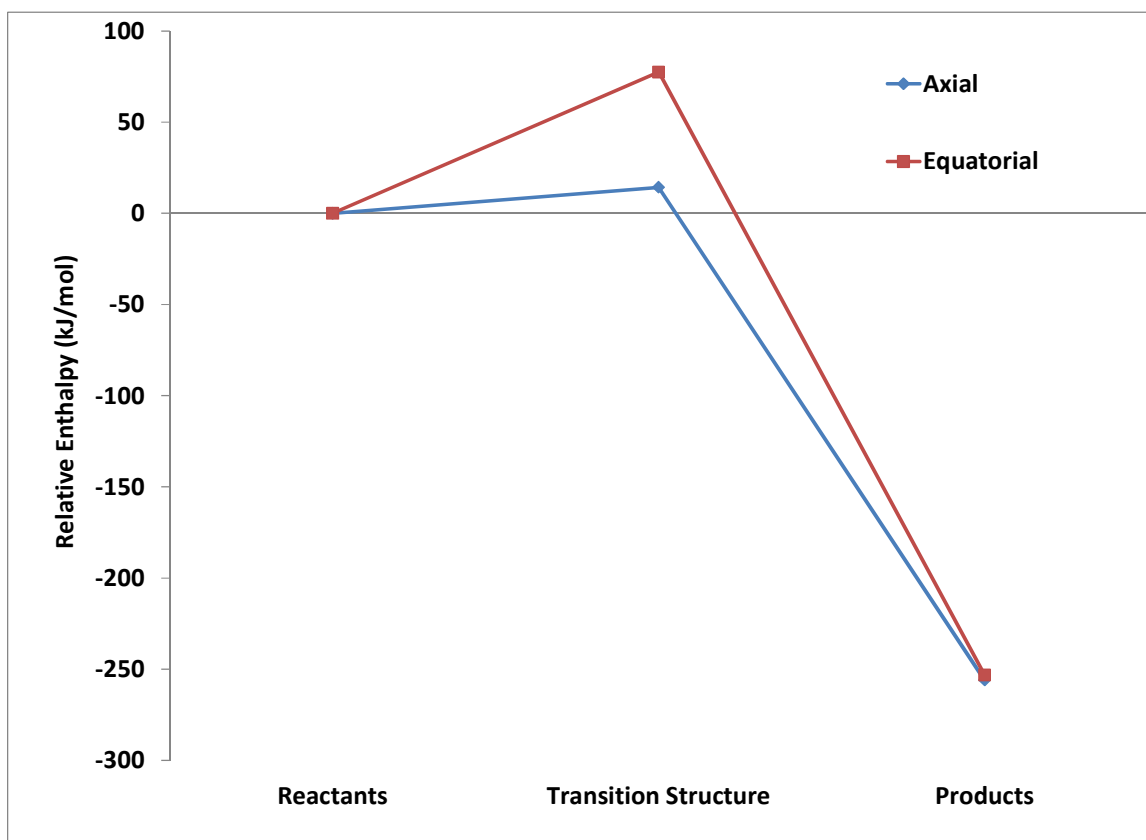


Figure 4.10. The B3LYP reaction coordinate for the 5 membered ring reaction with Li^+ starting from the nitrogen metalated reactant. Data shown is based on explicit / continuum hybrid solvation in THF.

<u>Distances (in Å)</u>	<u>Axial</u>	<u>Equatorial</u>
α-Carbon / Adding Methyl Carbon Distance	2.400	3.305
α-Carbon / Nitrile Carbon Distance	1.379	1.371
Nitrile Carbon / Nitrogen Distance	1.188	1.192
Nitrogen / Lithium Distance	1.968	1.939
Adding Methyl Carbon / Existing Methyl Carbon Distance	4.262	3.857
<u>Angles</u>		
Nitrile Carbon / Nitrogen / Cation	147.2	168.8

Table 4.5. Selected structural data for the two lithium based transition structures for the 5 membered ring reaction.

Though it became clear that the current strategy was not likely to yield the same information for the other scenarios, it was still desired that the data be obtained and used to complete the understanding of the landscape of this subject. To that end, an alternate strategy was investigated which made use of calculations using significantly smaller and computationally less expensive model chemistries.

4.3.3.2 Semi-Empirical Calculations

It was believed that beginning these transition structure calculations from a starting point which was closer to the optimized geometry might eliminate the problems seen with the calculations discussed in the previous chapter. To that end, the next strategy employed in this investigation was to find transition structures for the 16 combinations of geometry, cation, and ring size using a series of three semi-empirical model chemistries. The three model chemistries used were AM1, PM3, and PM6. However, due to the nature of the data sets used to develop the parameters used by the various methods, the two smaller models, AM1 and PM3, could not be applied over all of the cations being studied. The AM1 model does not have parameters for Na⁺, K⁺, or Cu⁺

and the PM3 model does not have parameters with Cu^+ , the PM6 model was, however, usable for all of the cations of interest. Unfortunately, as was the case with the direct DFT calculations that were discussed previously, the vast majority of these calculations could not be successfully completed due to several problems with the algorithms used by Gaussian09. The summary of which calculations did and did not successfully yield is shown in Table 4.6.

<u>Model</u>	<u>Cation</u>	<u>5 Membered Ring</u>		<u>6 Membered Ring</u>	
		<u>Axial</u>	<u>Equatorial</u>	<u>Axial</u>	<u>Equatorial</u>
AM1	Li	Successful	Unsuccessful	Unsuccessful	Unsuccessful
PM3	Li	Successful	Unsuccessful	Successful	Unsuccessful
	Na	Unsuccessful	Unsuccessful	Successful	Unsuccessful
	K	Unsuccessful	Unsuccessful	Unsuccessful	Unsuccessful
PM6	Li	Successful	Unsuccessful	Unsuccessful	Unsuccessful
	Na	Unsuccessful	Unsuccessful	Unsuccessful	Unsuccessful
	K	Unsuccessful	Unsuccessful	Unsuccessful	Unsuccessful
	Cu	Unsuccessful	Unsuccessful	Unsuccessful	Unsuccessful

Table 4.6. Summary of semi-empirical results for the calculations of transition structures using Gaussian 09.

Due to the computational problems experienced with the Gaussian software it was impossible to prove or disprove the hypothesis that the starting from a semi-empirically optimized structure would overcome issues observed during the DFT transition structure calculations. This hypothesis is still of very much interest, so an alternate software package was employed in a second attempt to answer this question. The results of this second attempt are discussed in the next section.

4.3.3.3 Alternate Software Calculations

In order to further explore the use of semi-empirical calculations as a tool to enable the completion of the desired B3LYP calculations an alternate software package, MOPAC, was used to carry out a series of calculations using the PM6 semi-empirical model chemistry. Due to the limitations of the AM1 and PM3 models, this work was limited to only the PM6 model.

A multiple step process was attempted using the MOPAC software. In the first step, all 16 structures were optimized to an energy minimum using the PM6 model chemistry, while the atoms of the reaction axis, as shown in Figure 4.8, were held frozen. After this step was successfully completed, the reaction axes were unfrozen and the 16 structures were again optimized to the transition structure. The issues that arose while using Gaussian to find these transition structures were not encountered while using MOPAC and the 16 transition structures were successfully determined using the MOPAC software. Those structures were optimized with explicit THF solvation, followed by single point energy calculations in which continuum solvation with THF was applied. The enthalpy results reported in this section are the values obtained from the calculations which employed explicit and continuum solvation with THF. The relative enthalpies of the transition structures are shown in Table 4.7, and several key structural features of the optimized geometries are shown in Tables 4.8 and 4.9.

Nitrogen Metallated Transition States (Relative Enthalpies in kJ/mol)				
Cation	5 Carbon Ring - Axial	5 Carbon Ring - Equatorial	6 Carbon Ring - Axial	6 Carbon Ring - Equatorial
Li	0.0	176.9	0.0	42.8
Na	0.0	1.4	0.0	59.1
K	0.0	7.4	0.0	27.9
Cu	0.0	8.3	0.0	38.1

Table 4.7. Relative energies of the MOPAC optimized transition structures

Distances (in Å)	Li-		Na-		K-		Cu-	
	Li - Axial	Equatorial	Na - Axial	Equatorial	K - Axial	Equatorial	Cu - Axial	Equatorial
α -Carbon / Adding Methyl Carbon Distance	2.258	2.298	2.317	2.315	2.234	2.331	3.348	3.396
α -Carbon / Nitrile Carbon Distance	1.383	1.368	1.374	1.371	1.376	1.374	1.331	1.335
Nitrile Carbon / Nitrogen Distance	1.182	1.177	1.177	1.178	1.175	1.174	1.208	1.202
Nitrogen / Cation Distance	1.955	2.001	2.404	2.381	2.726	2.740	1.853	1.853
Adding Methyl Carbon / Existing Methyl Carbon Distance	4.251	3.236	4.408	3.241	4.402	3.219	5.139	3.642
Angles								
Nitrile Carbon / Nitrogen / Cation	162.3	162.2	148.2	130.8	144.1	166.5	129.1	134.1

Table 4.8. Selected structural data for the PM6 transition structures for the 5 membered ring reaction.

Distances (in Å)	Li-		Na-		K-		Cu-	
	Li - Axial	Equatorial	Na - Axial	Equatorial	K - Axial	Equatorial	Cu - Axial	Equatorial
α -Carbon / Adding Methyl Carbon Distance	3.334	2.285	3.331	2.328	3.296	2.346	3.331	2.287
α -Carbon / Nitrile Carbon Distance	1.343	1.374	1.351	1.379	1.355	1.379	1.341	1.376
Nitrile Carbon / Nitrogen Distance	1.192	1.178	1.186	1.176	1.183	1.175	1.200	1.179
Nitrogen / Cation Distance	1.960	2.007	2.376	2.394	2.710	2.722	1.880	1.893
Adding Methyl Carbon / Existing Methyl Carbon Distance	3.719	3.638	3.664	3.696	3.784	3.685	3.742	3.682
Angles								
Nitrile Carbon / Nitrogen / Cation	146.1	164.9	139.7	160.2	149.4	155.8	134.6	155.9

Table 4.9. Selected structural data for the PM6 transition structures for the 6 membered ring reaction.

The energy values found in Table 4.7 are not as quantitatively accurate as those generated using ab initio and DFT methods, but are valuable in providing a qualitative understanding of how the different transition structures relate to each other. They also provide insight into the role of transition structure in determining the selectivity of the reactions. As shown in Table 4.7, for all of the cations studied the axial transition state was energetically preferred relative to the equatorial transition structure. This agrees with the B3LYP results obtained for Li^+ as shown in Figure 4.10. With the expectation of lithium, the values in in Table 4.7 show that magnitude of the energy preference is consistently higher in the case of the 6 membered ring reaction than in the 5 membered ring reaction.

Two interesting trends can be seen in the structural data shown in Tables 4.8 and 4.9. For the 5 membered ring reactions, as expected, the distance between the existing and the adding methyl group is much larger in the case of the axial addition, suggesting that sterics is a dominant factor in determining the preferred transition structure. In the case of the 6 membered ring reaction, however, the energy differences are generally larger, but the differences in methyl group distance are smaller. This suggests that there is a large electronic factor driving structure preference as well. In the 6 membered ring case, the preferred axial structures show a smaller nitrile carbon – nitrogen – cation bond angle. This brings the cation closer to the α -carbon, suggesting that the increased interaction with any negative charge on the α -carbon provides an energetic advantage that further stabilizes the axial transition structure.

The enthalpies of the PM6 optimized geometries for the reactants, transition structures, and products for the four cations were used to create the reaction coordinate energy profiles shown in Figures 4.11 – 4.18. The same trend is seen in all of these reaction coordinates; the axial transition structures were energetically preferred relative to the equatorial structure and the equatorial product was slightly more preferred than the axial product. This does not agree with the B3LYP result for Li^+ in that the products do not follow the same trend as the transition structures. This result, however, when coupled with the B3LYP results for the reaction products suggests that there is a large kinetic factor in the selectivity of the reaction which is as important thermodynamic factor. The much larger difference in the enthalpies of the two transition structures would lead to a large preference in the formation of the axial structure. The very large difference in the

energy of the transition structure relative to the final product would lead to a very rapid completion of the reaction. This would result in a significantly higher preference for the axial product than would be expected from the small differences in the energy of the products. This is in good agreement with experimental observations.¹²⁻²⁰

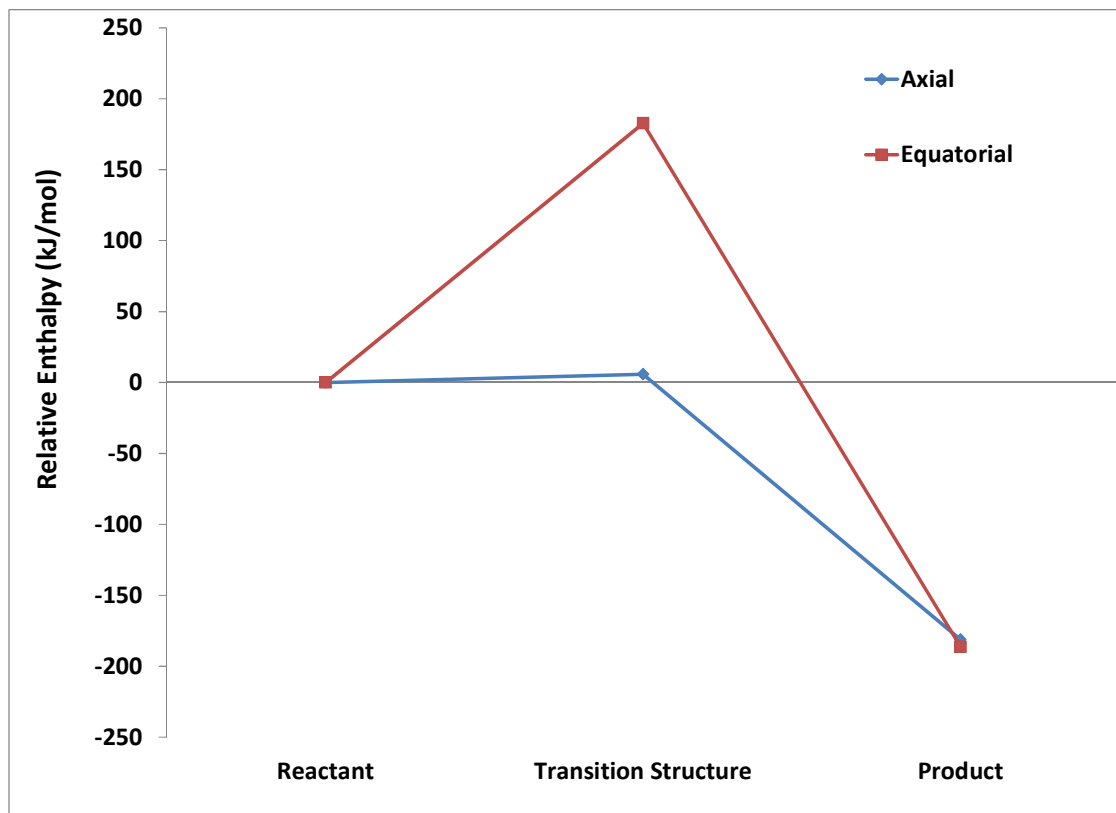


Figure 4.11. The PM6 reaction coordinate for the 5 membered ring reaction with Li^+ starting from the nitrogen metalated reactant. Data shown is based on explicit / continuum hybrid solvation in THF.

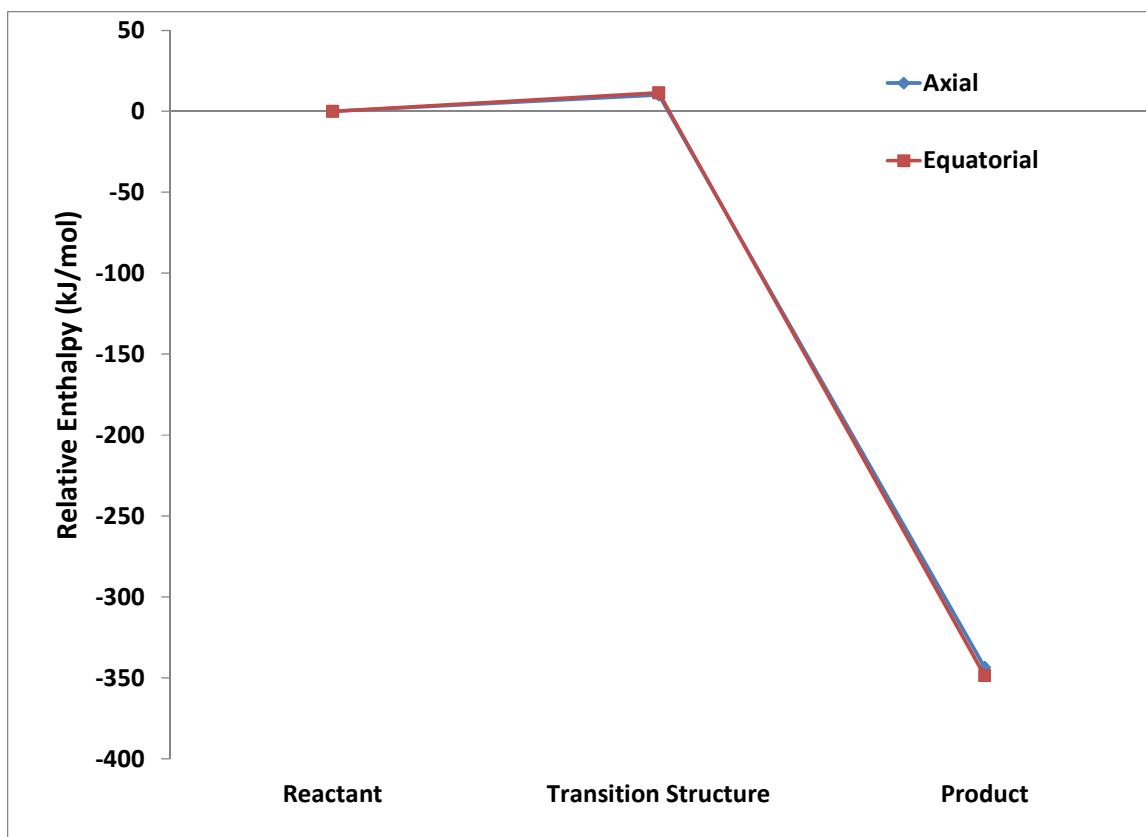


Figure 4.12. The PM6 reaction coordinate for the 5 membered ring reaction with Na^+ starting from the nitrogen metalated reactant. Data shown is based on explicit / continuum hybrid solvation in THF.

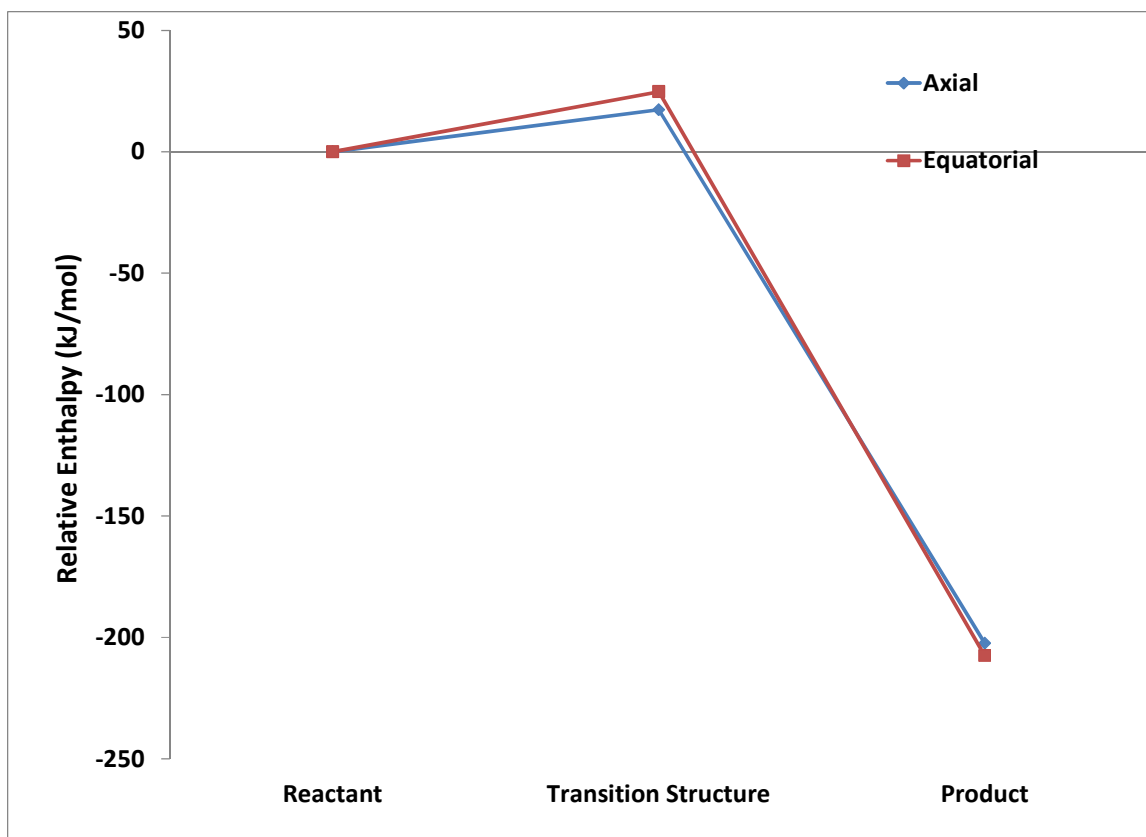


Figure 4.13. The PM6 reaction coordinate for the 5 membered ring reaction with K^+ starting from the nitrogen metalated reactant. Data shown is based on explicit / continuum hybrid solvation in THF.

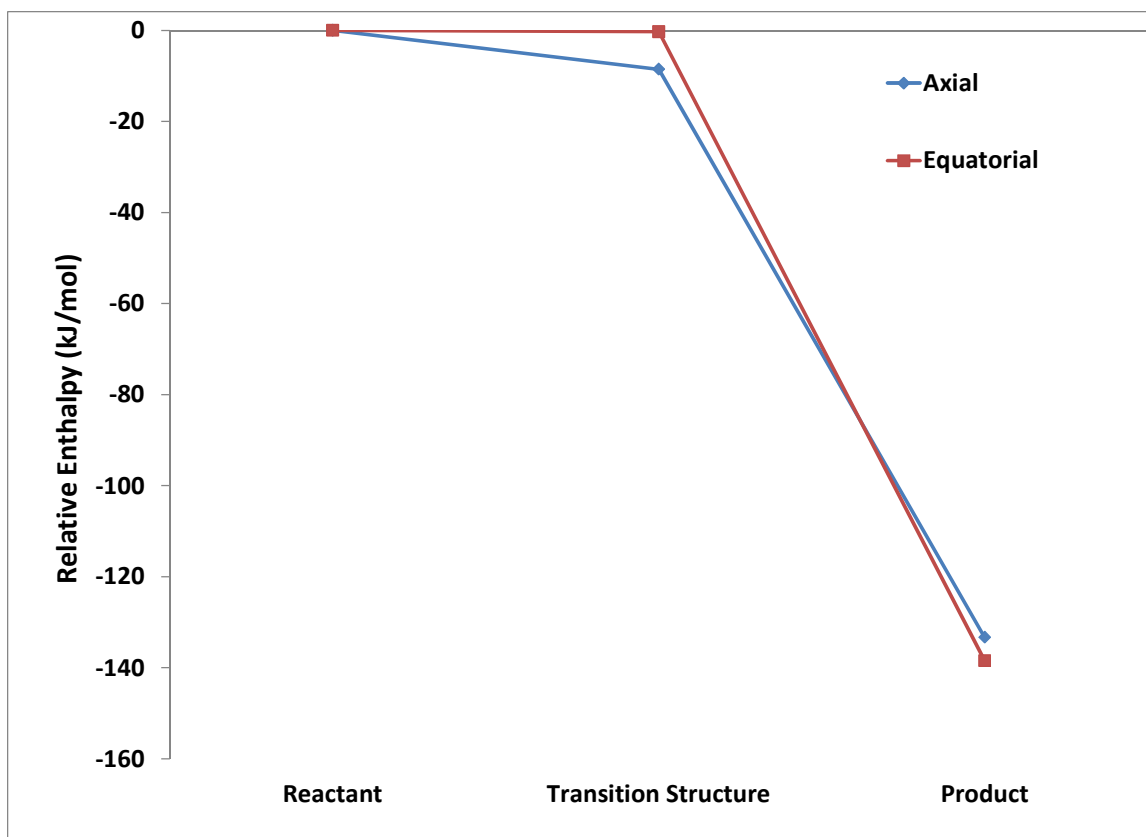


Figure 4.14. The PM6 reaction coordinate for the 5 membered ring reaction with Cu^+ starting from the nitrogen metalated reactant. Data shown is based on explicit / continuum hybrid solvation in THF.

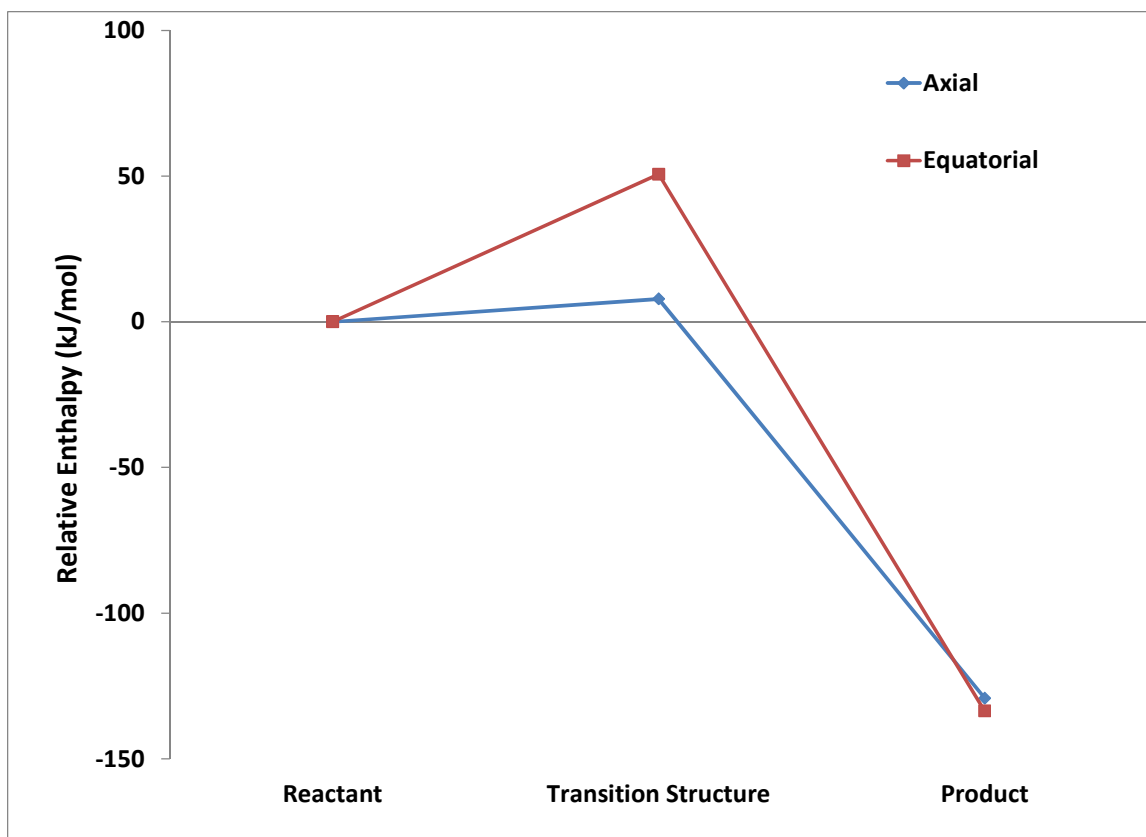


Figure 4.15. The PM6 reaction coordinate for the 6 membered ring reaction with Li^+ starting from the nitrogen metalated reactant. Data shown is based on explicit / continuum hybrid solvation in THF.

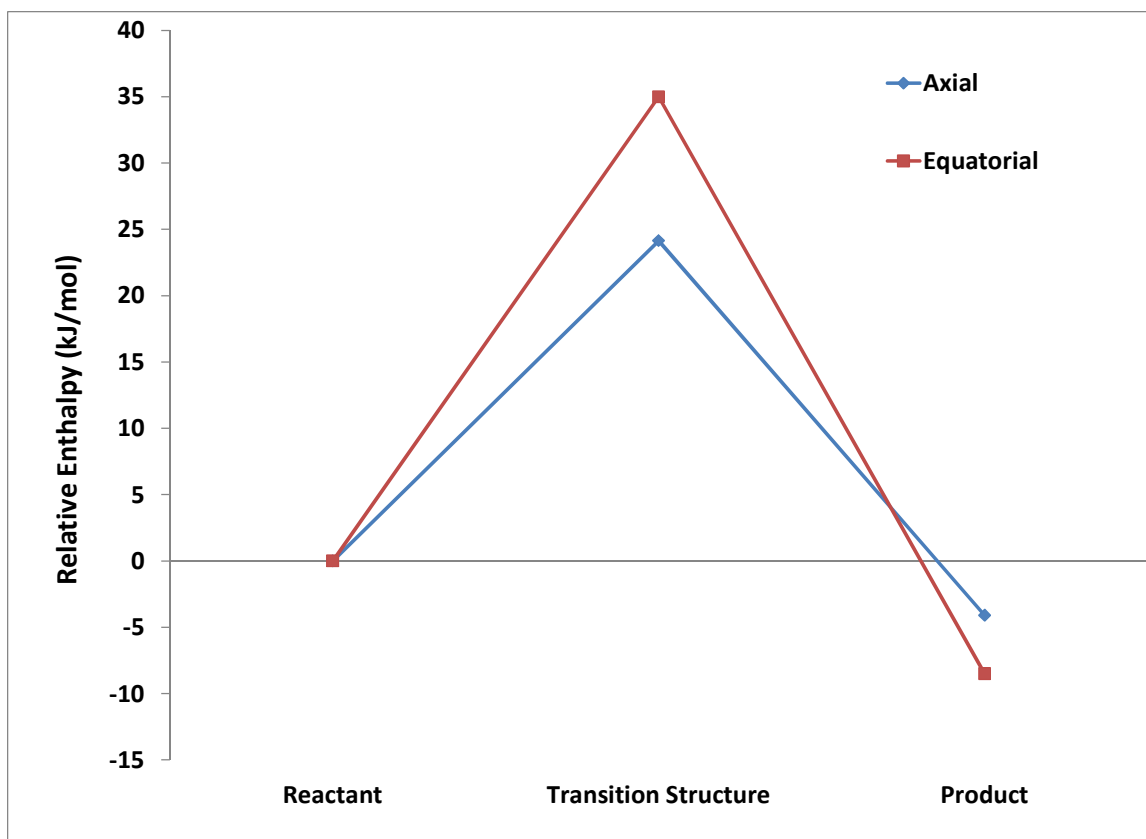


Figure 4.16. The PM6 reaction coordinate for the 6 membered ring reaction with Na^+ starting from the nitrogen metalated reactant. Data shown is based on explicit / continuum hybrid solvation in THF.

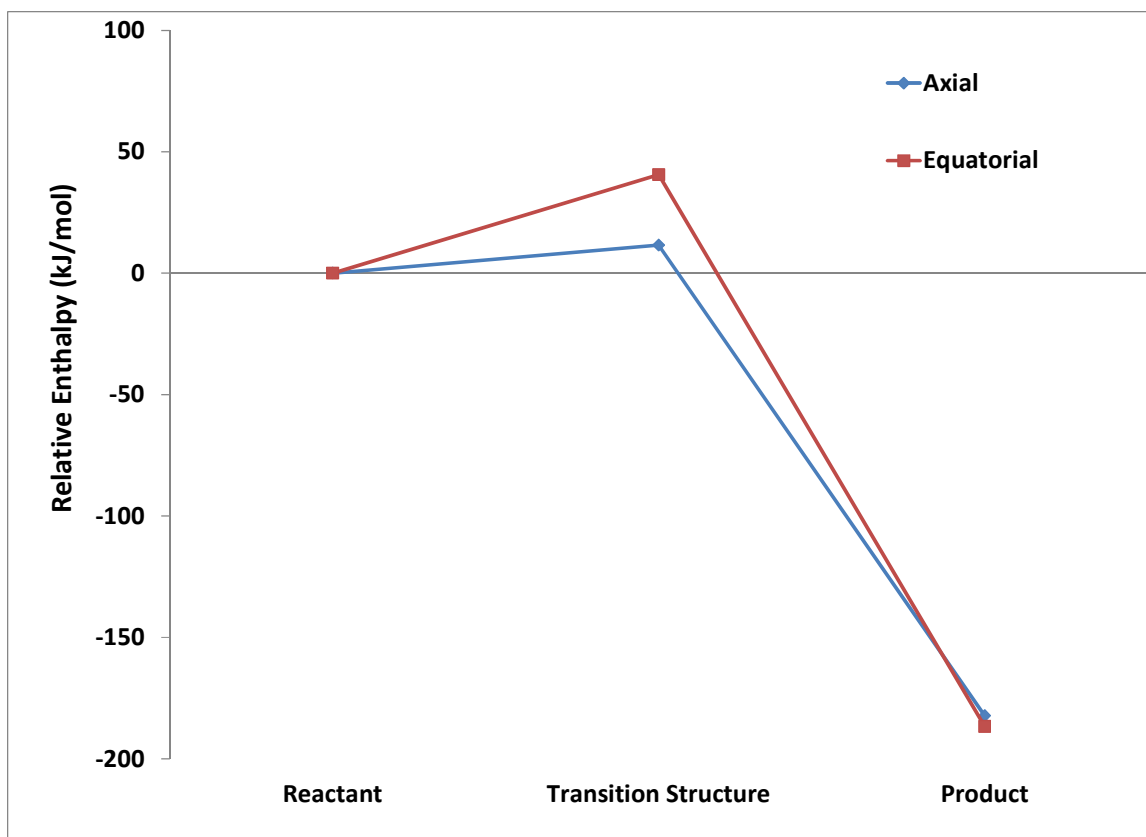


Figure 4.17. The PM6 reaction coordinate for the 6 membered ring reaction with K^+ starting from the nitrogen metalated reactant. Data shown is based on explicit / continuum hybrid solvation in THF.

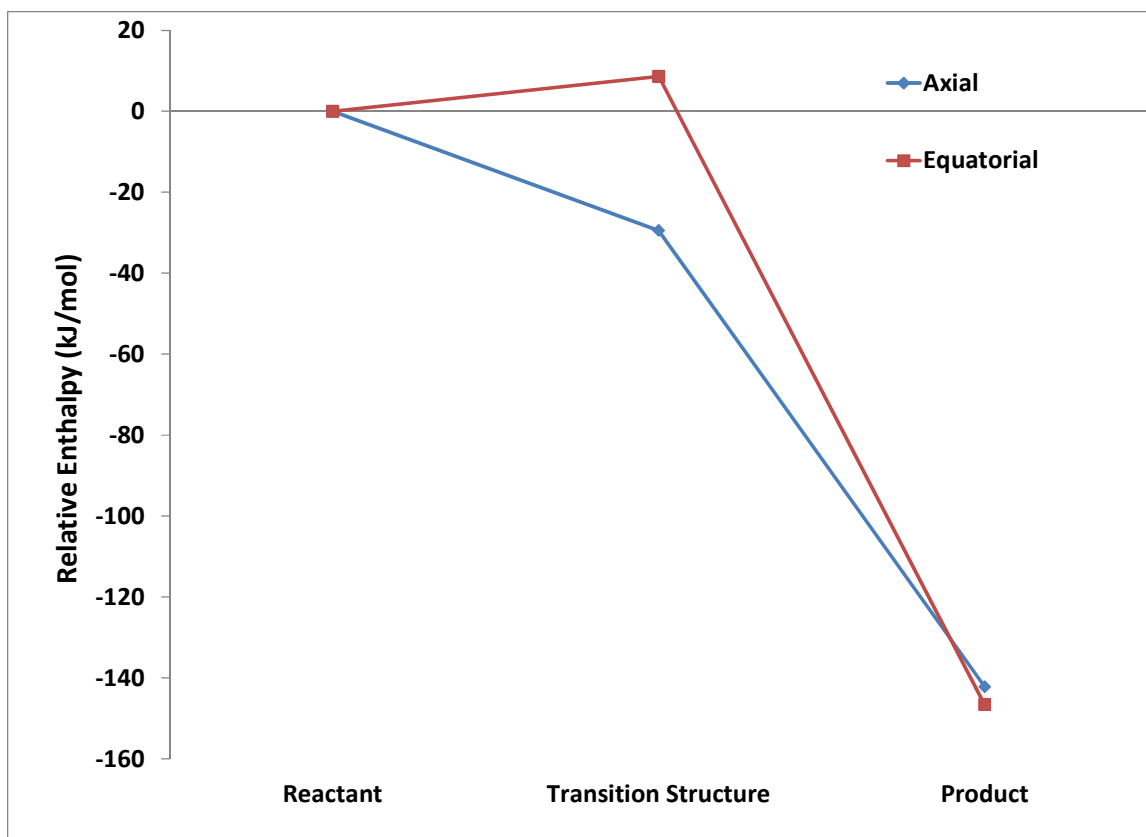


Figure 4.18. The PM6 reaction coordinate for the 6 membered ring reaction with Cu^+ starting from the nitrogen metalated reactant. Data shown is based on explicit / continuum hybrid solvation in THF.

The PM6 optimized transition structures were also important to the next step of this investigation, in which the hypothesis of avoiding the previously discussed problems in finding the B3LYP transition state by using a better, PM6 generated, starting geometry was tested. To this end, B3LYP frequency calculations were carried out on the PM6 optimized structures using Gaussian 09. None of the structures were found to have the one desired imaginary frequency corresponding to the transition structure, but all had between 5 and 11 imaginary frequencies. Using the PM6 optimized geometries, which were modified by having the atoms of the reaction axis frozen, and the force constants

obtained from the B3LYP frequency calculations, B3LYP geometry optimizations were carried out for the transition structures.

Unfortunately, using the PM6 optimized structures as starting point geometries did not eliminate the problem of cation and anion interaction which plagued the work described in Section 4.3.3.1, and no additional B3LYP transition structures were obtained using this process.

4.4 Conclusions

The overall objective of this portion of the dissertation investigation was to plot the reaction coordinate energy profile for two different substitution reactions which involved a reactant containing a nitrile anion and one of four cations, and in doing so, determine the effect of cation on the selectivity of the reaction. However, due to numerous difficulties in determining the transition structures of the reactions using the B3LYP/6-31+G(d) model chemistry, it was not possible to construct all of the desired reaction coordinates at the desired level of theory. Despite this, it was possible to understand the reactants and the products of the reactions at the desired level of theory and it was possible to construct full reaction coordinate energy profiles at the semi-empirical PM6 level of theory. From this data several insights into the nature of these reactions were obtained.

The first of these insights was the role of metalation of the nitrile anion at the α -carbon position. Initial investigations of these systems have focused on nitrogen metalation, which though valid for lithium may not be common conformation for other

metals. In the case of a nitrogen metalated species, there is a high level of freedom for a substitution reaction occurring at the α -carbon to proceed either above or below the plane in which the nitrile group exists. This makes the understanding of energetic differences in the two transition structures (above and below the nitrile anion plane) a key piece of information needed to understand the selectivity of the final product of the reaction. In the case of α -carbon metalation, the reaction is directed to the face of the plane opposite that of the cation. Based on this, there is only a single transition structure for a reaction proceeding from a carbon metalated reactant, and understanding the energy of that structure is of negligible value in understanding what drives selectivity of the reaction. Of more importance are the steric factors which drive the energetic preference for the direction in which the cation will approach the α -carbon and the direction in which the second reactant will approach and ultimately add to the nitrile anion containing molecule.

The second of these insights was the kinetic control of the selectivity of the final product of the reaction. For the nitrogen metalated reactants the differences in enthalpy for the two transition structure was found to be much larger than the energy difference of the final products. This implies that the selective of the reaction is driven more by the formation of the significantly preferred axial transition structure followed by rapid completion of the reaction, than it is by the thermodynamic preference of either of the products. This factor was only fully explored at the PM6 level of theory, but the agreement in results between PM6 and B3LYP for the 5 membered ring reaction with the lithium cation allows a reasonable level of confidence in the validity of this conclusion.

The third of these insights were the limitations of the models and model chemistries being used to study the transition structures associated with these reactions. The changes

in energetic preference seen in Table 4.3 strongly suggest that the 3 THF molecules used to approximate the primary solvation sphere are insufficient to fully account for the stabilization of solvation. Though results in the previous chapters showed that in very simple cases four ligands were sufficient to account for the energy of solvation, it is possible that the increased complexity of the systems studied in this chapter were no longer completely satisfied by the 3 solvent molecules and the nitrile group. It was also clear that the models used were not capable of managing, at the B3LYP level, the tendency of the cations to drift away from the nitrogen metalation point and toward the chlorine atom as the amount of negative charge/electron density on that atom increased.

The limited success in meeting the overall objective of this portion of the investigation, shows the opportunity for further investigation and implementation of different strategies to fully understand the factors that dictate the selectivity of these reactions definitely exist. The first of these would be the development of models which were are better able to handle the cation drift seen with calculations performed at the B3LYP level of theory. Perhaps the use of larger basis sets or additional molecules of explicit solvation would allow for better charge separation that would eliminate the drifting phenomenon. Of course, the computational expense of making these changes might be prohibitive at this time, but continued advances in the power and efficiency of computation software and hardware should eventually overcome this barrier.

4.5 References

1. Stork, G.; Boeckman, R. K., Mechanism and stereochemical control in the .alpha.-haloketal cyclization. Remarkable effect of metal cations. *Journal of the American Chemical Society* **1973**, 95, (6), 2016-2017.
2. Stork, G.; Gardner, J. O.; Beckman, R. K.; Parker, K. A., Haloketal cyclization. General method for the synthesis of functionalized cis bicyclic ketones. *Journal of the American Chemical Society* **1973**, 95, (6), 2014-2016.
3. Carlier, P. R.; Lo, K. M., 2,3-Anti Selective Aldol Reaction of Phenylacetonitrile. *The Journal of Organic Chemistry* **1994**, 59, (15), 4053-4055.
4. Rychnovsky, S. D.; Griesgraber, G.; Kim, J., Rapid Construction of the Roflamycoin System. *Journal of the American Chemical Society* **1994**, 116, (6), 2621-2622.
5. Rychnovsky, S. D.; Swenson, S. S., Alkylation and Reductive Decyanation of 4-Cyano-2,2-dimethyl-1,3-dioxanes (Cyanohydrin Acetonides). *The Journal of Organic Chemistry* **1997**, 62, (5), 1333-1340.
6. Fleming, F. F.; Shook, B. C.; Jiang, T.; Steward, O. W., β -Siloxy Unsaturated Nitriles: Stereoselective Cyclizations to cis- and trans-Decalins. *Organic Letters* **1999**, 1, (10), 1547-1550.
7. Arseniyadis, S.; Kyler, K. S.; Watt, D. S., *Organic Reactions* **1984**, 31, 1-364.
8. Fleming, F. F.; Shook, B. C., Nitrile anion cyclizations. *Tetrahedron* **2002**, 58, (1), 1-23.
9. Fleming, F. F.; Shook, B. C., Nitrile Anions: ϵ Solvent-Dependent Cyclizations. *The Journal of Organic Chemistry* **2002**, 67, (9), 2885-2888.

10. Fleming, F. F.; Wei, Y.; Liu, W.; Zhang, Z., Metalated Nitriles: Cation-Controlled Cyclizations. *Organic Letters* **2007**, 9, (14), 2733-2736.
11. Fleming, F. F.; Wei, Y.; Liu, W.; Zhang, Z., Metalated nitriles: stereodivergent cation-controlled cyclizations. *Tetrahedron* **2008**, 64, (32), 7477-7488.
12. Bare, T. M.; Hershey, N. D.; House, H. O.; Swain, C. G., Extent of bond formation in the transition state for alkylation at nitrogen and at carbon. *The Journal of Organic Chemistry* **1972**, 37, (7), 997-1002.
13. Boche, G., The Structure of Lithium Compounds of Sulfones, Sulfoximides, Sulfoxides, Thioethers and 1,3-Dithianes, Nitriles, Nitro Compounds and Hydrazones. *Angewandte Chemie International Edition in English* **1989**, 28, (3), 277-297.
14. Fleming, F. F.; Gudipati, S.; Zhang, Z.; Liu, W.; Steward, O. W., Cyclic Nitriles: Diastereoselective Alkylations. *The Journal of Organic Chemistry* **2005**, 70, (10), 3845-3849.
15. Fleming, F. F.; Liu, W.; Ghosh, S.; Steward, O. W., Metalated Nitriles: Internal 1,2-Asymmetric Induction. *The Journal of Organic Chemistry* **2008**, 73, (7), 2803-2810.
16. Fleming, F. F.; Zhang, Z., Cyclic nitriles: tactical advantages in synthesis. *Tetrahedron* **2005**, 61, (4), 747-789.
17. Fleming, F. F.; Zhang, Z.; Knochel, P., Metalated Nitriles: Halogen-Metal Exchange with $\hat{\pm}$ -Halonitriles. *Organic Letters* **2004**, 6, (4), 501-503.
18. Fleming, F. F.; Zhang, Z.; Liu, W.; Knochel, P., Metalated Nitriles: Organolithium, -magnesium, and -copper Exchange of $\hat{\pm}$ -Halonitriles. *The Journal of Organic Chemistry* **2005**, 70, (6), 2200-2205.

19. Fleming, F. F.; Zhang, Z.; Wei, G.; Steward, O. W., C-Metalated Nitriles: Electrophile-Dependent Alkylations and Acylations. *The Journal of Organic Chemistry* **2006**, 71, (4), 1430-1435.
20. Naota, T.; Tanna, A.; Murahashi, S.-I., Synthesis and Characterization of C- and N-Bound Isomers of Transition Metal $\hat{\text{I}}\pm$ -Cyanocarbanions. *Journal of the American Chemical Society* **2000**, 122, (12), 2960-2961.
21. Frisch, M. J.; Trucks, G. W.; Schlegel, H. B.; Scuseria, G. E.; Robb, M. A.; Cheeseman, J. R.; Scalmani, G.; Barone, V.; Mennucci, B.; Petersson, G. A.; Nakatsuji, H.; Caricato, M.; Li, X.; Hratchian, H. P.; Izmaylov, A. F.; Bloino, J.; Zheng, G.; Sonnenberg, J. L.; M. Hada; Ehara, M.; Toyota, K.; Fukuda, R.; Hasegawa, J.; Ishida, M.; Nakajima, T.; Honda, Y.; Kitao, O.; Nakai, H.; Vreven, T.; J. A. Montgomery, J.; Peralta, J. E.; Ogliaro, F.; Bearpark, M.; Heyd, J. J.; Brothers, E.; Kudin, K. N.; Staroverov, V. N.; Keith, T.; Kobayashi, R.; Normand, J.; Raghavachari, K.; Rendell, A.; Burant, J. C.; Iyengar, S. S.; Tomasi, J.; Cossi, M.; Rega, N.; Millam, J. M.; Klene, M.; Knox, J. E.; Cross, J. B.; Bakken, V.; Adamo, C.; Jaramillo, J.; Gomperts, R.; Stratmann, R. E.; Yazyev, O.; Austin, A. J.; Cammi, R.; Pomelli, C.; Ochterski, J. W.; Martin, R. L.; Morokuma, K.; Zakrzewski, V. G.; Voth, G. A.; Salvador, P.; Dannenberg, J. J.; Dapprich, S.; Daniels, A. D.; Farkas, O.; Foresman, J. B.; Ortiz, J. V.; Cioslowski, J.; Fox, D. J. Gaussian 09, Revision B.01; Gaussian, Inc.: Wallingford, CT, 2010.
22. Stewart, J. J. P. *MOPAC2009*, Version 9.351M; Stewart Computational Chemistry.
23. Becke, A. D., Density-functional thermochemistry. III. The role of exact exchange. *Journal of Chemical Physics* **1993**, 98, (7), 5648-5662.

24. Lee, C.; Yang, W.; Parr, R. G., Development of the Colle-Salvetti correlation-energy formula into a functional of the electron density. *Physical Review B* **1988**, 37, (2), 785-789.
25. Dewar, M. J. S.; Zoebisch, E. G.; Healy, E. F.; Stewart, J. J. P., Development and use of quantum mechanical molecular models. 76. AM1: a new general purpose quantum mechanical molecular model. *Journal of the American Chemical Society* **1985**, 107, (13), 3902-3909.
26. Stewart, J. J. P., Optimization of parameters for semiempirical methods I. Method. *Journal of Computational Chemistry* **1989**, 10, (2), 209-220.
27. Stewart, J. J. P., Optimization of parameters for semiempirical methods II. Applications. *Journal of Computational Chemistry* **1989**, 10, (2), 221-264.
28. Stewart, J., Optimization of parameters for semiempirical methods V: Modification of NDDO approximations and application to 70 elements. *Journal of Molecular Modeling* **2007**, 13, (12), 1173-1213.
29. Tomasi, J.; Persico, M., Molecular Interactions in Solution: An Overview of Methods Based on Continuous Distributions of the Solvent. *Chemical Reviews* **1994**, 94, 2027 - 2094.
30. Cossi, M.; Barone, V.; Cammi, R.; Tomasi, J., Ab initio study of solvated molecules: a new implementation of the polarizable continuum model. *Chemical Physics Letters* **1996**, 255, (4-6), 327-335.
31. Carlier, P. R.; Lo, C. W.-S., ⁷Li/³¹P NMR Studies of Lithiated Arylacetonitriles in THF-HMPA Solution: Characterization of HMPA-Solvated Monomers, Dimers, and Separated Ion Pairs. *Journal of The American Chemical Society* **2000**, 122, 12819-12823.

32. Carlier, P. R.; Lucht, B. L.; Collum, D. B., ^6Li PN NMR-Based Solution Structural Determination of EtzO- and TMEDA-Solvated Lithiophenylacetonitrile and a LiHMDS Mixed Aggregate. *Journal of The American Chemical Society* **1994**, 116, 11602-11603.
33. Carlier, P. R.; Zhang, Y., The First Enantioenriched Metalated Nitrile Possessing Macroscopic Configurational Stability. *Organic Letters* **2007**, 9, (7), 1319-1322.
34. Hilmersson, G.; Sott, R.; Granander, J., Mixed Complexes Formed by Lithioacetonitrile and Chiral Lithium Amides: Observation of ^6Li , ^{15}N and ^6Li , ^{13}C Couplings Due to Both C-Li and N-Li Contacts. *Journal of The American Chemical Society* **2004**, 126, 6798-6805.
35. Sott, R.; Granander, J.; Hilmersson, G., Solvent-Dependent Mixed Complex Formation—NMR Studies and Asymmetric Addition Reactions of Lithioacetonitrile to Benzaldehyde Mediated by Chiral Lithium Amides. *Chemistry – A European Journal* **2002**, 8, (9), 2081-2087.

5 Conclusion and Future Directions

The fundamental hypothesis of this investigation was that the structure and resultant reactivity of nitrile anions is strongly influenced by the nature of the cation that acts as counterion and the nature of the solvent in which the complex exists. Exploring this hypothesis through the use of electronic structure calculations resulted in the conclusion that the structure and reactivity of nitrile anions is definitely influenced by the cations with which they are associated and to a lesser extent by the solvent in which they exist. Specifically, it was found that different cations show substantial preferences for association with the nitrile anion at the nitrile nitrogen (lithium cation) or at the α -carbon position (copper cation and magnesium chloride cation). Complexes which displayed α -carbon metalation also showed significantly higher deformation and much more sp^3 character around the α -carbon than complexes which were nitrogen metalated. This carbon versus nitrogen metalation seems to be a key aspect in driving the selectivity of reactions involving nitrile anion functionalized molecules.

The first aspect of this investigation was described in Chapter 2 and was based on the study of various cation – solvent complexes using several different electronic structure calculation methods. The aim of this work was to determine the most effective method for studying these types of systems by comparing the calculated theoretical results with known experimental results. Based on this work it was determined that of the three model chemistries evaluated that the DFT model chemistry (B3LYP/6-31+G(d)) was the most accurate for determining the structure and electronic energy of these simple cation solvent complexes. Unlike the HF and MP2 models chemistries, the DFT method was able to accurately capture the strong influence of the d orbitals on how the copper

cation interacted with the solvent molecules ligating it. Finally, evaluations of explicit solvation and continuum solvation were conducted which demonstrated that continuum solvation alone was insufficient to fully provide the amount of stabilization that was expected for the various cations. From these results it also appeared that a combination of explicit and continuum solvation with at least three solvent molecules was sufficient to account for the expected amount of solvation energy.

There are several ways in which this part of the investigation could be interestingly extended by future researchers. One example would be a more thorough investigation of why the MP2 calculations, which were expected to be the most accurate, gave the poorest agreement with experimental data. Two ways to carry out this investigation would be to evaluate a range of basis sets to determine if the basis set used was too limited to provide accurate results with electron correlation containing MP2 model chemistry or to evaluate the MP2/6-31+G(d) model chemistry with several different software packages to determine if the poor results were due to a mathematical artifact of the software used in this investigation. It would also be of interest to investigate more thoroughly the number of solvent molecules which comprise the primary solvation sphere of the cations studied, and how this changes as the size of the solvent molecule changes. This information would very valuable in understanding the results of subsequent portions of this investigation as well the results of further investigations of the solvation of ionic species.

The second aspect of this investigation, which was described in Chapter 3, was an extension of the work in Chapter 2 in which acetonitrile anions are added to the cation – solvent complexes in place of one of the solvent molecules. The aim of this part of the

dissertation was to better understand the effect of cation and solvent on the structure of acetonitrile anion. The nature of the cation was found to have two key effects on the structure of acetonitrile anion. In either the nitrogen metalated or carbon metalated scenarios deformation angle, or degree of pyramidalization, increased as the size of the cation increased. However, in all cases the degree of deformation was sustainably larger for the carbon metalated complexes than for their nitrogen metalated analogs. As the size of the cation increased the preference for carbon metalation also increased. Further investigation of this observation, through the use of natural bond order analysis, showed a correlation between energetic preference for nitrogen or carbon metalation and the minimization of charge density on the cation. This correlation became weaker when continuum solvation was added to the complexes, suggesting that explicit solvation with three solvent molecules was insufficient to accurately describe the system. It also strongly suggests that solvation affects the charge density and charge stabilization on the cation, which in turn affects the energetic preference for carbon versus nitrogen metalation.

The most obvious and interesting extension of this work would be the broadening of the scope of solvents studied. Very little difference was seen, or expected, between the very similar THF and DME solvents used in this research. Expanding the scope of solvents to include non-polar aliphatic solvents such as hexane, non-polar aromatic solvents such as benzene or toluene, and polar non-ether solvents such as ketones or amines would significantly add to the understanding of how solvent affects these systems and also provide additional insight into how changes in the charge density of cation drive the preference for metalation position.

The third and final aspect of this investigation, which was described in Chapter 4, was an investigation into the relative energies of several structures along different reaction coordinates for a simple nucleophilic substitution reaction involving a nitrile anion containing cycloaliphatic molecule. The aim of that work was to determine if calculated differences in the electronic energies of the various reactants and transition structures could be used to predict the structure of the reaction product. The reactants and products of these reactions were calculated and demonstrated that several of the cations would direct a carbon metalated reactant which in turn would force the reaction to proceed via a single pathway leading to a single possible product. Numerous issues were encountered during the attempted calculation of the transition states of the reactions being studied at the desired level of theory. However, a complete reaction coordinate energy profile at the B3LYP/6-31+G(d) level of theory was obtained for the nitrogen lithiated 5 membered ring reaction. This reaction coordinate showed the expected preference for axial reaction product and the corresponding transition structure. A complete picture of both reactions with all four cations was developed from calculations carried out at the semi-empirical PM6 level of theory. These calculations showed a strong preference for the axial transition structures and lead to the possibility that the kinetic effect of the preference of the transition structure is more important to selectivity than the thermodynamic preference of the one product over the other.

One key extension of this work would be the previously discussed move toward a more effective method for managing the interaction between the cation and developing chlorine anion. This would, however, be extremely computationally expensive. Another extension would be the application of the current methodology to the study of more

complicated substitution reactions for which experimentally determined selectivity and structural data exists. Building a model which accurately reflects the experimental results would allow not just a more thorough understanding of electronic structure of the various participant molecules, but also would provide a confident starting point from which to study the effect of changes to the reaction conditions. A third extension would be to reconsider the reaction mechanism entirely and calculate transition structures and reaction coordinates which considers the transfer of the cation from the nitrile to anion to chlorine anion as the negative charge moved from the nitrile to the chlorine as an integral part of the mechanism, not an undesired artifact of the geometry optimization.

Overall, the objective of studying the effects of cation on the structure and reactivity of nitrile anions was reasonably well achieved and several interesting conclusions about this subject were drawn. The results of this investigation into the effects of cation and solvent on nitrile anions led to numerous additional questions which will provide fertile ground for the investigations of future researchers.